POLITECNICO DI MILANO

Facoltà di Ingegneria Industriale

Corso di Laurea in
Ingegneria Spaziale

The European Student Moon Orbiter
attitude determination and control
during the impulsive trajectory manoeuvres

Relatore: Prof.ssa MICHÈLE LAVAGNA

Co-relatore: Ing. GAVIN JOHNSTON

Tesi di laurea di :

MAURO CANNONE

Matricola 725129

Anno Accademico 2009-2010

Ringraziamenti

Index

List of figures

List of tables

Abstract

The aim of this work is to analyse the impulsive trajectory manoeuvres which will carry the European Student Moon Orbiter (ESMO) from the initial GTO (Geostationary Transfer Orbit) to the desired final moon orbit. The spacecraft attitude is estimated and controlled during these phases in order to define a reliable combination of sensors, actuators and algorithms capable of performing the manoeuvres with respect to the requirements. The simulations of attitude dynamic have pointed out system weakness and the importance of several parameters.

Available actuators (reaction wheels, cold gas thrusters, main engines) and sensors (sun sensor, star tracker, gyros) have been traded off to define the best architecture.

Attitude has been estimated processing measurements with a Kalman filter.

A closed loop control system has been developed in the Laplace domain considering all transmission delays and the presence of the sample & hold device.

System dynamic has then been implemented in Simulink and integrated over time considering all environmental disturbances acting on the spacecraft in order to obtain the attitude kinematic.

Several performance indices have been considered: First of all the ratio between the net velocity increment introduced perpendicularly to the required direction and the longitudinal one. Further indices are maximum values of angular rate, amplitude of attitude oscillations, manoeuvres duration etc..

During the transfer the spacecrafts centre of gravity is subject to shift within a band defined by the structure team. This is due to propellant consumption or any other undesired change in mass distribution. As the centre of gravity shifts away from the ideal position the thrusters arms are modified and slowly varying parasite torques appear.

The maximum value for shift has been considered in designing the system and the related torque introduced by main engines firing is by far the strongest disturbance acting on the spacecraft.

The main engines off-modulation is the only practical way of compensating it. It is important to notice that planning the thrusters off-time effectively change the disturbance torque acting on the spacecraft rather than compensating it with an additional torque, as is usually.

Since the centre of gravity position is required by the estimator to correctly propagate the attitude, an appropriate procedure has been designed to approximate it.

A key point is to understand whether the star tracker is able to supply measurements during the firing manoeuvres. In initial analyses it is assumed out

of work because of the system angular rates. Moreover the possibility of stopping the manoeuvres to quickly reset any estimation error is excluded. In this context analyses results pointed out that a second sensor is strongly recommended to reliably estimate the attitude. The second sensor shall be able to measure a vector in addition to the sun vector.

If no other sensor is admitted and the star tracker is out of work the attitude estimation will be affected by drift.

Diverse situations have been investigated and system performances have been evaluated against parameter variations.

In conclusions the requests, addressed to other subsystems, are exposed.

The simulation model is provided for those interested in exploring new situations and it is practically explained in the appendix.

Sommario

Il progetto di tesi ha l'obiettivo di analizzare le manovre orbitali che porteranno ESMO (European Student Moon Orbiter) dall'orbita di trasferimento geostazionaria (GTO) all'orbita operativa lunare. L'assetto del sistema è stato stimato e controllato durante tali fasi con l'obiettivo di individuare una configurazione di sensori attuatori e algoritmi in grado di affrontare le manovre richieste rispettando i requisiti.

La simulazione della dinamica del sistema ha permesso di evidenziare i punti deboli e di valutare l'importanza dei diversi parametri di progetto.

Gli attuatori a disposizione (ruote di reazione, razzetti a gas freddo, motori principali) sono stati confrontati così come i sensori (giroscopi, sensore di sole, sensore di stelle) per capire quale fosse la combinazione più affidabile in grado di adempiere la missione.

La stima dell'assetto è basata sull'utilizzo di un filtro di Kalman mentre il sistema di controllo in anello chiuso è stato progettato nel dominio di Laplace considerando i ritardi di linea e la presenza del circuito sample/hold.

La dinamica del sistema è stata quindi implementata in ambiente Simulink e integrata nel tempo considerando tutti i disturbi ambientali presenti, così da ricavare la cinematica d'assetto.

Sono stati considerati diversi indici di prestazione: primo fra tutti il rapporto tra l'incremento netto, finale di velocità in direzione transversa a quella di manovra (imposta nel riferimento inerziale) e quello in direzione longitudinale. Ulteriori indici di prestazione sono i valori massimi di velocità angolare, l'ampiezza delle oscillazioni dell'assetto, la durata delle manovre etc.

Durante la fase di trasferimento il centro di massa del sistema è soggetto ad una traslazione indefinita, i cui valori massimi sono stati fissati dal gruppo strutture; Tale spostamento è causato dal consumo di propellente o da indesiderate variazioni nella distribuzione di massa e, anche se piccolo, modifica le coppie introdotte dai motori principali. All'accensione del sistema propulsivo compare dunque una coppia di disturbo lentamente variabile nel tempo. Per garantire robustezza del progetto, il dimensionamento è stato effettuato considerando il più alto valore possibile di traslazione. La coppia parassita risultante è di gran lunga il disturbo più intenso agente sul sistema e l'unico modo per compensarlo è tramite off-modulation dei motori principali: l'impulso associato alla coppia di controllo è stato tradotto, ogni secondo in una sequenza di spegnimento dei propulsori. E' importante notare che questa strategia non introduce una coppia che si oppone all'azione del disturbo, come avviene in situazioni canoniche, ma di fatto, programmando la sequenza di spegnimento, si modifica la storia temporale del disturbo che risulta quindi accoppiato all'azione dei motori/attuatori.

Per quanto riguarda l'osservatore, dal momento che la propagazione dell'assetto necessita di una stima della posizione del centro di massa, è stata ideata una procedura ad hoc per ottenerne un'approssimazione.

Un punto chiave è capire se le misure del sensore di stelle siano disponibili durante la fase propulsa. In prima analisi esso è stato considerato non funzionante quando i propulsori sono accesi per via delle accelerazioni e velocità angolari risultanti. Inoltre si è esclusa la possibilità che ciascuna manovra possa essere più volte, ma brevemente, sospesa e subito ripresa, per azzerare in ogni intervallo l'errore accumulato nella stima d'assetto. In tal caso i risultati dell'analisi hanno mostrato come un secondo sensore sia fortemente raccomandato al fine di rendere l'osservatore affidabile. Tale sensore dovrebbe essere in grado di misurare un ulteriore vettore in aggiunta al vettore sole. In caso nessun'altro sensore sia ammesso allora la stima dell'assetto sarà soggetta a deriva. Diversi scenari sono stati esplorati e le prestazioni del sistema sono state studiate e correlate alla variazione dei parametri.

In conclusione sono raccolte le richieste agli altri sottosistemi derivanti dall'analisi.

Il modello realizzato per le simulazioni è disponibile per chi voglia analizzare una qualsiasi condizione di manovra e una sua pratica descrizione è fornita in appendice.

Chapter 1   Introduction

The guideline of the whole mission is to design a reliable machine able to achieve the mission objectives with respect to all given requirements.

Typical designing procedures have been revisited since components are usually selected to fulfil requirements; conversely ESMO philosophy imposes to use several either available or university made components to achieve objectives respecting requirements.

System dynamic has been implemented in Simulink and several analyses have been carried out to prove the system capability in obtaining the desired Δv with the required accuracy. The obtained results are important input to all the other subsystem. The whole project involves several aspects such as the system dynamic modelling, the estimator and compensator designs and tuning, the influence of all disturbances, sensors and actuators measurements error and saturation modelling, performances evaluation against parameters variation and finally verifications of results. Many problems arose while the model has been developed and ad hoc solutions has been arranged to optimize performances.

The attitude determination and control concern all the mission phases. Different ADCS modes are related to different mission phases. What follows refers only to the manoeuvre mode.

1.1   About the European Student Moon Orbiter (ESMO)

ESMO is an education satellite project of the ESA Education Office, and if successful will be the first ever student-built spacecraft to leave Earth orbit and achieve an orbit around another solar system body. This would be a remarkable achievement, and would allow a student mission to join a long list of previously successful government agency missions to the Moon such as Apollo, Luna, Clementine, Lunar Prospector, and more recently ESA's first lunar mission, SMART-1.

ESMO is built upon a solid foundation of experience and lessons learned gained on ESA's education satellite programme (the SSETI Express and YES2 missions), industry, and academia, in order to fulfill its educational and mission objectives. The success of small lunar missions such as Clementine (424 kg), Lunar Prospector (295 kg) and SMART-1, as well as recent studies by European industry/academia on deep space missions to asteroids (SIMONE), Mars (MicroMars, MMM) and the Moon utilizing micro- or mini-satellites with low-cost auxiliary payload opportunities, gives some confidence in the technical feasibility of the ESMO mission.

1.2   Mission objectives:

The objectives of the ESMO mission are:
1. Launch the first lunar spacecraft to be designed, built and operated
   by students across ESA Member and Cooperating States;
2. Place the spacecraft in a lunar orbit;
3. Acquire images of the Moon from a stable lunar orbit and transmit
   them back to Earth for education outreach purposes;
4. Perform experiments relevant to future human lunar missions.

1.3   Mission Description

ESMO will be launched as a secondary payload into a highly elliptical, low inclination Geostationary Transfer Orbit (GTO). From GTO, the small spacecraft would use its on-board chemical propulsion system for lunar transfer, lunar orbit insertion and orbit transfer to its final orbit around the Moon. A miniaturized payload would perform measurements during the lunar orbit phases over a period of a few months. The core payload is a Narrow Angle Camera for optical imaging of the lunar surface, principally for education outreach purposes. A secondary scientific payload being considered is a biology experiment to study the effects of trans-lunar space environment on bacterial growth. If the NASA American Student Moon Orbiter (ASMO) is in lunar orbit at the same time as the ESMO spacecraft, then joint operations are foreseen, for example through stereo imaging using cameras on both spacecraft and an inter-satellite Lunar Internet communication protocol demonstration.

1.4   Manoeuvres

The mission analysis team (University of Glasgow) has supplied information about the ESMO orbit and manoeuvres. In particular it has furnished the complete orbital state vector at the beginning of each manoeuvre and the required Δv. Below the spacecraft altitude and absolute required Δv are listed:

Tab 1.1 Impulsive trajectory manoeuvres, altitude and required Δv

	1	2	3	4	5	6	7
$h\ [km]$	545	815	$2.14e5$	$3.79e3$	$1.37e6$	$3.55e5$	$3.6e5$
$\Delta v\ [^m/_s]$	404	244	6.3	142	71	200	101

Chapter 2   Requirements and performance evaluation

2.1   Subsystem requirements

The following strict requirement will lead the whole development of the project:

The applied delta-v along the required direction shall be within ±1% of the demanded value with an error of ±1% transverse to the required direction (3σ).

The lower the spacecraft angular rate is kept the more likely the star camera is going to be operative.
Accurate analyses have to test the system capability to respect what above. New requirements will be derived and will flow down to all other subsystems.

2.2   System performances evaluation

System performances have been calculated projecting the firing axis (which is directed as –y in body frame) onto the inertial axes. The thrust component onto the required direction is named Δv_2. The transverse projection, i.e. the component onto the plane perpendicular to Δv_2, is named Δv_T. It is important to note that a Δv_T in a certain direction and time can be compensated by a Δv_T in the opposite direction in a different time.
In order to verify the requirement in section 2.1 the following criterion has been developed:
I, J, K, the versors of the inertial frame are considered. J is the direction along which the impulse is required. In order to calculate an expression for $err_\%$ the evolution in time of the firing axis $\Delta \underline{v}(t)$ is considered.
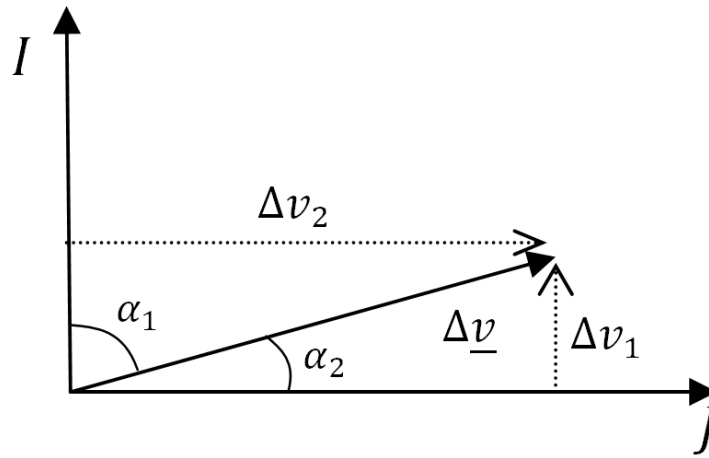
Fig 2.1 Actual velocity increment in the inertial frame, $I - J$ plane
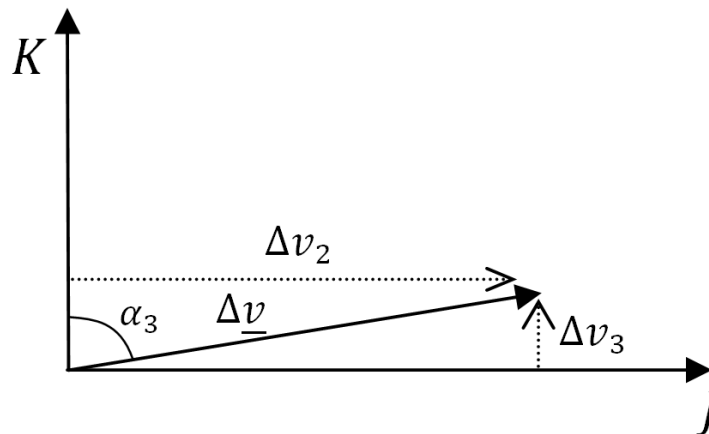
Fig 2.2 Actual velocity increment in the inertial frame, $K - J$ plane

Time dependence is not shown in the figures (to simplify the notation) but it is reported in the following relations

$$\Delta v_1(t) = \Delta v cos(\alpha_1(t)) = \Delta v c_1(t)$$
$$\Delta v_2(t) = \Delta v cos(\alpha_2(t)) = \Delta v c_2(t)$$
$$\Delta v_3(t) = \Delta v cos(\alpha_3(t)) = \Delta v c_3(t)$$

2.1

The effective applied $\Delta\bar{v}$ along the 3 inertial direction at time T is defined as the mean value of $\Delta v_i(t)$ on the period T[1]

$$\Delta\bar{v}_i(T) = \frac{1}{T}\int_0^T \Delta v_i(t)\,dt \qquad 2.2$$

Therefore the applied $\Delta\bar{v}_T$, transverse to the required direction (which means on the $K - I$ plane) is

$$\Delta\bar{v}_T(T) = \sqrt{\Delta\bar{v}_1^2(T) + \Delta\bar{v}_3^2(T)} \qquad 2.3$$

Remembering the requirement:
The error on the applied delta-v shall not exceed ±1% transverse to the required direction.
Hence,

$$err_{\%}(T) = 100\frac{\Delta\bar{v}_T(T)}{\Delta\bar{v}_2(T)} = \frac{100}{\int_0^T c_2(t)dt}\sqrt{\left(\int_0^T c_1(t)\,dt\right)^2 + \left(\int_0^T c_3(t)\,dt\right)^2} \qquad 2.4$$

This is a pessimistic evaluation because it assumes the thrusters force constant during the whole manoeuvre while it is function of the thrusters off times (which are averagely longer at the beginning of the manoeuvre where the thrust vector misalignment is more accentuated). Moreover the applied Δv is proportional to the spacecraft acceleration which is inversely proportional to the system mass. At the end of the manoeuvre mass is lower (because of propellant consumption) therefore the same thrust produces bigger Δv.
It will be shown in section 4.5 that the off modulation is the only practicable way to control the spacecraft. Since the thrusters off time is unknown previously to the manoeuvre, the applied Δv is calculated while the firing is performed:

$$\Delta v = \sum_j^N \frac{T'_{men}}{m}\left(4T_s - \sum_i^4 t_{off}^i\right)cos\alpha \qquad 2.5$$

Time dependence of the elements of eq. 2. 5 is not represented.
T'_{men} is the thrust provided by each thruster along the y body axis: 22cos (10°) [N].
α is the angle between $\Delta\underline{v}$ and J
T_s is the sampling time, t_{off}^i is the i-th thruster off time.

---

[1] A justification of the mean value is obtained thinking that different Δv in opposite directions (with respect to the average) compensate each other.

The manoeuvre is stopped as the estimated applied Δv reaches the desired value, therefore N is the number of seconds required to perform the manoeuvre.

Chapter 3   AOCS hardware

Components choice is a delicate issue since mission budget is limited. Therefore university made or spare components are preferred even if TRL level is surely lower.
A subsystem preliminary design brought up the following components selection: 1 Star tracker, 1 coarse sun sensor, three axes gyro, 3/4 reaction wheels, 4 pre-acceleration thrusters, 4 cold gas thrusters and 4 main engines.
During the manoeuvre the spacecraft angular rates are impulsively forced by the engines firing; it is important to understand whether the sensors capabilities are compromised.
Several aspects guide the choice of the actuators such as force/torque provided, precision, bandwidth. It will be shown that the most compelling constraint on the choice is the torque provided.

3.1 Actuators trade off

Different ways to control the spacecraft attitude are available: Main engines off-modulation, cold gas thrusters on-modulation, wheels. A preliminary design pointed out the wheels inability to supply enough torque.
A trade off between cold gases on modulation and main engines off modulation has been carried out. The first choice is the cold gases thrusters for two reasons: first they ensure finer control torque as they got an inferior nominal thrust, and second no power is subtracted from the main engines.

Unfortunately it will be shown that they cannot supply torque enough to compensate the parasite momentum introduced by the main engines firing.
Indeed they offer 0.2 N each and even assuming two thrusters firing in the same direction of the X-Z plane, the following maximum torque is introduced:

$$T_{CG}^{max} = 0.178 \, Nm$$

T_{CG}^{max} is obtained from the cross product between thrust and arm (assuming orthogonal vectors).
Although it is an overestimation of the effective available torque (remember that we need to cant the thrusters to obtain some torque out of the X-Z plane) it is much weaker than T_d, which is the biggest disturbance (defined in section 4.5).
Therefore the off modulation of the main engines resulted as the only solution rather than the best between several strategies. However an on modulation of the

cold gas thrusters is suitable if much stronger thrusters are employed and the arms length is increased.

Since the disturbance impulses vary with the commanded OFF-time, the OFF-modulation of the main engines not only introduces control torques to compensate some constant disturbances, but actually modifies the disturbance torques switching on and off the engines.

Moreover the prediction of the manoeuvre duration becomes more complex because it depends on the main engines off-time which is function of the centre of gravity (CoG) shift. It means that the performed Δv is calculated on board and as it reaches the required value the engines are cut off.

Stabilizing wheel

Some preliminary analyses demonstrated the stabilising effect of a fast spinning wheel on the firing axis. Further analysis, where the ON/OFF modulation of the thrusters was accounted, pointed out how the benefits were achievable merely with a continuous control. A justification to this fact could be related to the gyroscopic effect of the spinning wheel which corrupts control torques with any perpendicular component to the wheel rotation axis.

3.2 Sensors trade off

A key point is to understand whether the star tracker is able to supply reliable measurements during firing manoeuvres. Since no information is available diverse configurations have been investigated with or without the star camera measurements as the engines are switched on. Anyway, it is very important to contain the spacecraft angular rate while the main engines are firing to increase the chance for the star tracker of being operative.

Gyros and sun sensors are surely working during the manoeuvres but in case no other sensor is operative the longer the manoeuvre is the bigger the drift of the estimated attitude is (around the s/c to sun vector).

It will be shown how useful would be another sensor, able to measure a second vector during the manoeuvres. Its precision is not very important and its presence would avoid any gyro drift.

Chapter 4   Disturbances

4.1 Gravity Gradient

$$\underline{N}_{gg} = \frac{3k_t}{R^3}\begin{Bmatrix} (I_z - I_y)c_3 c_3 \\ (I_x - I_z)c_1 c_3 \\ (I_y - I_x)c_1 c_2 \end{Bmatrix} \tag{4.1}$$

Where $k_t = 3.98\ 10^{14}\frac{m^3}{s^2}$, $R = h + 6372 Km$ and $c_1 c_2 c_3$ are radial direction cosines on principal axes.

Gravity gradient torque is a quantifiable disturbance once attitude and moments of inertia are available.
In any case, considering the worst case and the lowest orbit, the gravity gradient induced torque respects the following (with a 20 % margin):

$$\left|\underline{N}_{gg}\right| < 2.7e - 5\ Nm \tag{4.2}$$

4.2 Drag induced torque

The lowest manoeuvre is performed at perigee (about 500 Km height). Just statistical data about atmosphere density are available:

$$\rho_{min}^{550} = 3.63\ e - 14;$$
$$\rho_{av}^{550} = 2.21\ e - 13;$$
$$\rho_{max}^{550} = 9.25\ e - 13;$$

A random number within the above boundaries has been assumed. The drag torque vector direction is randomly defined on a plane normal to the rolling axis. The torque magnitude is defined as follow:

$$\underline{N}_D = \frac{1}{2}\rho S C_D |v|\underline{v} \wedge \underline{b} \tag{4.3}$$

Where v is the s/c maximum velocity during the manoeuvre; S is the s/c front section normal to the y axis; C_D is the drag coefficient, conservatively assumed to be 2.3.
The arm length b has been guessed because centre of pressure(Cp) position is not yet defined. To be conservative the same thrusters arm has been hypothesized.

Therefore this disturbance torques cannot be exactly quantified. A maximum value has been defined (with a 20 % margin)

$$\left|\underline{N_D}\right| < 1.5e - 5 Nm \qquad\qquad 4.4$$

4.3 Magnetic Field

It is defined by the cross product between spacecraft residual dipole vector $\underline{m}$, usually unknown, and Earth magnetic field vector $\underline{B}$, usually known.

$$\underline{N_{MF}} = \underline{m} \wedge \underline{B} \qquad\qquad 4.5$$

even if an accurate model of the Earth magnetic field is available it will be hard to define $\underline{m}$.

Therefore the magnetic field disturbance torque has been estimated, accordingly to Wertz[2], as follow:

$$N_{MF} = mB \qquad\qquad 4.6$$

With $m = 1\, A \cdot m^2$ and $B = 2M/R^3$

$M = 7.96e15\, Tesla \cdot m^3$ and $R = (545 + 6371)\, Km$

Giving

$$\left|\underline{N_{MF}}\right| < 5.8e - 5 Nm \qquad\qquad 4.7$$

This approximation refers to the first manoeuvre because the lower the orbit is the stronger N_{MF} is.

4.4 Solar Pressure

Solar pressure has been neglected since its magnitude is two orders lower than other disturbances'.

---

[2] W . Larson, J. Wertz, *Space Mission Analysis And Design 3Rd Ed* , Academic Publishers Kluwer, 1999

4.5 Centre of gravity shift

It is the last to be described but the most important.

The thrust vector (22N for each thruster) is directed along the negative Y axis. The thrusters are located on the X-Z plane of the reference system (accurate within $5 \div 10\ cm$).

The 4 thrusters are arranged on the diagonals of that plane on a ring ($d = 340\ mm$) and numbered anticlockwise from thruster 1 viewed from above.
Thruster 1 (+X,+Y), Thruster 2 (+X,-Z), Thruster 3 (-X ,-Z), Thruster 4 (-X,+Z)
With zero cant angle, the thrusters forces are aligned with -Y. The cant angle is a rotation around Z applied positive to thrusters 3 and 4 and negative to thrusters 1 and 2.
The spacecraft centre of gravity initial position is $[0 - 445.5\ \ 0]\ mm$
The centre of gravity undesired shift is assumed not to exceed the following value $[37.7\ - 384.2\ - 68.7]\ \ mm$
The worst case (maximum shift) has been considered in the trade off.
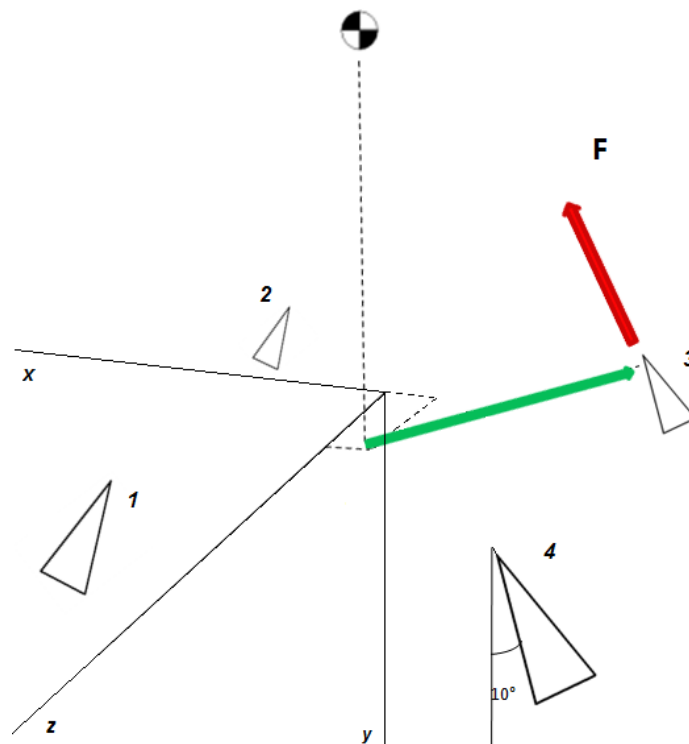
Fig 4.1 Thrusters configuration and numbering

Calculating the cross product between thrusters arms and forces the torque provided by each thruster firing is obtained:

Tab 4.1 Torques introduced by main engines firing when the CoG shift is maximum

	T_1 [Nm]	T_2 [Nm]	T_3 [Nm]	T_4 [Nm]
X	6.6972	-3.7204	-3.7204	6.6972
Y	-1.1809	0.6560	-0.6560	1.1809
Z	-2.9243	-2.9243	4.5579	4.5579

Each column refers to a thruster and each row is a different body axis.
It can be easily obtained the parasite torque introduced by all the engines firing:

$$\underline{T_d} = \begin{Bmatrix} 5.9538 \\ 0 \\ 3.2672 \end{Bmatrix} [Nm] \qquad 4.8$$

This torque vector is several orders larger than the others. The only way to compensate it is the off modulation of the main engines.

Chapter 5   System modelling

5.1   Dynamic model

System dynamic is described by Euler equation:

$$\underline{\underline{J}}\underline{\dot{\omega}} + \underline{\omega} \wedge \underline{\underline{J}}\underline{\omega} + \underline{\omega} \wedge \underline{\underline{A}}_w \underline{h}_w = \underline{T} + \underline{D} \qquad\qquad 5.1$$

$\underline{\omega}$ is the spacecraft angular rate

$\underline{\underline{J}}$ is a diagonal matrix with inertia momenta

$\underline{\underline{A}}_w$ is a matrix defining wheels orientation

$\underline{h}_w$ is the spacecraft angular rate

$\underline{T}$ are control torques

$\underline{D}$ are disturbance torques

Dynamic is integrated by Simulink using Heun method.
A fixed integration step has been chosen to simplify the PWM implementation.
Indeed the torques profile is planned at the beginning of each sample (in order to deliver the desired impulse for that sample) and more problems would have arisen if a varying step had been applied.

5.2   Kinematics

The body axes orientation is described by quaternions. At the simulation starting epoch the three references (body, orbital, inertial) are assumed to be coincident with no loss of generality. Knowing the control torques acting on the spacecraft and introducing every determinant environmental disturbance (exactly, where known, or randomly within maximum and minimum value where unknown) attitude is propagated as follow:

$$\dot{\vec{q}} = \frac{1}{2}\Omega\vec{q} \qquad \text{with } \Omega = \begin{bmatrix} 0 & \omega_3 & -\omega_2 & \omega_1 \\ -\omega_3 & 0 & \omega_1 & \omega_2 \\ \omega_2 & -\omega_1 & 0 & \omega_3 \\ -\omega_1 & -\omega_2 & -\omega_3 & 0 \end{bmatrix} \qquad 5.2$$

Therefore

$$\vec{q}_{k+1} = \vec{q}_k + \dot{\vec{q}}_k \Delta t \qquad\qquad 5.3$$

5.3 Delay

Line delays have been considered. They are defined as the time required to the signal to go from an hardware device to another.
700 ms of global line delay is considered:
The effects of delay in closed-loop feedback systems resemble the effects of lowering the sampling frequency.
The biggest obstacle to handling delay in design lies in the fact that the delay cannot be exactly expressed as a rational polynomial. Fortunately there are some approximations that have rational polynomial form:

$$e^{-sT_d} \cong \frac{1}{\left[1 + \frac{sT_d}{n}\right]^n} \qquad 5.4$$

$$e^{-sT_d} = \frac{1 - k_1 s + k_2 s^2 + \cdots \pm k_n s^n}{1 + k_1 s + k_2 s^2 + \cdots + k_n s^n} \qquad 5.5$$

Their accuracy raises as n is increased.
The second one is the Pade approximation and is based on a minimization of the truncation errors in a finite series expansion of e^{-sT_d}. The approximation order is n. k_i are function of n.

The polynomials above should track (in both magnitude an phase) the Bode plot of e^{-st} over the range of frequencies corresponding to the bandwidth of the designed system.
It will be shown in Chapter 6 that the system bandwidth is similar for all the 3 axes (remember that the bandwidth is the set of frequencies where the magnitude of the closed loop transfer function is bigger than -3dB):

$$bandwidth \cong [0 \quad 10^{-0.25}] \ rad/s$$

Therefore the goodness of diverse orders polynomial approximation has been investigated over that frequencies band:
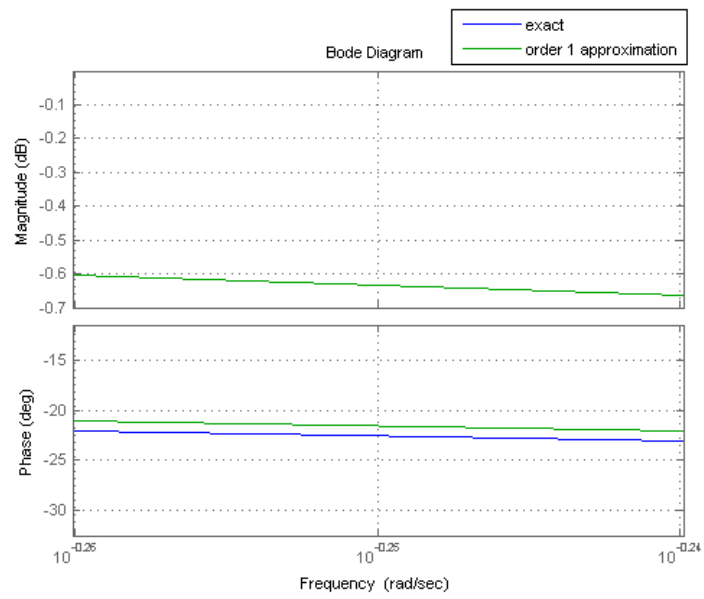
Fig 5.1 Line delay 1°order approximation versus exact bode diagram
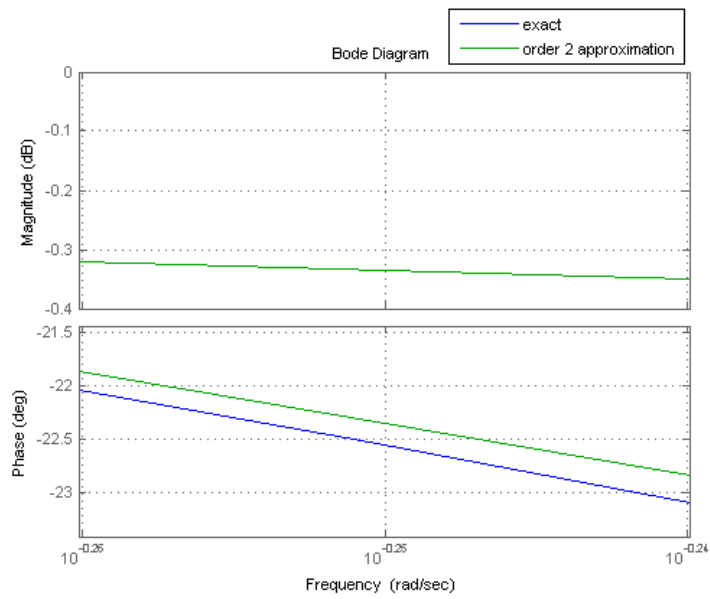
Fig 5.2 Line delay 2°order approximation versus exact bode diagram
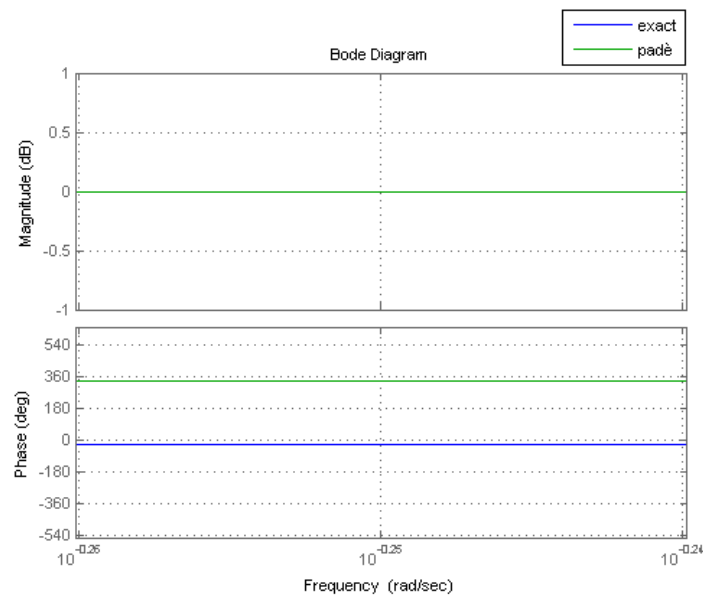
Fig 5.3 Line delay 2°order Pade approximation versus exact bode diagram

The second order approximation is acceptable and the maximum error (at the upper edge of the bandwidth) on magnitude and phase is -0.32dB and 0.2 deg respectively. A second order Pade approximation does better: no error on magnitude and -0.04deg on phase

In order to verify the validity of the approximations the exact closed-loop step response is drawn. The step response refers to the following transfer function between y_{ref} e y

$$F(s) = \frac{C(s)G(s)E(s)}{1 + C(s)G(s)E(s)} \qquad 5.6$$

Where E(s) is represented in 3 different ways:
By the 2 approximations described earlier and by the exact expression ($E(s) = e^{-sT_d}$). In this case the 'exact' step response is obtained using the Matlab function "Feedback" which requires a state space representation of the system.
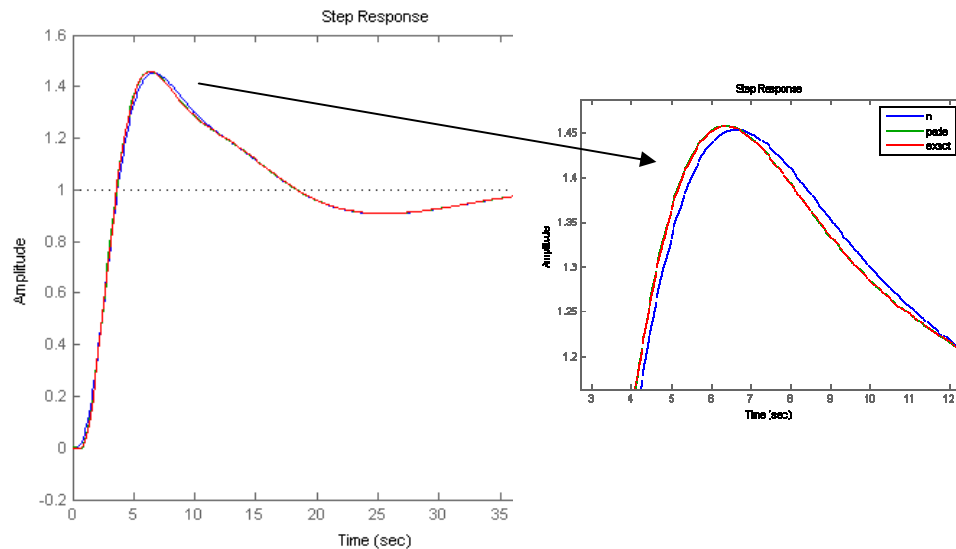
Fig 5.4 Step responses for the 3 different expressions of delay

Looking to the graph it is clear that using the pade approximation the system response is closer to the exact solution.

Second order approximations have been used for the comparison but higher orders offer the same conclusions.

5.4   Sample and hold

The sampler and the zero-order hold circuit have the net effect of adding some delay to the open-loop transfer function of the feedback system, which has to be taken into consideration when designing with continuous control analysis techniques. The Laplace transform of the sample and hold circuit is

$$\frac{1 - e^{-sT_{SH}}}{sT_{SH}} \qquad 5.7$$

As well as line delay the sample and hold transfer function has been approximated using a second order pade polynomial.

It is important to distinguish the simulation integration step from the real system sampling rate. The first one is 0.1 s while the second is 1s.

5.5 Actuators

Once torque request is defined it needs to be converted into thrusters off time. A Pulse Width Modulation (PWM) strategy is adopted:
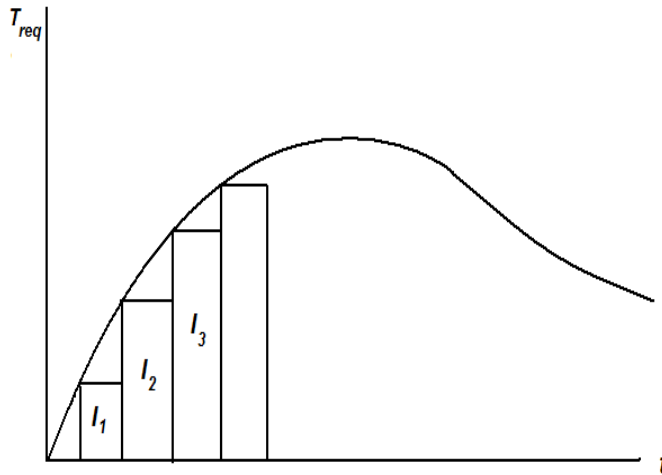
Fig 5.5 PWM strategy

The required torque is sampled at 1Hz and the desired control impulse is calculated

$$\underline{I}_{req} = \underline{T}_{req} t_s \qquad\qquad 5.8$$

The torques introduced by each thruster firing has been calculated before, when the effects of the centre of gravity shift have been analyzed.
The required impulse is converted to axis off time (a_{OFF}) by the following relation:

$$\underline{a}_{OFF} = \frac{\underline{I}_{req}}{\underline{T}_{PWM}} \qquad\qquad 5.9$$

The division above is element by element.
$\underline{T}_{PWM}$ is the maximum torque available on each axis (The torques introduced by each thruster firing has been calculated before, when the effects of the centre of gravity shift have been analyzed)

$$T_{PWM}(1) = T_{1x} + T_{4x}$$
$$T_{PWM}(2) = T_{2y} + T_{4y} \qquad\qquad 5.10$$
$$T_{PWM}(3) = T_{3z} + T_{4z}$$

As the CoG position is estimated previously to the manoeuvre it is spontaneous to think about correcting the vector above with the contributions due to the CoG shift. Simulations results pointed out that better performances of the compensator are obtained assuming a symmetric configuration for the main engines.

t_{OFF} is related to a_{OFF} trough the following matrix

$$\underline{a}_{OFF} = \begin{bmatrix} -0.5 & 0.5 & 0.5 & -0.5 \\ 0.5 & -0.5 & 0.5 & -0.5 \\ 0.5 & 0.5 & -0.5 & -0.5 \end{bmatrix} \underline{t}_{OFF} \qquad 5.11$$

This is an underdetermined system.

Summing rows 1 and 2 , 2 and 3, 1 and 3 gives

$$t_{OFF}(3) = t_{OFF}(4) + a_{OFF}(1) + a_{OFF}(2)$$
$$t_{OFF}(1) = t_{OFF}(4) + a_{OFF}(2) + a_{OFF}(3) \qquad 5.12$$
$$t_{OFF}(2) = t_{OFF}(4) + a_{OFF}(1) + a_{OFF}(3)$$

Since an off modulation strategy has been chosen, during the manoeuvres all the main engines fire together and the control system properly stops them to introduce the required impulse.

The global t_{OFF} should be minimized not to deprive the manoeuvre of thrust.

The indeterminateness on one component of $\underline{t}_{OFF}$ is exploited to guarantee that at least one component of $\underline{t}_{OFF}$ is zero.

$$t_{OFF}(4) = \max \begin{pmatrix} -(a_{OFF}(1) + a_{OFF}(2)) \\ -(a_{OFF}(2) + a_{OFF}(3)) \\ -(a_{OFF}(1) + a_{OFF}(3)) \\ 0 \end{pmatrix} \qquad 5.13$$

The main engines off time is introduced at the beginning of each sample.

If any component of $\underline{t}_{OFF}$ is bigger than t_s all the vector is multiplied by $t_s / \max(\underline{t}_{OFF})$.

The thrusters have a minimum on time (MOT) , derived from the minimum impulse bit that the thruster is rated to provide. When the impulse demand equals the minimum impulse bit, the thruster can be fired. However, the actuation of the thruster is governed by a linearization factor, $\Gamma = 0.65$, derived from a describing function analysis to allow the PWM to be treated as a linear function.
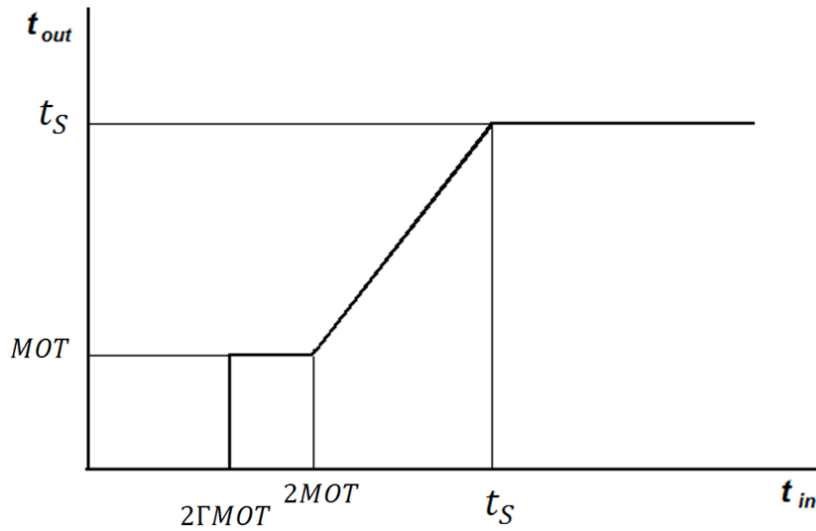
Fig 5.6 Thrusters off time conditioning

5.5.1   Torque modulation to introduce the exact impulse

Any required off time bigger than 2MOT has a temporal resolution of 1 millisecond. Therefore exact modeling of main engines (MEN) behavior requires a simulation time step of 1 ms, which is not suitable for long manoeuvres (1500s would become 1,5 millions of steps).

Another solution is to keep 100 ms as simulation time step and to modify the torques magnitude to introduce the desired impulse.

$$\underline{\tilde{T}} = \frac{\underline{T} t_{off}}{n t_S} \qquad\qquad 5.14$$

Where n is the positive integer which minimizes $\left| n t_S - t_{off} \right|$.

This is another approximation which requires to be tested by comparison with a 1 ms system on a limited time interval.

5.6   Sensors

The dynamic Euler equations described in section 5.1 are assumed to exactly represent the system dynamic. So given the initial condition on attitude the attitude kinematic is easily calculated. This means the exact solution is available to be compared with the approximated one (the one which is estimated on board). In other words the exact data have been corrupted with several noise sources to model the real components behaviour. The on board software will

struggle with corrupted data to obtain the best estimate of the state vector (using a Kalman filter).

5.6.1   Gyro

To model gyro behaviour several error sources have been considered.
This model simulates the behaviour of a single attitude rate channel. The behaviour is the same for all three axes.
Most of the parameters used in this model are measured during calibration. Values that can be used in place of these measurements are summarized in Table 5.1.

Tab 5.1 Gyro error sources

Parameter	Value
Noise, σ_{noise}	0.02 deg/sec/ $\sqrt{Hz}$
Bias stability, σ_{bias}	20 deg/hour over 1 hour
Nominal bias	0.5 deg/sec
Bias error	0.15 deg/sec

Noise

White Gaussian noise values are generated at a frequency of 10Hz, the frequency at which the sensor head is sampled. The RMS raw noise is 1.0 and the PSD is constant within 10Hz (Gaussian white noise). This noise is scaled by the gain K1, which is defined below. The parameter σ_{noise} is the noise characteristic for this channel. This value will be no greater than $0.02 \; deg/sec/ \sqrt{Hz}$ and will be specified for each channel with the module test. The scaled noise is added to the truth inertial rate about the measurement axis.

$$K1 = \sigma_{noise} \sqrt{8}$$

Bias stability

White Gaussian noise values are generated at a frequency of 10Hz, the frequency at which the sensor head is sampled. The RMS raw noise is 1.0 and the PSD is shown below. This noise is scaled by the gain K2, which is defined below. The parameter σ_{bias} is the bias stability characteristic for this channel.

This value will be no greater than 20deg/hour and will be specified for each channel with the module test.

$$K2 = \frac{\sigma_{bias} \sqrt{8}}{2160000}$$

The scaled white noise is integrated in a discrete time manner at 10Hz to give the bias stability.

The bias stability is added to the truth inertial rate about the measurement axis.

Nominal Bias

The nominal bias is a constant bias that will be no greater than 0.5deg/sec and will be specified for each channel with the module test. This is added to the truth inertial rate about the measurement axis.

Bias Error

The bias error represents unknown variations in the bias due to environmental effects and bias repeatability. These bias errors are expected to be less than 0.15deg/sec, excluding bias drift at switch on. This is added to the truth inertial rate about the measurement axis.

5.6.2 Sun coarse sensor

The sun coarse sensor is able to measure one vector, the sun versor in body frame $\underline{\tilde{v}}_s^b$.

$\underline{v}_s^i$ is the sun versor in the inertial frame

$$\underline{v}_s^b = \underline{\underline{A}}_{i2b} \underline{v}_s^i \qquad\qquad 5.15$$

A_{i2b} is obviously the rotation matrix between the two frames.
The exact versor $(\underline{v}_s^b)$ is corrupted accordingly to the sensor accuracy :
A random unit vector $\underline{r}$ normal to v_s^b and a random angle α_r with the sensor accuracy as standard deviation have been generated.
$\underline{r}$ and α_r represent Euler axis and angle respectively.
The corrupted sun versor $\underline{\tilde{v}}_s^b$ has then been obtained:

$$\underline{\tilde{v}}_s^b = \underline{\underline{A}}_{err} \ \underline{v}_s^b \qquad\qquad 5.16$$

With

$$\underline{\underline{A}}_{err} = \begin{bmatrix} c_\alpha + e_1^2(1 - c_\alpha) & e_1 e_2(1 - c_\alpha) + e_3 s_\alpha & e_1 e_3(1 - c_\alpha) - e_2 s_\alpha \\ e_1 e_2(1 - c_\alpha) - e_3 s_\alpha & c_\alpha + e_2^2(1 - c_\alpha) & e_3 e_2(1 - c_\alpha) + e_1 s_\alpha \\ e_1 e_3(1 - c_\alpha) + e_2 s_\alpha & e_3 e_2(1 - c_\alpha) - e_1 s_\alpha & c_\alpha + e_3^2(1 - c_\alpha) \end{bmatrix}$$

α_r has a 0 zero mean and a standard deviation of $0.3°$
The sun vector is assumed constant in the inertial frame with no loss of generality.

5.7   Data uncertainty

The analyses require many data related to the spacecraft and its components which are not exactly defined yet, or which are not exactly known even during the mission, for example change in spin rate resulting from the conservation of angular momentum as propellant flows from storage tanks to thrusters has not been considered. The change in center of mass and moments of inertia as propellant is consumed can be easily estimated given the geometry of the tanks and the propellant flow rate but the uncertainty in the distribution of the propellant within the tanks remains.

Errors on the knowledge of the moments of inertia have been voluntarily introduced, it means that the 3 values used in the dynamic model are different from those used for attitude propagation and for the estimation of the CoG position.

Gyros bias is estimated previously to the manoeuvres. The analyses evaluated the estimation error.

It will be shown that such errors, especially on the inertial data, seriously affect the centre of gravity position estimation. Therefore a precise evaluation of the moments of inertia is required and a correlation with the CoG position is required to the structure team.

No errors on the initial attitude and rate have been assumed because as long as MEN are off the attitude and the angular rate estimation is based on accurate measurements and the wheels offer fine control torques. Any small initial error is negligible compared to the attitude displacement suddenly introduced as engines are fired.
Errors on sensors measurements have been described in previous chapters.

5.8 Initial condition

As initial condition the body, the orbital and the inertial frame are assumed to be coincident. Particularly the y body axis is assumed coincident with the orbital rolling axis and with the inertial -J axis.
Initial error on attitude estimation is zero.
Initial torque request is zero.

5.9 Integration scheme

Algorithm and time step choice has to guarantee accuracy in integrating the model while integration time is kept within reasonable limits.
Heun method has been chosen. Its equations are presented later. Time step is 0.1s

5.10 Implementation

The equations presented in this project have been implemented in Simulink. Required data are loaded using a Matlab m-file. Other m-files have been used to evaluate system performances from the data acquired with the analyses.

Chapter 6　Compensator design

An uncoupled control strategy is adopted. Single axis linear dynamic is considered to design the compensator:

$$J\underline{\dot{\omega}} = \underline{T_C} \tag{6.1}$$

then non-linear terms are algebraically added to the required torque to obtain the effective required torque:

$$\underline{T} = \underline{T_C} + \underline{\omega} \wedge J\underline{\omega} + \underline{\omega} \wedge \underline{A_w}\underline{h_w} \tag{6.2}$$

A double phase lead controller has been chosen to improve the system's phase margin.

$$C(s) = K\frac{(1 + \alpha\tau s)^2}{(1 + \tau s)^2} \tag{6.3}$$

Improvements in phase margin are accompanied by improvements in bandwidth.

Parameters definition

$$\alpha = \frac{1 + \sin\left(\tilde{\Phi}/2\right)}{1 - \sin\left(\tilde{\Phi}/2\right)} \tag{6.4}$$

$$\omega = \sqrt{\frac{K\alpha^{\frac{3}{2}}}{J}} \tag{6.5}$$

$$\tau = \frac{1}{\omega\alpha^{\frac{1}{4}}} \tag{6.6}$$

Where $\tilde{\Phi} = \Phi + \pi\omega_c T_d$ with ω_c and T_d cross-over frequency and line delay respectively. $\tilde{\Phi}$ is used in place of Φ (required phase margin) to compensate the delay presence.
Phase lead has been selected because it was successfully employed in previous mission and because the LQR (Linear Quadratic Regulator) requires more computational efforts and has a lower TRL.

In order to project a reliable system, which is robust against parameters uncertainty the following constraints are imposed on phase and gain margin:
Phase margin shall be bigger than 30 deg.
Gain margin shall be within 2 and 2.5 (6÷8 dB)

6.1 Domain

At first sight the z domain appears to better fit the problem background. This is because the stability problems are clearly related to the control frequency, therefore to the discrete world.
As far as line delays and the sample and hold device are not encountered stability is guaranteed with the compensator preliminary design.
Introducing lag in the loop it's an easy operation until the delay is a sample time multiple. Being the line lag approximately 0.7 s it was decided to operate the analysis in the s domain.

6.2 Cross-over frequency

Since the samples frequency is 1 Hz for both the control torques and the measurements rate, the Nyquist theorem imposes a limit on the open loop bandwidth: 0.5 Hz.
Moreover the sampling rate should be 5÷20 times the crossover frequency (ω_C), therefore a maximum frequency of 0.2 Hz has been imposed.
Note that as ω_C increases towards 0.2 the control system loses smoothness.

6.3 Disturbance torque rejection

A disturbance is considered on the forward path
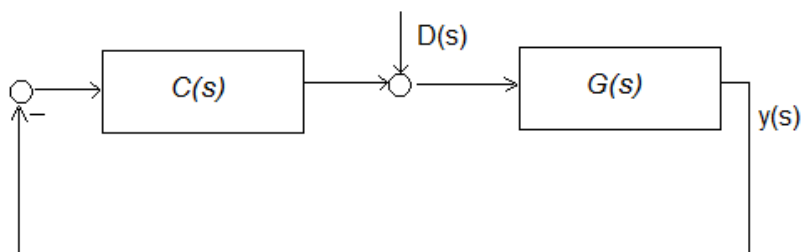
Fig 6.1 System loop, disturbance action

The closed loop transfer function between a disturbance torque T(s) and the controlled variables (for an input of zero) is

$$\frac{Y(s)}{D(s)} = \frac{G(s)}{1 + C(s)G(s)} \qquad\qquad 6.7$$

Where $G(s) = \dfrac{1}{Js^2}$

Considering the step function $\frac{A}{s}$ as disturbance, and applying the final value theorem the steady state error is obtained

$$\vartheta_{err}^{ss} = lim_{s \to 0} \ s \ \frac{G(s)}{1 + C(s)G(s)} \ \frac{A}{s}$$

$$= lim_{s \to 0} \ \frac{1/Js^2}{1 + C(s)/Js^2} \ A \qquad\qquad 6.8$$

$$= lim_{s \to 0} \ \frac{1}{Js^2 + C(s)} \ A$$

Since $lim_{s \to 0} C(s) = K$

$$\vartheta_{err}^{ss} = \frac{A}{K} \qquad\qquad 6.9$$

Considering the disturbance torques introduced by the thrusters

$$T_{CG} = \begin{Bmatrix} 5.9538 \\ 0 \\ 3.2672 \end{Bmatrix} \ [Nm]$$

The related steady state angular error is huge.
Raising the compensator gain helps to low the steady state error, but unfortunately it cannot be raised without lowering the close loop phase and gain margin.

6.4 Integrator

The steady state error can be eliminated by the action of an integrator which is placed in parallel to the compensator.
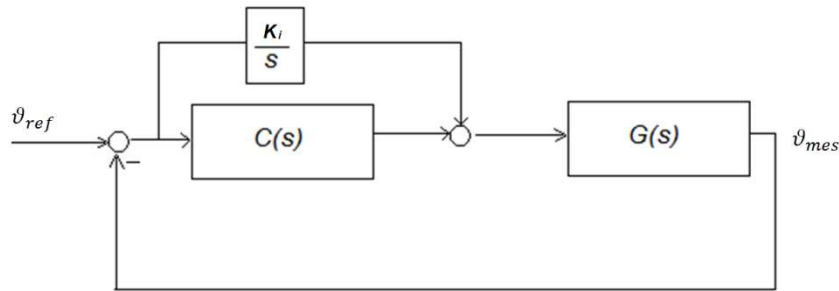
Fig 6.2 System block diagram, with integrator

Even the integrator gain cannot be raised much for the same reasons exposed earlier.

Note that the delay and the sampler are not sketched in Fig.6.2 not to crowd the illustration but they should be represented by blocks on the forward path and they have been considered in the designing phase.

$\tilde{C}(s) = C(s) + \frac{k_i}{s}$ is the updated compensator block.

Fine tuning of the double phase lead parameters has been performed following these rules:

- Raise compensators gain.
- Ensure the required phase and gain margins.
- Adjust phase peak at magnitude crossover.
- Keep the crossover frequency within the required band

The table below shows all the definitive parameters:

Tab 6.1 Compensator parameters

	ω_C [Hz]	K [Nm/rad]	K_i [Nm/rad/s]	α	τ [s]
X	0.1261	1.55	0.2	3.3276	1.3243
Y	0.1256	0.9	0.1	3.3276	1.3439
Z	0.1265	1.47	0.19	3.3276	1.3069

A bode diagram of the open loop transfer function $\tilde{C}(s)G(s)$ has been drawn for each axis.
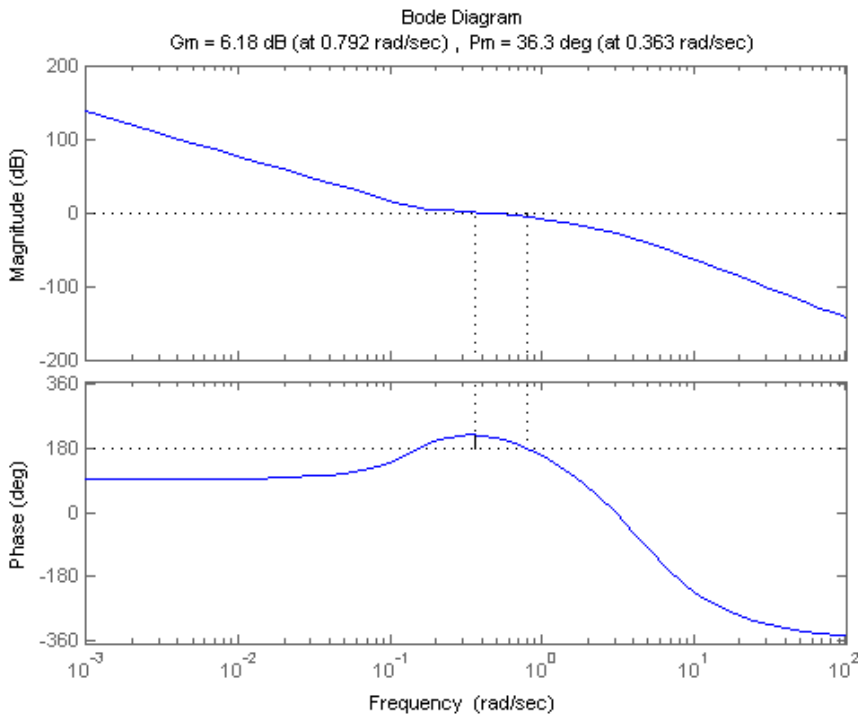
Fig 6.3 Open loop Bode diagram. X axis
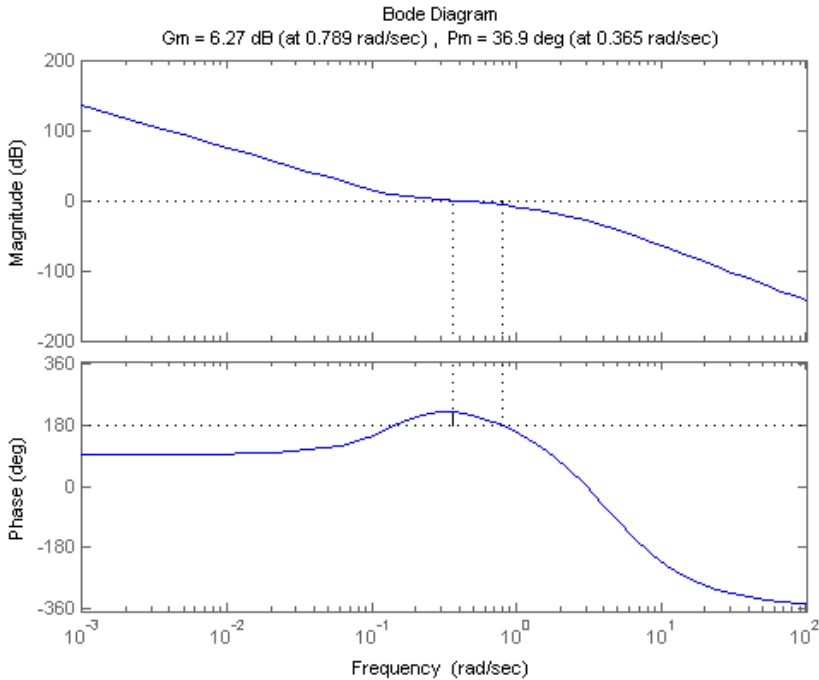
Fig 6.4 Open loop Bode diagram. Y axis
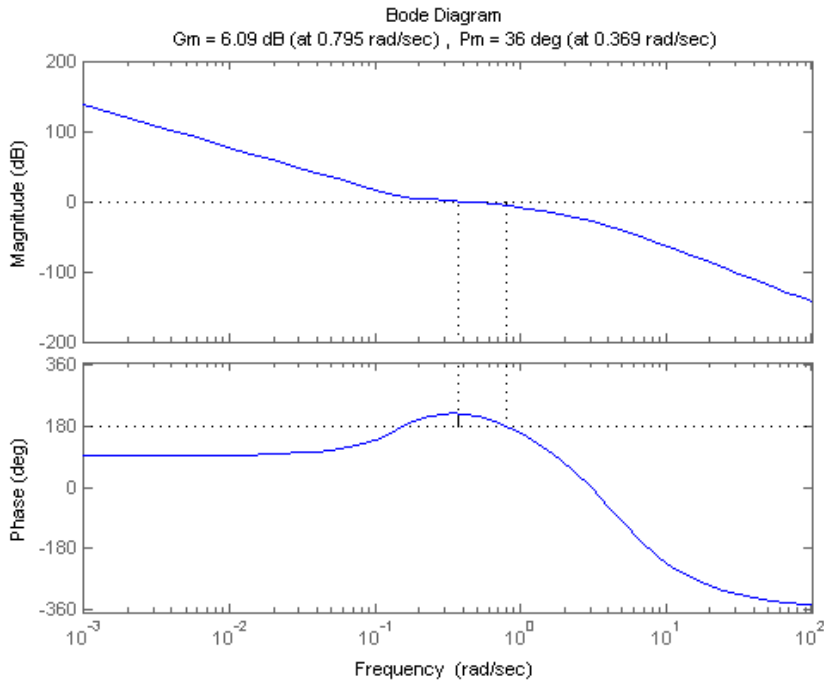
Fig 6.5 Open loop Bode diagram. Z axis

The peak on phase diagram at the module cross over is due to the benefic action of the double phase lead compensator.

6.5 Angle error to torque request

Attitude is defined using quaternions.

Since quaternion math doesn't allow additional algebra it is useful to rapidly explain how to treat successive rotations ($\vec{p}$ and $\vec{q}$ in this case):

$$T(\vec{p})T(\vec{q}) \ = \ T(\vec{p} \otimes \vec{q}) \qquad\qquad 6.10$$

Where $T(\vec{p})$ and $T(\vec{q})$ are rotation matrices associated with the quaternions $\vec{p}$ and $\vec{q}$

$$\vec{p} \otimes \vec{q} = \begin{bmatrix} p_4 & p_3 & -p_2 & p_1 \\ -p_3 & p_4 & p_1 & p_2 \\ p_2 & -p_1 & p_4 & p_3 \\ -p_1 & -p_2 & -p_3 & p_4 \end{bmatrix} \begin{bmatrix} q_1 \\ q_2 \\ q_3 \\ q_4 \end{bmatrix}$$

It is possible to define an error quaternion ($\delta\vec{q}$) which defines the rotation from the estimated to the target attitude[3].

$$\vec{q}_T = \delta\vec{q} \otimes \vec{q}_{est}$$
<div align="right">6.11</div>

$$\delta\vec{q} = \vec{q}_T \otimes \vec{q}_{est}^*$$
<div align="right">6.12</div>

where * defines conjugate quaternion

$$\vec{q}^* = [\ q_1 \quad q_2 \quad q_3 \quad -q_4]^T$$
<div align="right">6.13</div>

As the compensator inputs are angular errors, a quaternion-angles relation has been defined

$$\alpha_x = -2\ q_1$$
$$\alpha_y = -2\ q_2$$
$$\alpha_z = -2\ q_3$$
<div align="right">6.14</div>

Which is defined with small angles but it is proven to work even with big rotation.

6.5.1   Implementation

Since the analysis is performed in time and the compensator equation lives in the s-domain, a transformation is required to obtain the torque request in time. The conversion travels throw the z-domain to eventually reach the time domain.

$$\frac{T(s)}{\vartheta(s)} = K\frac{(1 + \alpha\tau s)^2}{(1 + \tau s)^2}$$
<div align="right">6.15</div>

$$T(s)(1 + \tau^2 s^2 + 2\tau s) - K(1 + \alpha^2\tau^2 s^2 + 2\alpha\tau s)\vartheta(s) = 0$$
<div align="right">6.16</div>

Compensator transfer function lives in the s-domain. It is converted to the z-domain using a bilinear transform (also known as Tustin method)

---

[3] The estimated attitude is the approximation of the actual attitude. Next Chapters will describe the estimation process. The target attitude is defined by the firing axis laying on the required inertial direction. The rotation around that vector shall ensure some conditions such as sun in the sun sensor field of view.

$$s \rightarrow \frac{2}{T_s} \frac{z-1}{z+1} \qquad \text{6.17}$$

It is obtained:

$$T(z)\left(1 + 4\frac{\tau^2}{T_s^2}\frac{(z-1)^2}{(z+1)^2} + 4\frac{\tau}{T_s}\frac{z-1}{z+1}\right) +$$

$$\left(1 + 4\alpha^2\frac{\tau^2}{T_s^2}\frac{(z-1)^2}{(z+1)^2} + 4\alpha\frac{\tau}{T_s}\frac{z-1}{z+1}\right)\vartheta(s) = 0 \qquad \text{6.18}$$

T_s is the simulation time step.
Now Dividing by z^2 and remembering that z^{-n} represents a n steps delay, the following expression, for the required torque at step k, is obtained:

$$\boldsymbol{T_k} = (T_s^2 + 4\tau^2 + 4\tau T_s)^{-1}[K(T_s^2 + 4\alpha^2\tau^2 - 4\alpha\tau T_s)\boldsymbol{\vartheta_{k-2}} +$$

$$K(2T_s^2 - 8\alpha^2\tau^2)\boldsymbol{\vartheta_{k-1}} + K(T_s^2 + 4\alpha^2\tau^2 + 4\alpha\tau T_s)\boldsymbol{\vartheta_k} - (T_s^2 + 4\tau^2 - \qquad \text{6.19}$$

$$4\tau T_s)\boldsymbol{T_{k-2}} - (2T_s^2 - 8\tau^2)\boldsymbol{T_{k-1}}]$$

Defining

$$a_0 = (T_s^2 + 4\tau^2 + 4\tau T_s)^{-1} K(T_s^2 + 4\alpha^2\tau^2 - 4\alpha\tau T_s)$$

$$a_1 = (T_s^2 + 4\tau^2 + 4\tau T_s)^{-1} K(2T_s^2 - 8\alpha^2\tau^2)$$

$$a_2 = (T_s^2 + 4\tau^2 + 4\tau T_s)^{-1} K(T_s^2 + 4\alpha^2\tau^2 + 4\alpha\tau T_s) \qquad \text{6.20}$$

$$b_0 = (T_s^2 + 4\tau^2 + 4\tau T_s)^{-1} (T_s^2 + 4\tau^2 - 4\tau T_s)$$

$$b_1 = (T_s^2 + 4\tau^2 + 4\tau T_s)^{-1} (2T_s^2 - 8\tau^2)$$

Therefore

$$\boldsymbol{T_k} = a_0\boldsymbol{\vartheta_{k-2}} + a_1\boldsymbol{\vartheta_{k-1}} + a_2\boldsymbol{\vartheta_k} - b_0\boldsymbol{T_{k-2}} - b_1\boldsymbol{T_{k-1}} \qquad \text{6.21}$$

the required torque is expressed by a combination of the current error angle and previous torque demands and angle errors.
This scheme is suitable to be implemented on the on board computer.

Chapter 7   Model verification

A verification of delay modeling has been presented in section 5.3.
Now the system model is verified without any line delay and without the integrator action. The verification is carried out examining the system settling time (the time taken for the response to settle following a step demand).
The settling time can be estimated in a second order approximation. Starting from the compensator transfer function:

$$\frac{\ddot{\vartheta}}{\vartheta} = -K_x \frac{(1 + \alpha\tau s)^2}{(1 + \tau s)^2} \qquad 7.1$$

And remembering that a time derivation becomes a multiplication by s in the Laplace domain, it is obtained (neglecting the third and fourth derivative):

$$(1 + K_x \alpha^2 \tau^2)\ddot{\vartheta} + 2K_x \alpha\tau\dot{\vartheta} + K_x\vartheta = 0 \qquad 7.2$$

$$\ddot{\vartheta} + \frac{2K_x \alpha\tau}{1 + K_x \alpha^2 \tau^2}\dot{\vartheta} + \frac{K_x}{1 + K_x \alpha^2 \tau^2}\vartheta = 0 \qquad 7.3$$

This equation will produce under-damped oscillations as long as

$$\left(\frac{2K_x \alpha\tau}{1 + K_x \alpha^2 \tau^2}\right)^2 < \frac{K_x}{1 + K_x \alpha^2 \tau^2} \qquad 7.4$$

Remembering the generic equation related to second order systems

$$s^2 + 2\xi\omega s + \omega^2 = 0 \qquad 7.5$$

and the definition of settling time ST

$$ST \approx \frac{4.6}{\xi\omega} \qquad 7.6$$

Remember that the settling time is the time elapsed from the application of an ideal instantaneous step input to the time at which the output has entered and remained within a $\pm 1\%$ band symmetrical about the final value.
Therefore the second-order approximations gives:

Tab 7.1 Theoretical settling times to step command

axis	ST [s]
X	20.94
Y	21.72
Z	20.72

These theoretical results have been compared with the settling time of the system response to a step command. The following close loop transfer function has been considered:

$$\frac{Y(s)}{Y_0(s)} = \frac{C(s)G(s)}{1 + C(s)G(s)}$$

7.7

remember that line delays, s/h and the integration action are not considered.
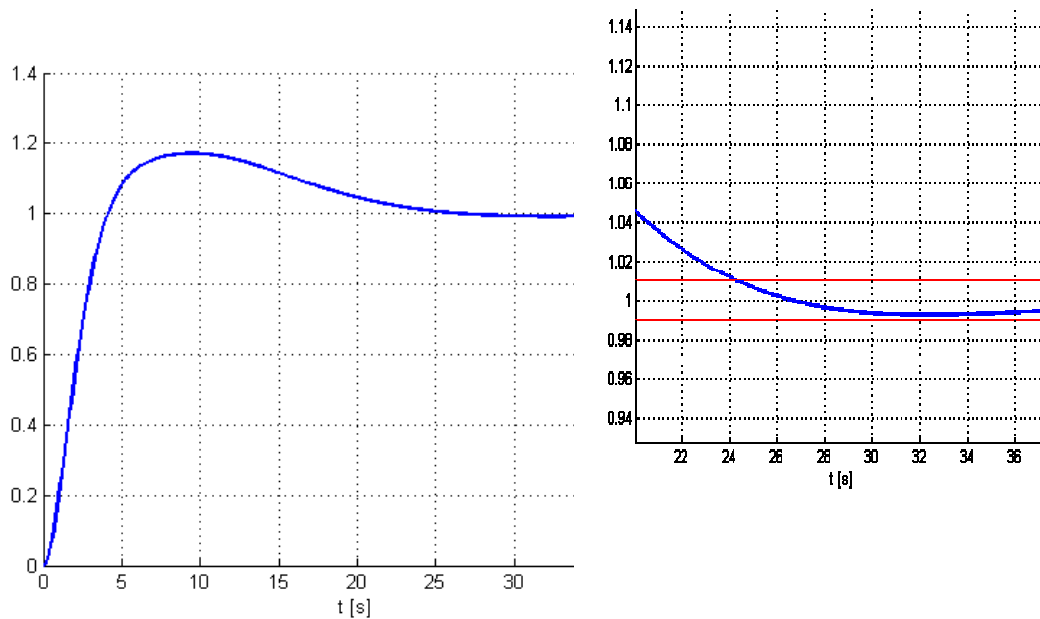
Fig 7.1 X axis settling time to step command

Small disagreements are due to the fact that third and fourth derivative have been discarded in defining the theoretical settling time.
Accordance is found on the y and z axes as well.

Chapter 8   System performances

In order to evaluate system performances the whole system is considered.
The whole adjective includes integrators, line delay end the fact that system is digital.
System readiness is evaluated watching the closed loop transfer function

$$\frac{Y(s)}{Y_0(s)} = \frac{\tilde{C}(s)G(s)\tilde{E}(s)}{1 + \tilde{C}(s)\tilde{E}(s)}$$

8.1

Where $\tilde{E}(s)$ is the Pade approximation of line delay and sample and hold continuous function $\left(e^{-sT_d}, \frac{1-e^{-sT_s}}{sT_s}\right)$.

System responses to step commands $\left(Y_0(s) = \frac{1}{s}\right)$ are exposed
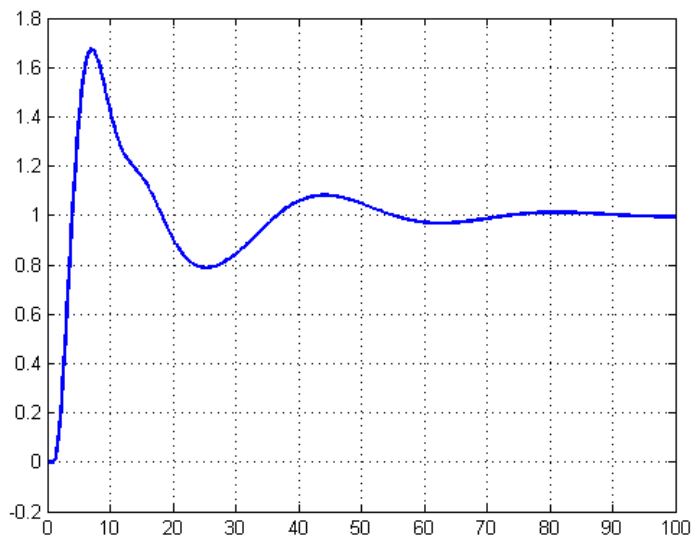
Fig 8.1 X axis response to step command
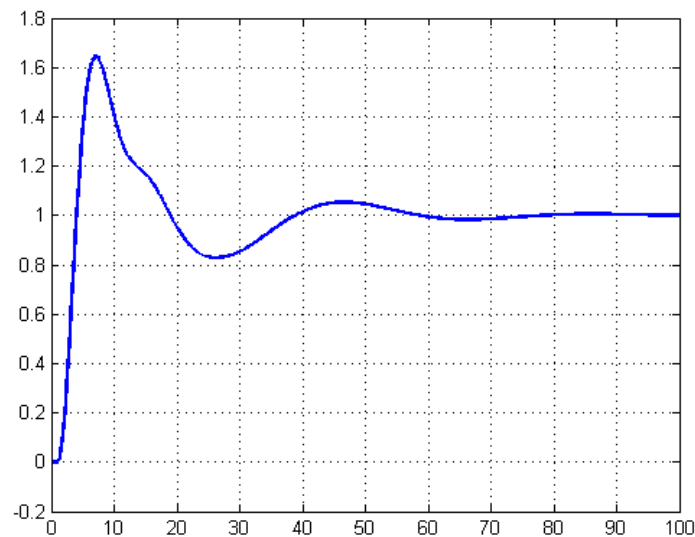
Fig 8.2 Y axis response to step command

The Z axis response is very similar to the X axis one and it is not represented. The step response in Fig. 8.1 looks worse than the one in Fig. 7.1. Comparing the two the negative actions of delays, digitization and integrators come out. System would be more prompt without the integrator but the faster response would lead the attitude to unacceptable steady state errors.

8.1   Structural dinamyc

In attitude feedback control loops based on PWM, the sampling frequency is constant and the reaction pulses are applied at equal time intervals. If the dynamics of the plant contains additional structural dynamics with low damping coefficients and eigenfrequencies equal to the sampling frequency of the control loop, then the structural dynamics might be excited, thus degrading the quality of the feedback control loop. Special precautions, such as adequate structural filters, must be incorporated to account for this phenomenon.

Chapter 9   Attitude estimation

Attitude estimation is one of the most challenging problems that came out during the system design.
The fact is manoeuvres are very critical phases of the mission and the strict requirement on their accuracy increases design criticality. A viable solution could have been found quite easily if inputs for the components choice could have been given but unfortunately this was not the case. Since the guideline of the ESMO mission imposes low budget and self developed components the required accuracy cannot be simply achieved.
With some preliminary analysis it will be shown how important is the contribution of a Kalman filter in estimating the attitude.

9.1   Configurations trade off

As already stated in section 3.2 it is very important to understand whether the star tracker is able to supply reliable measurements while the main engines are firing. Two different cases have been investigated with or without the star tracker contribution, but both of them relying on gyros and sun sensors measurements.
Two different error sources affect attitude propagation using gyros measurements only: The first one is related to gyro bias which is an error (assumed constant or slowly changing) affecting rate measurements. The second one descends from can bus inability to transfer data at 10 Hz. Angular rate is measured at 1 Hz while changing in torque has 1 ms resolution (for any off time which is longer than 20ms). Therefore the angular rate is correctly estimated but not the attitude.
Both of these have the net effect of forcing the evaluated attitude to drift away from the exact one.

Bias estimation is described in section 9.4, unfortunately the MEN firing compromises the estimation procedure, therefore it is recommended to perform it previously to the manoeuvre and it's easy to understand how important is accuracy in that procedure.

Two configurations are presented in the following section:

1)   3 axis gyros working at 10 Hz and 1 sun sensor working at 1Hz

2)   3 axis gyros and 1 sun sensor + a second sensor, all working at 1Hz

Both the above updating the control torque at 1Hz[4].

Configuration 1
Discrete results have been obtained with the first configuration where attitude quaternion is the state vector, propagated by gyros data (angular rate measurements are filtered from bias) and updated by sun sensor measurements.
This kind of system is quite sensitive to parameter tuning. The updating rotation around the sun vector is not reliable and causes the attitude to slowly drift around that vector. The error versus time graph has usually got a minimum at some point but there are no clues to identify it in order to stop the manoeuvre.
It means configuration 1 is not robust. It can be employed as long as the accepted final error is increased.
No estimation of the CoG position is required because ω is not in the state vector and it is not propagated.
This configuration is very sensitive to precision in bias estimation.

Configuration 2
It relies on two vector sensors[5] and gyros. The attitude is properly estimated. A second sensor has been introduced. The quaternion and the angular rate are the state vector, bias is still assumed constant during the manoeuvre. The error versus time is often a monotonically decreasing function to attest the configuration 2 robustness.
Another solution is to bypass the CoG estimation simply cutting out ω from the state vector and using gyros data to propagate the state (as for configuration 1).

9.2   Attitude Propagation

State variables propagation:

$$\vec{q}_{k+1} = \tfrac{1}{2}\Omega\vec{q}_k \qquad \Omega = \begin{bmatrix} 0 & \omega_3 & -\omega_2 & \omega_1 \\ -\omega_3 & 0 & \omega_1 & \omega_2 \\ \omega_2 & -\omega_1 & 0 & \omega_3 \\ -\omega_1 & -\omega_2 & -\omega_3 & 0 \end{bmatrix} \qquad 9.1$$

---

[4] As stated before the control torques are calculated every second but the effective applied torques can change every millisecond. This is related to the PWM scheme and to the high precision in controlling the engines off time.

[5] A vector sensor is a sensor which provides a vector as measurement. That vector is defined in the sensor frame and usually points to a celestial body.

$$\begin{cases} \underline{\dot{\omega}}_k = \underline{T}_k - \underline{\omega}_k \wedge \underline{\underline{J}}\,\underline{\omega}_k - \underline{\omega}_k \wedge \underline{\underline{A}}_w \underline{h}_{w\,k} + \underline{\Delta N}_{GG} \\ \underline{b}_{k+1} = \underline{b}_k \end{cases}$$ 9.2

Where $\underline{\underline{A}}_w, \underline{h}_w$ are defined in section 5.1 and $\underline{\Delta N}_{GG}$ in section 4.1

The generic differential equation below governs the state evolution

$$\dot{x} = f(x)$$ 9.3

Several approximated integration schemes have been compared:

- Explicit Euler

$$\dot{x} = \frac{x_{k+1} - x_k}{DT} = f(x_k)$$ 9.4

- Centred finite differences (second order)

$$\dot{x} = \frac{x_{k+1} - x_{k-1}}{2DT}$$ 9.5

- Backward finite differences (second order)

$$\dot{x} = \left(\frac{3}{2}x_k - 2x_{k-1} + \frac{1}{2}x_{k-2}\right)\frac{1}{DT}$$ 9.6

- Predictor corrector (Heun):

$$\tilde{x}_{k+1} = x_k + f(x_k)DT \quad \text{(prediction)}$$
9.7
$$x_{k+1} = x_k + \frac{1}{2}\big(f(x_k) + f(\tilde{x}_{k+1})\big)DT \quad \text{(correction)}$$

The effects of using different schemes have been compared to finally choose the predictor/corrector because it minimizes the propagation error.
As soon as an efficient Kalman filter is introduced all the above schemes become equivalent because any error due to propagation inaccuracy is cut off. This is not the only error the Kalman filter can eliminate. Indeed a well designed filter is able to compensate any disturbance torques which are not modelled.

9.3   Kalman filter

The Kalman filter is a computer algorithm for processing discrete measurements (the input) into optimal estimates (the output). Its operating can be sketched as follow: Attitude at time k (assumed to be known) is propagated to k+1. An estimation of sensors measurements is derived from the propagated attitude and it is subtracted to the actual sensors measurements. This error is multiplied by the Kalman gain to obtain the state updating vector, which is finally summed to the state propagated vector to give the updated state vector. The figure below better explain what has just been explained.
The Kalman gain calculus is described below.
This is just a step but it could be extended in a recursive way.
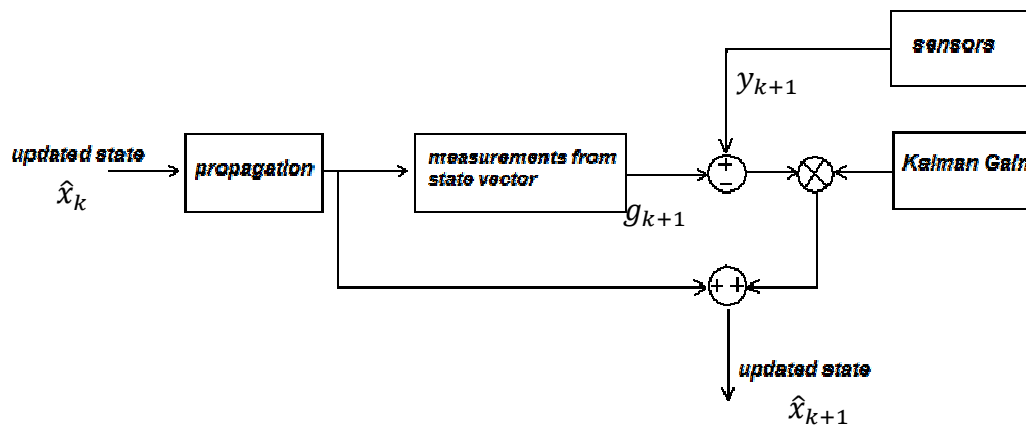
Fig 9.1 Kalman filter scheme

Some definitions:
State vector $\underline{x}$: array with the variables the analyst is interested in. In this case it contains attitude quaternion, angular rate and gyro bias.

Measurement vector $\underline{g}$: array with estimated measurements. For instance sun vector or gyro angular rates which are obtained propagating attitude and angular rate.

It is important to define the observation matrix (H), which is the ideal (noiseless) connection between measurements and state vector.

$$\underline{g} = \underline{\underline{H}}\underline{x} + \underline{v} \qquad\qquad 9.8$$

Where $\underline{v}$ is measurement error assumed to be white noise with known covariance structure.

The state vector evolution in time is

$$\underline{x}_k = \underline{\underline{\Phi}}_{k-1}\underline{x}_{k-1} + \underline{w}_{k-1}$$

9.9

Where $\underline{\underline{\Phi}}$ is the state transition matrix which is presented in subsection 9.3.2 and $\underline{w}$ is the driven response due to the presence of white noise.

At some point in time (t_k) a first estimate of the state vector is obtained from all the process data prior to t_k and it is defined with $\underline{\hat{x}}_k^-$ where the hat denotes estimation and the super minus is a reminder that this is the best estimate prior to assimilating the measurements at t_k.

The error covariance matrix P_k^- related to $\underline{\hat{x}}_k^-$ is defined as

$$\underline{\underline{P}}_k^- = E\left[\underline{e}_k^-\underline{e}_k^{-T}\right] = E\left[\left(\underline{x}_k - \underline{\hat{x}}_k^-\right)\left(\underline{x}_k - \underline{\hat{x}}_k^-\right)^T\right]$$

9.10

Where $E[x]$ indicates the expected value which is the weighted average of all possible values that the argument can take on

If x is a discrete random variable

$$E[x] = \sum_{1=1}^{\infty} x_i p_i$$

9.11

p_i are the probabilities related to the possible values x_i.

If x is a continuous and ergodic signal

$$E[x] = \lim_{T \to \infty} \frac{1}{2T} \int_{-T}^{+T} x \, dt$$

9.12

At time t_k measurement data are acquired $(\underline{y}_k)$ and the a posteriori estimate of the state vector is obtained:

$$\underline{\hat{x}}_k = \underline{\hat{x}}_k^- + \underline{\underline{K}}_k(\underline{y}_k - \underline{g}_k)$$

9.13

Where $\underline{K}_k$ is the Kalman gain and it is calculated using a minimum mean square error as performance criterion.

The error covariance matrix P_k related to the a posteriori estimate is

$$\underline{P}_k = E\left[\underline{e}_k \underline{e}_k^T\right] = E\left[\left(\underline{x}_k - \hat{\underline{x}}_k\right)\left(\underline{x}_k - \hat{\underline{x}}_k\right)^T\right] \qquad 9.14$$

Substituting Eq. 9.8 into the updating equation (Eq. 9.13) and inserting the resulting expression for $\hat{\underline{x}}_k$ into Eq. 9.14, it gives:

$$\underline{P}_k = E\left\{\left[\left(\underline{x}_k - \hat{\underline{x}}_k^-\right) - \underline{K}_k\left(\underline{H}_k \underline{x}_k + \underline{v}_k - \underline{H}_k \hat{\underline{x}}_k^-\right)\right]\left[\left(\underline{x}_k - \hat{\underline{x}}_k^-\right) - \underline{K}_k\left(\underline{H}_k \underline{x}_k + \underline{v}_k - \underline{H}_k \hat{\underline{x}}_k^-\right)\right]^T\right\} \qquad 9.15$$

Now, performing the indicated expectation and noting that $\left(\underline{x}_k - \hat{\underline{x}}_k^-\right)$ is the a priori estimation error which is uncorrelated with the measurements error v, it is obtained

$$\underline{P}_k = \left(\underline{I} - \underline{K}_k \underline{H}_k\right) P_k^- \left(\underline{I} - \underline{K}_k \underline{H}_k\right)^T + \underline{K}_k \underline{R}_k \underline{K}_k^T \qquad 9.16$$

The aim is to obtain the particular K that minimize the individual terms along the major diagonal of P because these terms represent the estimation error variance for the elements of the state vector being estimated.

The optimization is done with a straightforward differential calculus approach, and to do so two differentiation formulas are required:

$$\frac{d[trace(AB)]}{dA} = B^T \text{ (AB must be square)} \qquad 9.17$$

$$\frac{d[trace(ACA^T)]}{dA} = 2AC \text{ (C must be symmetric)} \qquad 9.18$$

Where the derivative of a scalar with respect to a matrix is defined as

$$\frac{ds}{dA} = \begin{bmatrix} \dfrac{ds}{da_{11}} & \dfrac{ds}{da_{12}} & \cdots \\ \dfrac{ds}{da_{21}} & \ddots & \\ \vdots & & \end{bmatrix} \qquad 9.19$$

$\underline{P}_k$ expression is expanded

$$\underline{P}_k = \underline{P}_k^- - \underline{K}_k\underline{H}_k\underline{P}_k^- - \underline{P}_k^-\underline{H}_k^T\underline{K}_k^T + \underline{K}_k(\underline{H}_k\underline{P}_k^-\underline{H}_k^T + \underline{R}_k)\underline{K}_k^T \qquad 9.20$$

The two differentiation formulas can now be applied. The aim is to minimize the trace of P because it is the sum of the mean-square errors in the estimates of all the elements of the state vector (the individual mean square-error is assumed to be minimized as soon as the total is minimized provided that there are enough degree of freedom in the variation of $\underline{K}$). Noting that the trace of $\underline{P}_k^-\underline{H}_k^T\underline{K}_k^T$ is equal to the trace of its transpose $\underline{K}_k\underline{H}_k\underline{P}_k^-$ it is obtained:

$$\frac{d[trace(\underline{P}_k)]}{d\underline{K}_k} = -2\left(\underline{H}_k\underline{P}_k^-\right)^T + 2\,\underline{K}_k(\underline{H}_k\underline{P}_k^-\underline{H}_k^T + \underline{R}_k) \qquad 9.21$$

Setting the derivative equal to zero and solving for the optimal (Kalman) gain:

$$K_k = \underline{P}_k^-\underline{H}_k^T(\underline{H}_k\underline{P}_k^-\underline{H}_k^T + \underline{R}_k)^{-1} \qquad 9.22$$

An a priori estimate of the state vector $\underline{\hat{x}}_k^-$ and of the error covariance matrix $\underline{P}_k^-$ is needed. The first one can easily be obtained as

$$\underline{\hat{x}}_k^- = \underline{\Phi}_{k-1}\underline{\hat{x}}_{k-1} \qquad 9.23$$

Note that w_k is neglected because it has zero mean and it's not correlated with any of the previous w's.

The error covariance matrix associated with $\underline{\hat{x}}_k^-$ is obtained by first forming the expression for the a priori error

$$\underline{e}_k^- = \underline{x}_k - \underline{\hat{x}}_k^- = \left(\underline{\Phi}_{k-1}\underline{x}_{k-1} + \underline{w}_{k-1}\right) - \underline{\Phi}_{k-1}\underline{\hat{x}}_{k-1} = \underline{\Phi}_{k-1}\underline{e}_{k-1} +$$
$$\underline{w}_{k-1} \qquad\qquad 9.24$$

$\underline{w}_{k-1}$ and $\underline{e}_{k-1}$ have zero cross-correlation[6], thus

---

[6] since $\underline{w}_{k-1}$ is the process noise that accumulates during the step ahead from t_{k-1} to t_k and it contributes only to the state vector after time t_{k-1}, and not before

$$\underline{P}_k^- = E[\underline{e}_k^- \underline{e}_k^{-T}] = E\left[\left(\underline{\Phi}_{k-1}\underline{e}_{k-1} + \underline{w}_{k-1}\right)\left(\underline{\Phi}_{k-1}\underline{e}_{k-1} + \underline{w}_{k-1}\right)^T\right] =$$
$$= \underline{\Phi}_{k-1}\underline{P}_{k-1}\underline{\Phi}_{k-1}^T + \underline{Q}_{k-1}$$

9.25

P matrix is automatically propagated and updated by the algorithm but a first guess is required. Small values mean the initial guess for the state vector can be trusted.
The following section contextualize the theoretical approach presented above.

9.3.1 Observation matrix

Attitude quaternion, angular rate and bias compose the state vector $\underline{x}$ (which is true only previously to the firing, remember that bias is not estimated during the manoeuvre).
Sun versor and angular rate compose the observation vector $\underline{g}$

$$\underline{x} = \begin{Bmatrix} \delta\vec{q} \\ \delta\underline{\omega} \\ \delta\underline{b} \end{Bmatrix}$$

9.26

$$\underline{g} = \begin{Bmatrix} \underline{v}_s^b \\ \underline{\omega} \end{Bmatrix}$$

9.27

It is required to relate measurements to variation in the state vector. A relation between $\delta\vec{q}$ and $\underline{v}_s$ is needed in order to design the observation matrix.
The updated $\vec{q}$ is defined as

$$\vec{q} = \delta\vec{q} \otimes \vec{q}_p$$

9.28

Where $\vec{q}_p$ is the propagated quaternion and $\delta\vec{q}$ is the error quaternion which relates the propagated attitude to the updated one.
The estimated sun vector in body frame, $\hat{\underline{v}}_s^b$, is related to the inertial one $\underline{v}_s^i$ by:

$$\hat{\underline{v}}_s^b = \underline{A}(\vec{q})\underline{v}_s^i$$

9.29

Where $\underline{A}(\vec{q})$ is the estimated attitude matrix and can be manipulated

$$A(\vec{q}) = A(\delta\vec{q} \otimes \vec{q}_p) = A(\delta\vec{q})A(\vec{q}_p) \qquad \qquad 9.30$$

Hence

$$\hat{\underline{v}}_s^b = A(\delta\vec{q})\underline{v}_{s\,p}^b \qquad \qquad 9.31$$

The components of $A(\delta\vec{q})$ are obtained linearizing the generic rotation matrix related to quaternion $\vec{q}$.

$$A(\vec{q}) = \begin{bmatrix} q_1^2 - q_2^2 - q_3^2 + q_4^2 & 2(q_1q_2 + q_3q_4) & 2(q_1q_3 + q_2q_4) \\ 2(q_1q_2 - q_3q_4) & -q_1^2 + q_2^2 - q_3^2 + q_4^2 & 2(q_2q_3 + q_1q_4) \\ 2(q_1q_3 + q_2q_4) & 2(q_2q_3 + q_1q_4) & -q_1^2 - q_2^2 + q_3^2 + q_4^2 \end{bmatrix}$$

Assuming small rotations, therefore $q_1, q_2, q_3 \ll 1$ and $q_4 \approx 1$, it becomes

$$A(\delta\vec{q}) = \begin{bmatrix} 1 & 2\delta q_3 & -2\delta q_2 \\ -2\delta q_3 & 1 & 2\delta q_1 \\ 2\delta q_2 & -2\delta q_1 & 1 \end{bmatrix} \qquad \qquad 9.32$$

Where $\underline{v}_{s\,p}^b$ is the sun versor in body frame obtained from the propagated quaternion[7].

$$\hat{\underline{v}}_s^b = \begin{bmatrix} 1 & 2\delta q_3 & -2\delta q_2 \\ -2\delta q_3 & 1 & 2\delta q_1 \\ 2\delta q_2 & -2\delta q_1 & 1 \end{bmatrix} \begin{Bmatrix} v_{sp1}^b \\ v_{sp2}^b \\ v_{sp3}^b \end{Bmatrix} =$$

$$= \begin{bmatrix} 0 & -2v_{sp3}^b & 2v_{sp2}^b \\ 2v_{sp3}^b & 0 & -2v_{sp1}^b \\ -2v_{sp2}^b & 2v_{sp1}^b & 0 \end{bmatrix} \begin{Bmatrix} \delta q_1 \\ \delta q_2 \\ \delta q_3 \end{Bmatrix} + \underline{v}_{s\,p}^b = C(2\underline{v}_{s\,p}^b)\delta\vec{q} + \underline{v}_{s\,p}^b \qquad 9.33$$

Therefore the H matrix will have the following shape

---

[7] $C(\underline{v})$ indicates the following emisymmetric matrix $\begin{bmatrix} 0 & -2v_3 & 2v_2 \\ 2v_3 & 0 & -2v_1 \\ -2v_2 & 2v_1 & 0 \end{bmatrix}$

$$\underline{\underline{H}} = \begin{bmatrix} C(2\underline{v}^b_{S\,p}) & 0 & 0 \\ \Delta\underline{N}_{gg} + \Delta\underline{N}_{MF} + \Delta\underline{N}_D & I & I \\ 0 & 0 & I \end{bmatrix} \qquad 9.34$$

Where $\Delta\underline{N}_{gg}, \Delta\underline{N}_{MF}, \Delta\underline{N}_D$ relate $\underline{\omega}$ to $\delta\vec{q}$ describing torques introduced by variations in attitude. For preliminary analyses they can be neglected because their influence is limited.

If two vectors ($\underline{v}^b_S$ and $\underline{v}^b_{SS}$) are provided by sensors the H matrix will be:

$$\underline{\underline{H}} = \begin{bmatrix} C(2\underline{v}^b_{S\,p}) & 0 & 0 \\ C(2\underline{v}^b_{SS\,p}) & 0 & 0 \\ \Delta\underline{N}_{gg} + \Delta\underline{N}_{MF} + \Delta\underline{N}_D & I & I \\ 0 & 0 & I \end{bmatrix} \qquad 9.35$$

$\underline{v}^b_{SS\,p}$ is the predicted measurement vector in body frame associated with the second sensor and it is obtained from the propagated quaternion. The measurements vector will be

$$\underline{g} = \begin{Bmatrix} \underline{v}^b_S \\ \underline{v}^b_{SS} \\ \underline{\omega} \\ \underline{b} \end{Bmatrix} \qquad 9.36$$

The second sensor mentioned above has been considered capable of measuring one vector (like the sun sensor). It could be a new sensor, which is not part of the ESMO equipment or the star tracker if operative during the manoeuvre.

9.3.2 State transition matrix Φ

State transition matrix is defined by

$$\underline{\underline{\Phi}} = \underline{\underline{I}} + \underline{\underline{F}}\Delta t \qquad 9.37$$

F incorporates the linearized relation between state variables and their derivatives:

$$\delta\dot{\vec{q}} = -C(\underline{\omega})\,\delta\vec{q} + \frac{1}{2}\delta\underline{\omega} \qquad 9.38$$

$$J\delta\underline{\dot{\omega}} = \left[\Delta N_{gg} + \Delta N_{MF} + \Delta N_D\right]\delta\vec{q} - \left[C(\underline{\omega})J - C(J\underline{\omega} + \right.$$
$$\left. +\underline{h})\right]\delta\underline{\omega} + J\underline{\eta}_D \qquad 9.39$$

$$\delta\underline{\dot{b}} = \underline{\eta}_G \qquad 9.40$$

$\underline{\eta}_D$ and $\underline{\eta}_G$ represent disturbance torques that have not been accounted for and the gyro bias instability process noise vector respectively.

Therefore

$$\underline{\underline{F}} = \begin{bmatrix} -C(\underline{\omega}) & \frac{1}{2}I & 0 \\ \Delta N_{gg} + \Delta N_{MF} + \Delta N_D & -\left[C(\underline{\omega})J - C(J\underline{\omega} + \underline{h})\right] & 0 \\ 0 & 0 & 0 \end{bmatrix} \qquad 9.41$$

9.3.3   Process noise matrix Q

System equations in state space are considered

$$\underline{\dot{x}} = \underline{\underline{F}}\underline{x} + \underline{n} \qquad 9.42$$

Where $\underline{n}$ is a vector forcing function whose elements are white noise.
State vector is propagated using the following

$$\underline{x}_k = \underline{\underline{\Phi}}_{k-1}\underline{x}_{k-1} + \underline{w}_{k-1} \qquad 9.43$$

$\underline{\underline{\Phi}}_{k-1}$ is the state transition matrix for the step from t_{k-1} to t_k

$\underline{w}_{k-1}$ is the driven response at t_k due to the presence of white-noise input during the t_{k-1}, t_k interval

$$\underline{w}_{k-1} = \int_{t_{k-1}}^{t_k} \underline{\underline{\Phi}}(t_k, \tau)n(\tau)d\tau \qquad 9.44$$

Process noise matrix is defined by

$$\underline{\underline{Q}}_k = E\left[\underline{w}_k \underline{w}_k^T\right] =$$

$$E\left\{\left[\int_{t_k}^{t_{k+1}} \underline{\underline{\Phi}}(t_{k+1}, u)n(u)du\right]\left[\int_{t_k}^{t_{k+1}} \underline{\underline{\Phi}}(t_{k+1}, v)n(v)dv\right]^T\right\} =$$

$$= \int_{t_k}^{t_{k+1}} \int_{t_k}^{t_{k+1}} \underline{\underline{\Phi}}(t_{k+1}, u)E\left[\underline{n}(u)\underline{n}(v)^T\right]\underline{\underline{\Phi}}^T(t_{k+1}, u)dudv$$

9.45

It is assumed that

$$E\left[\underline{n}(u)\underline{n}^T(v)\right] = \begin{bmatrix} 0 & 0 & 0 \\ 0 & \underline{\underline{S}}_D\delta(u-v) & 0 \\ 0 & 0 & \underline{\underline{S}}_G\delta(u-v) \end{bmatrix}$$

9.46

Where δ is Dirac delta function which is 1 when u equals v and is zero otherwise. $\underline{\underline{S}}_D$ and $\underline{\underline{S}}_G$ are diagonal matrices which correspond to the effects of disturbance torques and bias instability respectively.

Considering $t_k = 0$ and $t_{k+1} = \Delta t$ the process noise matrix is obtained

$$\underline{\underline{Q}} = \begin{bmatrix} \frac{1}{12}\underline{\underline{S}}_D\Delta t^3 & \frac{1}{4}\underline{\underline{S}}_D\Delta t^2 & 0 \\ \frac{1}{4}\underline{\underline{S}}_D\Delta t^2 & \underline{\underline{S}}_D\Delta t & 0 \\ 0 & 0 & \underline{\underline{S}}_G\Delta t \end{bmatrix}$$

9.47

In order to derive the equation above a simplified $\underline{\underline{\Phi}}$ has been assumed

$$\underline{\underline{\Phi}} \approx \begin{bmatrix} \underline{\underline{I}} & \frac{1}{2}\tau\underline{\underline{I}} & 0 \\ 0 & \underline{\underline{I}} & 0 \\ 0 & 0 & \underline{\underline{I}} \end{bmatrix}$$

9.48

$\underline{\underline{I}}$ represents a 3x3 identity matrix.

The calculus of element 1,1 of the Q matrix is shown below

$$Q(1,1) = \int_0^{\Delta t} \int_0^{\Delta t} \frac{1}{4}uvS_D\delta(u-v)dudv = \int_0^{\Delta t} \frac{1}{4}u^2S_D du =$$

$$\frac{1}{12}S_D\Delta t^3$$

9.49

The smaller $\underline{S_D}$ and $\underline{S_G}$ are set the more reliable the propagation model is considered.

9.3.4   Measurements noise matrix R

The measurements noise matrix is a diagonal matrix which contain the measurements errors variances.

$$\underline{\underline{R}} = \begin{bmatrix} \sigma_{SCS} & 0 \\ 0 & \sigma_G \end{bmatrix} \tag{9.50}$$

σ_{SCS} and σ_G are acquired from the sensors data sheets or defined through a test campaign.
If two sensors measurements are available the R matrix will be:

$$\underline{\underline{R}} = \begin{bmatrix} \sigma_{SCS} & 0 & 0 \\ 0 & \sigma_{SS} & 0 \\ 0 & 0 & \sigma_G \end{bmatrix} \tag{9.51}$$

9.3.5   Sensor accuracy

SCS (by satellite services): 0.3 deg
Second Sensor (Hypothesis): 0.5 deg
These values represent the standard deviations of sensor measurements.
Which means

$$\sigma_{SCS} = 2.74e-5 \; rad^2$$
$$\sigma_{SS} = 7.62e-5 \, rad^2$$
$$\sigma_G = 1e-6 \left(rad/_s \right)^2$$

σ_{SCS} and σ_{ST} are simply defined by the variance, which is the square of the standard deviation defined above.
Since the gyro measurements are affected by errors coming from different sources σ_G is empirically calculated processing some acquired data.

9.4   Gyro Bias Estimation

Since gyro bias affects all rate measurements it is useful to estimate it while the manoeuvres are performed.
It will be pointed out how the thrusters firing and the consequent angular rate quick changing interfere with the bias evaluation. Therefore it was decided to

estimate it in a previous phase, when the thrusters are off, and to assume it constant during the manoeuvre.

The estimation procedure is now described:

Thrusters are off and only external disturbances affect the attitude. Parameters have been set as follow:

$$P_{fg} = diag(10^{-9} \quad 10^{-9} \quad 10^{-9} \quad 10^{-9} \quad 10^{-9} \quad 10^{-9} \quad 10^{-6} \quad 10^{-6} \quad 10^{-6})$$

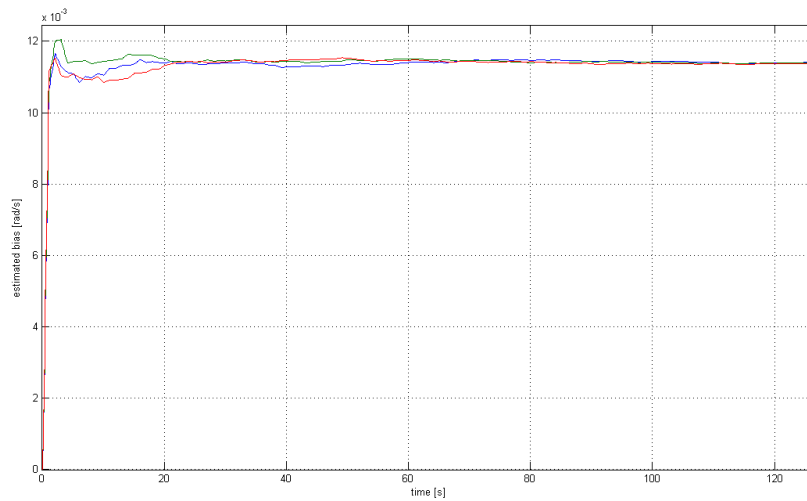$$b_{fg} = [0\ 0\ 0]$$

$$S_D = S_G = 10^{-12}$$

The *fg* subscript means first guess.

Fig 9.2 Bias estimation

As gyros bias has been voluntarily introduces it can be easily verified the estimation correctness:

Introduced total bias: $0.65\ deg/sec = 0.0113 rad/sec$ (neglecting gyro bias stability).

The graph show how bias is correctly estimated after about 10 seconds. The accuracy is showed in table 9.1

Tab 9.1 Error on bias estimation

Axis	X	Y	Z
err [%]	1.1434	1.0375	0.7392

As the parameters are varied, the transient phase duration changes. E.g. an increment of the last 3 terms of P_{fg} makes the settling time longer.

9.5   Estimation with gyros

Before diving in complex estimation calculus it is opportune to try to determine the attitude from gyros measurements. The accuracy in estimating gyro bias determines the accuracy of the whole propagation procedure.
Attitude is propagated using a conventional formula:

$$\vec{q}_{k+1} = \frac{1}{2}\underline{\underline{\Omega}}\vec{q}_k \qquad \underline{\underline{\Omega}} = \begin{bmatrix} 0 & \omega_3 & -\omega_2 & \omega_1 \\ -\omega_3 & 0 & \omega_1 & \omega_2 \\ \omega_2 & -\omega_1 & 0 & \omega_3 \\ -\omega_1 & -\omega_2 & -\omega_3 & 0 \end{bmatrix} \qquad 9.52$$

Where $\underline{\omega}$ is a filtered (from bias) value of measured angular rate.
Now the control system is working and in order to judge the estimation precision exact attitude $\vec{q}$ is compared with the estimated one $\vec{\hat{q}}$ to find the error quaternion $\delta\vec{q}$ (This is similar to the calculus of error angles required by the compensator which is described in section 6.5).

$$\vec{q} = \delta\vec{q} \otimes \vec{\hat{q}} \qquad 9.53$$

$$\delta\vec{q} = \vec{q} \otimes \vec{\hat{q}}^* \qquad 9.54$$

With

$$\vec{\hat{q}}^* = [\hat{q}_1 \quad \hat{q}_2 \quad \hat{q}_3 \quad -\hat{q}_4]^T \qquad 9.55$$

The two reference systems are supposed to be close and the angular error around each axis is evaluated:

$$\begin{aligned} \alpha_x^{err} &= 2\hat{q}_1 \\ \alpha_y^{err} &= 2\hat{q}_2 \\ \alpha_z^{err} &= 2\hat{q}_3 \end{aligned} \qquad 9.56$$

The problem is rate measurements are processed at 1 Hz while control torques change with much higher frequency (because thrusters off time has 1ms resolution). This fact introduces big errors and the attitude propagation fails.

As far as gyros data are processed at 10Hz the propagation is feasible but the attitude slowly drift away from the exact one.

Manouvre number 2 is considered (see Tab. 1.1). The maximum value for the centre of gravity shift is assumed, a 5% overestimation of the spacecraft actual moments of inertia is hypothesized and a limit of 400 ms is imposed on the minimum thrusters off time. Assuming 1.5% error on bias estimation (equal on each axis) a marked attitude drift is obtained:
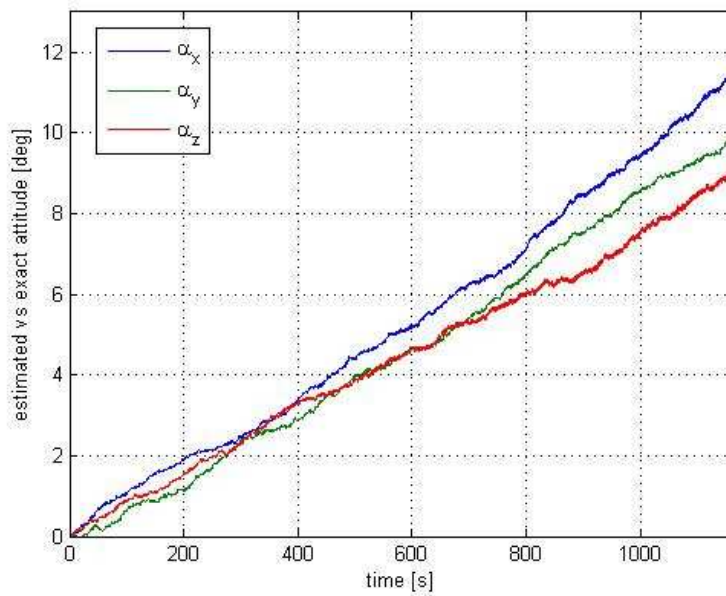

Fig 9.3 Estimation with gyros only. Attitude drift (1.5% bias overestimation)
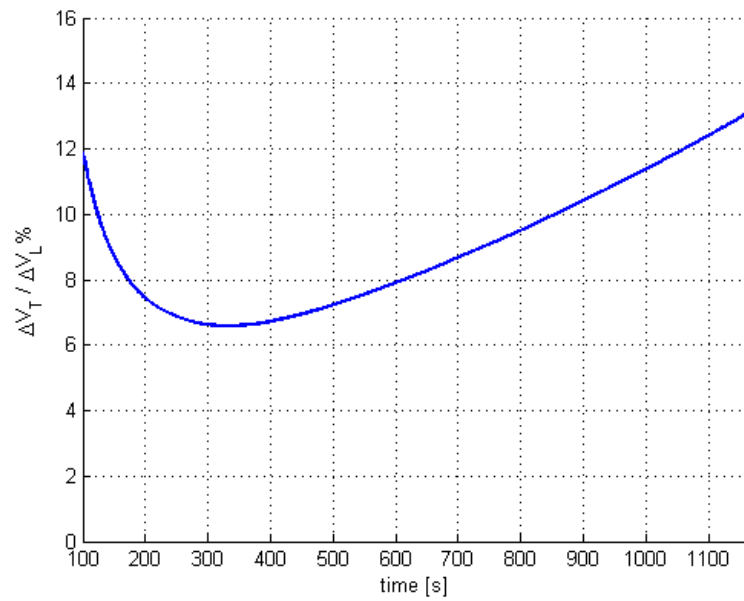
Fig 9.4 Transverse on longitudinal velocity component, percental error (1.5% bias overestimation)

Causes of drift has been searched and identified:

Errors on bias estimation radically influence the error on attitude propagation and consequently system performances.
Diverse values of bias error have been considered
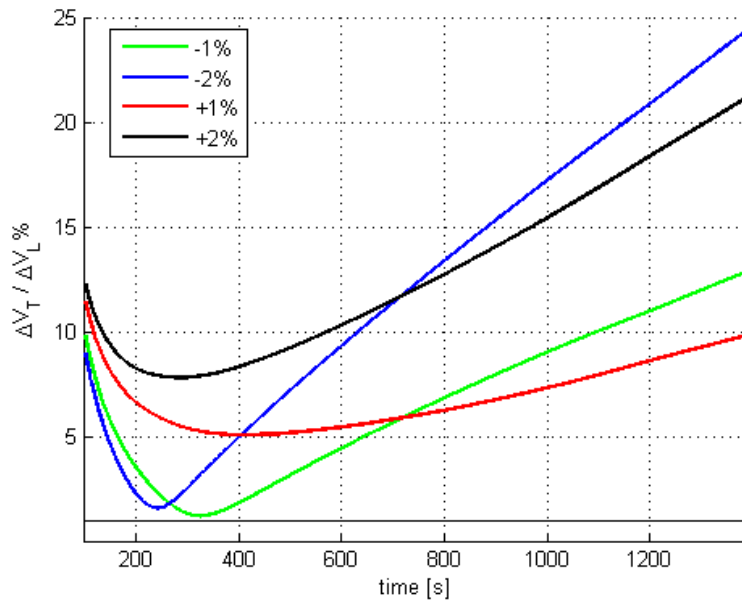
Fig 9.5 Transverse on longitudinal velocity component, percental error. Effects of errors on bias estimation

As mentioned earlier the error on bias valuation totally influences the results. Actually if error is negative a sort of compensation to the initial peak is provided.

In other words as thrusters are fired the s/c goes far from the desired attitude and accumulates a big angle error which in half of the cases is compensated by bias misestimation, in the other half is accentuated.

Another source of error is the measuring frequency. Samples every 1 ms are required not to lose any attitude variation while samples every 100ms will likely be available. In order to investigate this problem the dynamic should be integrated with a 1ms time step. Since the unacceptable results, exposed in this section, have been obtained considering bias error and 10 Hz torque variation, an higher rate of torque changing would surely lead to worse results, especially without any compensation of the attitude drift (supplied by vector sensors). Therefore this situation is not even analyzed.

This kind of system is unreliable because the bias error sign is unpredictable. It is important to notice that even assuming a zero error in estimating gyro bias, a small drift appears. This is due to bias stability.

9.6   Estimation with gyros and sun sensor

The sun coarse sensor measurement is introduced to improve performances. *Two different strategies* have been employed to determine the spacecraft orientation: The *first* one is based on Kalman filtering with $\underline{\omega}$ and $\vec{q}$ in the state vector. Discrete results are obtained if the effective control torque is used for propagation (unfortunately the control torque used in propagation is an approximation of the effective applied torque because the centre of gravity position is not precisely known). In this case the estimation error around two axes is inversely proportional to sun sensor accuracy while around the third axis it descends from the gyros limitations that have been described above. Indeed gyros data are helpful in angular rate estimation but useless in attitude estimation because even a small error on bias estimation causes the estimation drift moreover their measurements flow is too slow compared to the control torque variation rate.

The sun coarse sensor measured vector is useful in updating the state vector even if the rotation around that vector is undetermined.

At the beginning of the manoeuvre the required attitude has been assumed having sun on the x axis[8] and the initial orientation being coincident with the required one.

What stated before is clearly visible in the following graph where the uncertainty in x rotation is showed.
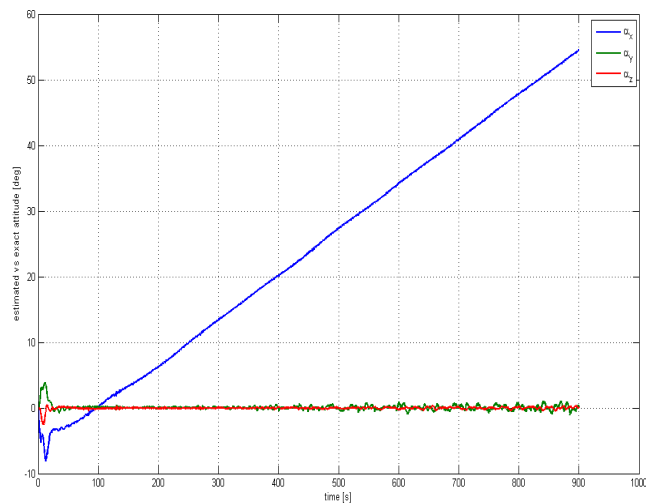

Fig 9.6 True/estimated attitude error angles

---

[8] Since y is the axis along which thrust is provided, attitude uncertainty around any axes perpendicular to y maximizes the error on the performed Δv

As soon as the centre of mass uncertainty, even a small one, is encountered (introducing a wrong torque into the propagation block) the estimation get worse, especially around the sun vector. The slow drift noticed before turns into wide oscillations and after 400 seconds the scheme becomes even unstable.
Working on parameters tuning, a stable scheme can be eventually achieved but results are far to be acceptable and the system is far to be reliable

Since the problem in estimating arises as the $\underline{\omega}$ propagation is fed by the approximated control torque and not by the actual torque (which is unknown) a *second* scheme has been developed: attitude propagation is performed by gyro acquired measurements, where the previously evaluated bias is filtered. The attitude updating is performed without Kalman filter but using a rotation defined by the following Euler axis $\underline{e}$ and angle ϑ:

$$\underline{e} = \underline{v}^b_{s\,p} \wedge \underline{v}^b_{s\,m} \qquad 9.57$$

$$\vartheta = acos\left(\underline{v}^b_{s\,p} \cdot \underline{v}^b_{s\,m}\right) \qquad 9.58$$

Where $\underline{v}^b_{s\,p}$ is the estimated sun vector in body frame (based upon sun position in the inertial frame and the propagated attitude) and $\underline{v}^b_{s\,m}$ is the measured sun vector.
This scheme works well as far as rate data are processed at 10Hz; the uncertainty around the sun versor causes the calculated attitude to slowly drift around that axis. But as the measurements flow is slowed down to 1Hz the propagation collapse.
Similar results are expected from both the schemes because they are different ways of optimizing the same problem with the same hardware.
Similar results have been obtained properly tuning S_D and S_G of the process noise matrix of the Kalman filter.

9.7   Estimation with gyros and 2 vector sensors

A second sensor is modeled, hence another versor is introduced in the estimation process. The second sensor introduction produces three axes compensation of gyro bias provided that the vectors measured by the sensors have got different directions (the best would be orthogonal vectors). Even if the second sensor accuracy is rough, attitude doesn't drift away but error oscillations are wider (Oscillation of the estimated attitude around the actual one becomes actual system oscillations around the target attitude).

The following results have been obtained with a second sensor accuracy of 0.3 deg and assuming the second vector on the diagonal of the x-z plane at the beginning of the manoeuvre.
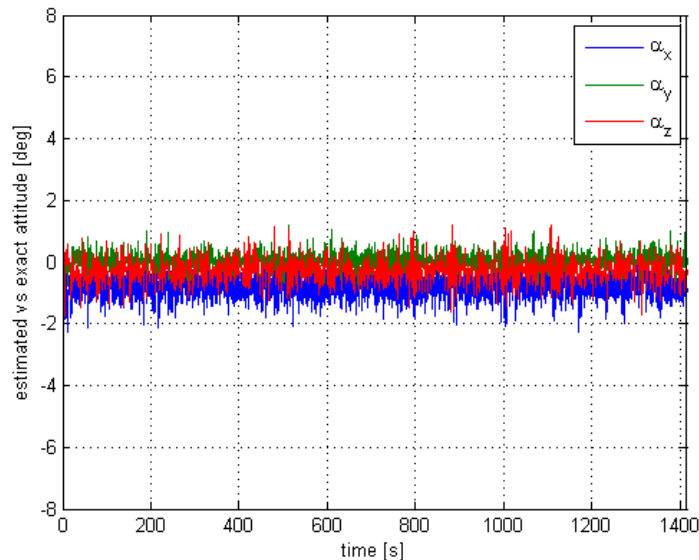

Fig 9.7 True/estimated attitude error angles, corrupted propagation

Oscillations amplitude depends on sensor accuracy and not on the relative angle between the measurements vectors (a minimum angle of 20 deg has been considered without performances degradation). Usually that noise is smoothed properly setting the Kalman filter parameters in order to relay more on propagation rather than on measurements. In this case it is not so simple because propagation is affected by errors resulting from the uncertainty on the centre of gravity shift.

Looking carefully at Fig. 9.7 it is important to notice that the errors around x and z axes have a non zero mean. This behaviour is explained by inaccuracy in propagating the attitude and by weakness in updating. The filter parameter S_D, described in subsection 9.3.3, allows to move reliability from propagation to measurements (increasing S_D) and vice-versa. Fig. 9.7 has been obtained with $S_D = 9x10^{-13}$. As S_D is increased the update acquires strength at the expense of propagation. As a result error mean get closer to zero but oscillations amplitude rises (to become finally unstable).

In order to verify what stated above the centre of gravity shift is supposed to be exactly known. Therefore the only errors affecting propagation are due to the environmental disturbances. S_D has been set to $9x10^{-16}$ and the attitude error of Fig. 9.8 has been obtained.
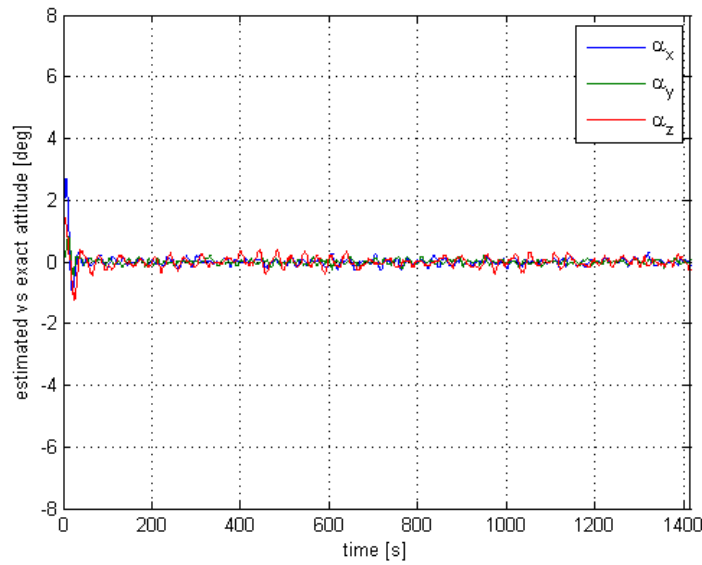
Fig 9.8 True/estimated attitude error angles, exact propagation

A zero mean error is obtained; the important role of accuracy in estimating the centre of gravity position is highlighted. Since it is very difficult to obtain that accuracy the Kalman filter has to relay much more on measurements rather than on propagation and as a consequence the estimated attitude looks rougher.

Chapter 10 Estimation of Center of Gravity position

Knowledge of the centre of gravity position is required as attitude propagation is employed in estimating the attitude. In that case a particular procedure is performed previously to the manoeuvre:

At the beginning the spacecraft shall acquire a steady attitude (zero angular rates) so that any coupling (due to $\underline{\omega} \wedge \underline{\underline{J}}\underline{\omega}$) of the dynamic equations is minimized; this could be done by wheels which ensure fine control. Then A couple of main engines are fired together for the minimum on time to produce one axis torque. The spacecraft angular rate is estimated and the centre of gravity shift is evaluated.

A generic axis and its dynamic equation is considered

$$J\dot{\omega} = T + D_e \qquad\qquad 10.1$$

$\dot{\omega}$ is approximated by finite differences.

$$\dot{\omega} = \frac{\omega_{k+1} - \omega_k}{t_{ON}} \qquad\qquad 10.2$$

T is split into 4 contributions:

T_0 ideal torque produced by the two engines firing when the centre of gravity is in the ideal position $[0 - 445.5 \; 0] \; mm$.

$DT_x(\Delta x)$, $DT_y(\Delta y)$, $DT_z(\Delta z)$ are the corrective torques associated with the centre of gravity shift $(\Delta x, \Delta y, \Delta z)$. Given the main engines configuration it is easy to relate them to the shift.

D_e are evaluable disturbances such as gravity gradient and drag.

Torques introduced by the wheels gyroscopic effect are not considered because watching to their contribution

$$\underline{\omega} \wedge \underline{h}_w = \begin{Bmatrix} \omega_y h_z - \omega_z h_y \\ \omega_z h_x - \omega_x h_z \\ \omega_x h_y - \omega_y h_x \end{Bmatrix} \qquad\qquad 10.3$$

it is clear that starting the procedure from a steady attitude and introducing torque around one axis any spinning around the other two axes are negligible and so is the wheels contribution.

Similar considerations allow not to consider the coupling terms $\underline{\omega} \wedge \underline{\underline{J}}\underline{\omega}$.

Hence

$$J\omega_{k+1} = \left(T_0 + DT_x(\Delta x) + DT_y(\Delta y) + DT_z(\Delta z) + D_e\right)t_{ON} \qquad 10.4$$

Three coupled equations in three variables have been defined.

This procedure requires moments of inertia knowledge. Moments of inertia change as the centre of gravity shifts. Therefore a relation between the centre of gravity shift and moments of inertia is required to the structure team.

The procedure above has been tested. Since no relation between CoG shift and moments of inertia is available, 5% error has been considered affecting the moments of inertia knowledge.

Tab 10.1   Centre of gravity position, actual and estimated values

	Actual [m]	Estimated [m]	Error [%]
X	0.0377	0.0392	+4
Y	-0.3842	-0.3243	-15.6
Z	-0.0687	-0.0847	+23.3

Chapter 11 Results

At the beginning the s/c has no angular rate and the firing axis coincides with the required Δv vector. As the MEN are fired the initial kick rotates the s/c far from the desired attitude. The control system kills that displacement in less than 1 minute. In this phase Δv_T is even bigger than Δv_L but after that the attitude gets close to the required one and the error starts decreasing.

It means that most of the final error is accumulated in the first 20 seconds and long manoeuvres are required to compensate it.

In order to minimize the initial peak and rise time a fast response is required but the system and its hardware impose some limits.

The propulsion system is very powerful and even a small CoG shift generates big disturbance torques. This causes accentuated initial displacement because the s/c inertia momenta are small and because the demanded torque is sampled at 1 Hz and the control torque is delayed of 0.7 s by the line transmission.

ESMO has to perform several manoeuvres. System performances have been obtained considering all of them. It can be shown that the shortest manoeuvres do not last enough to kill the initial error. A viable solution to this problem is to provide smaller impulses imposing a top limit on the MEN on time; which is the same as imposing a bottom limit on the MEN off time: the required off times are raised so that the lowest one meets the bottom limit and they are all scaled if the biggest exceed the sampling time.

The above artifice induces longer manoeuvres which ensure the requirements to be met (the error plot is often monotonically decreasing).

Given the required Δv series and the thrusters specific impulse ($I_{sp} = 289\ s$) the s/c mass evolution has been estimated:

Tab 11.1 Impulsive trajectory manoeuvres, mass evolution and required Δv

m [Kg]	$\Delta v\ [m/s]$
189	404
163	244
149	142
141	71
137	200
127	101
122	

For example the first manoeuvre requires 404 m/s of velocity increment and the mass reduction due to propellant consumption is calculated using the Tsiolkovsky rocket equation:

$$m_1 = m_0 e^{-\frac{\Delta v}{I_{sp}g}} \qquad\qquad 11.1$$

As mentioned before the most critical manoeuvres, in terms of final Δv error, are those which require the lowest Δv with the lowest s/c mass i.e. the shortest one $(71,101\ m/s)$

The uncertainty in m knowledge will generate the longitudinal Δv error. Here the assumed m is an average value between the manoeuvre initial and final mass.

In order to demonstrate the system efficiency in every condition all the manoeuvre are analyzed. Some parameters are not predictable such as errors affecting the moments of inertia knowledge or the centre of gravity shift, therefore their variation have been analyzed.

It is important to remember that all the results, which are exposed below, refer to the worst case of maximum shift of the centre of gravity. Therefore the system actual performances will be better in any condition.

Due to the spacecraft low moments of inertia and to the powerful engines the attitude error and angular rates show marked initial peaks. In order to get rid of them the minimum thrusters off-time is not imposed with a step command but with an exponential function which starts from 1 and eventually reaches the minimum off-time that was designed for the specific manoeuvre $\left(\bar{t}_{OFF}^{min}\right)$.

$$t_{OFF}^{min}(t) = \bar{t}_{OFF}^{min} + \left(1 - \bar{t}_{OFF}^{min}\right)e^{-t/\tau} \qquad\qquad 11.2$$

τ is the time constant of the exponential function. The bigger τ is the smaller the initial peak and the longer the transitory are. Several values of τ have been considered.

Manoeuvre n°1

Required $\Delta v = 404\ m/s$

Average mass $= 176\ Kg$

Minimum thruster off time (per sample) $= 0.1\ s$

Error on the assumed moments of inertia $= -10\%$ of the actual values

Error on CoG estimation $=\ [4; -15.6; 23.3]\%$ of the actual values

Error on bias estimation = 11.5% of the actual values

Manoeuvre duration = $1442\ s$ (24 min)
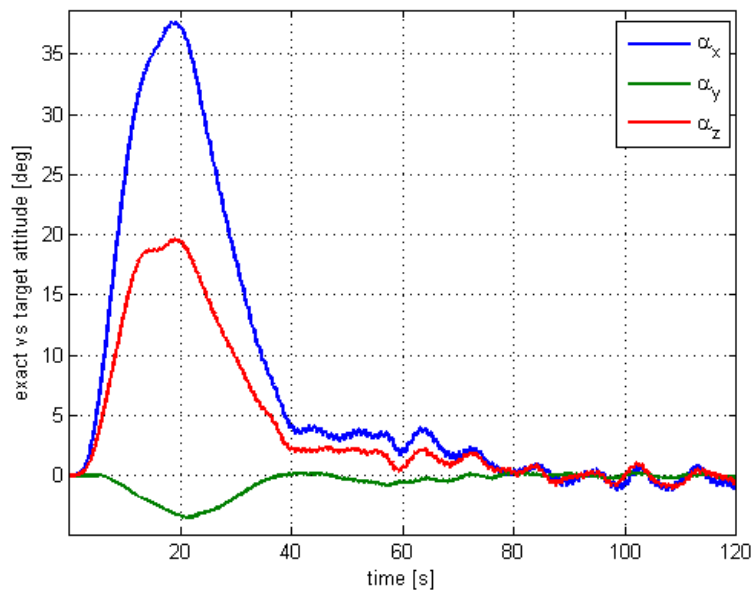
Fig 11.1 True/desired attitude error angles, initial transitory (manoeuvre n°1)

The maximum thruster on time is 0.9s (big disturbance impulse), therefore a big error is introduced by the initial kick. Error which is slowly erased by the long manoeuvre duration (about 24 minutes). Fig. 11.1 represents only the beginning of the firing (about 120 s). The oscillations for $t > 80s$ are typical of the whole manoeuvre.
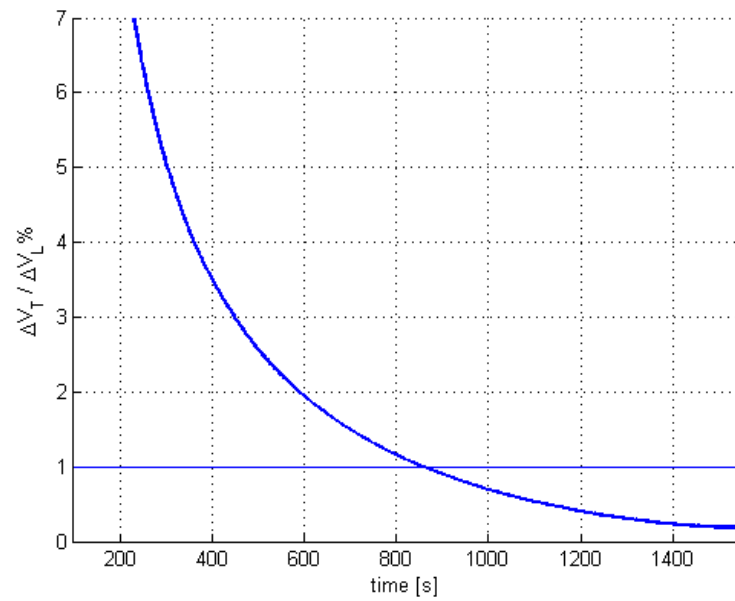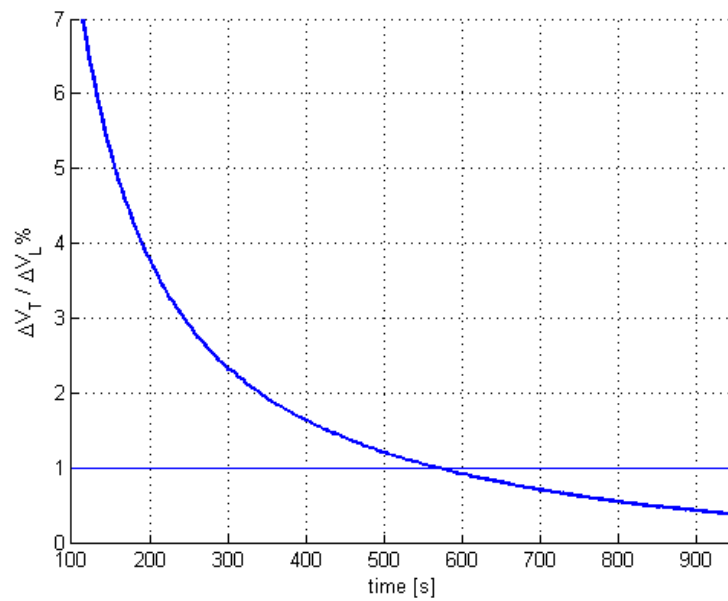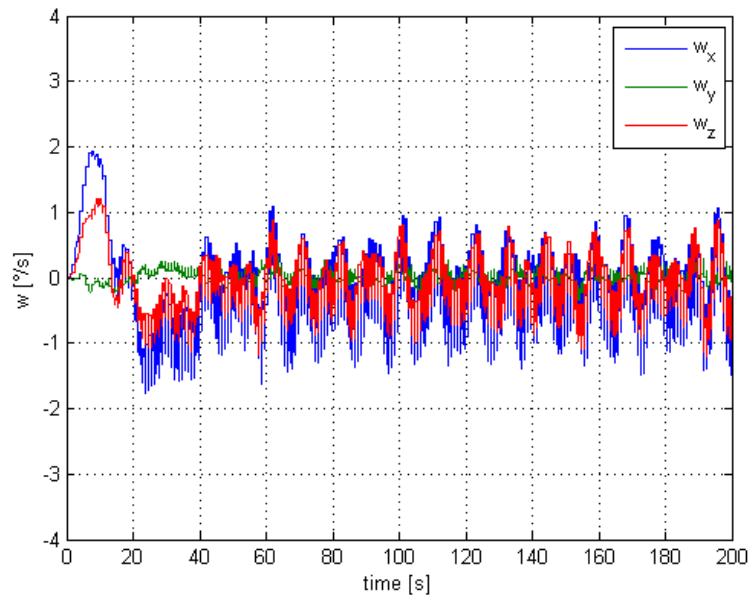
Fig 11.2 Transverse on longitudinal velocity component, percental error (manoeuvre n°1)
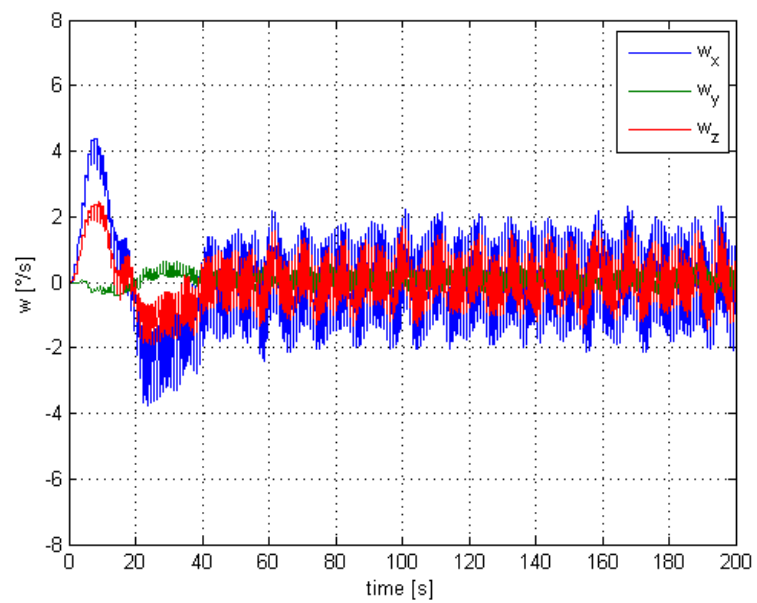
Fig 11.3 Angular rate (manoeuvre n°1)
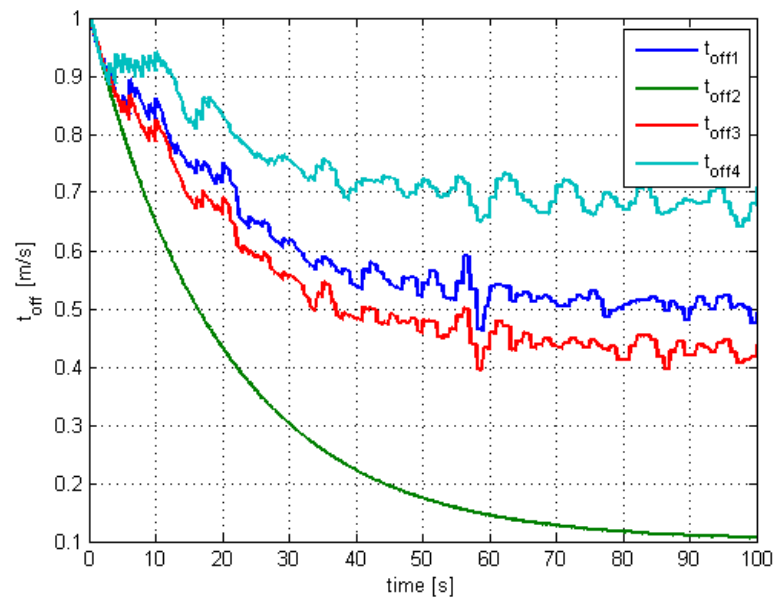
11.4 Thrusters off-time, initial transitory (manoeuvre n°1)

Manoeuvre n°2

Required $\Delta v = 244\ m/s$

Average mass $= 156\ Kg$

Minimum thruster off time (per sample)$= 0.4\ s$

Error on the assumed moments of inertia $= -5\%$ of the actual values

Error on CoG estimation $=\ [4; -15.6; 23.3]\%$ of the actual values

Error on bias estimation $= 11.5\%$ of the actual values
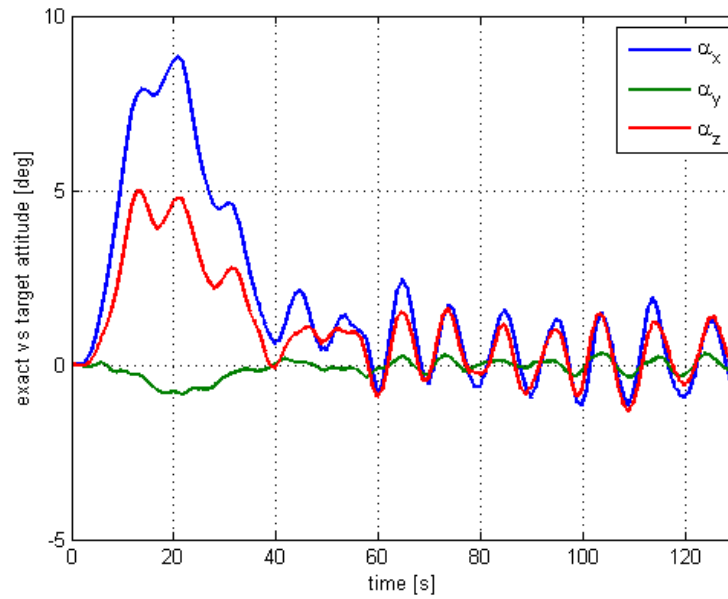
Manoeuvre duration $1198\ s$ ($\approx$20 min)
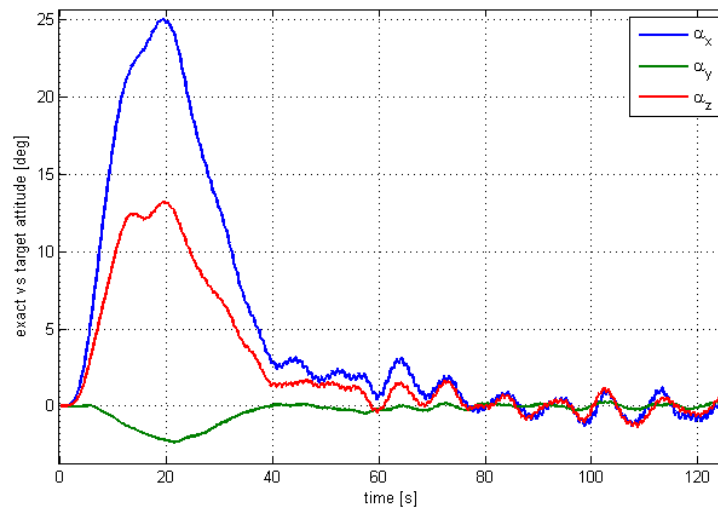
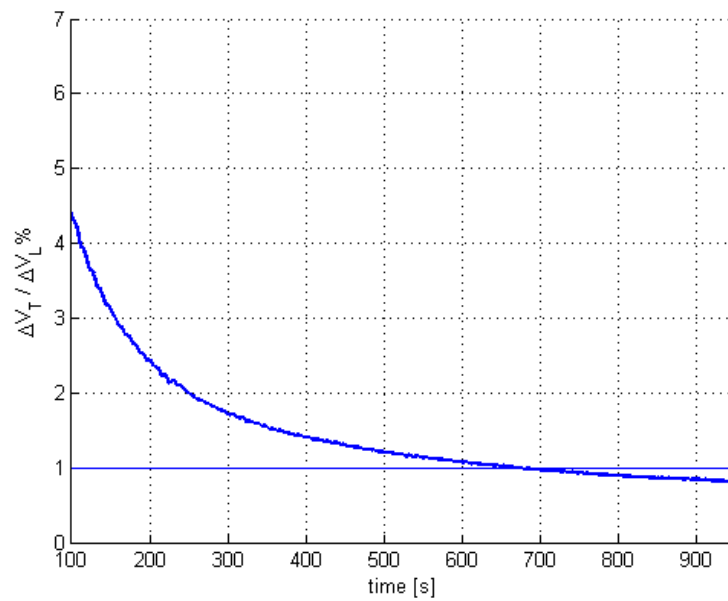Fig 11.5 True/desired attitude error angles, initial transitory (manoeuvre n°2)
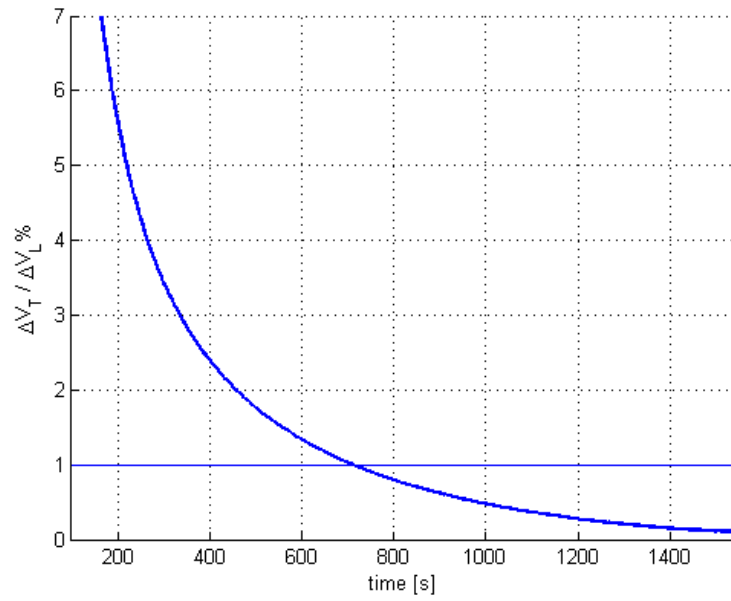
Fig 11.6 Transverse on longitudinal velocity component, percental error (manoeuvre n°2)
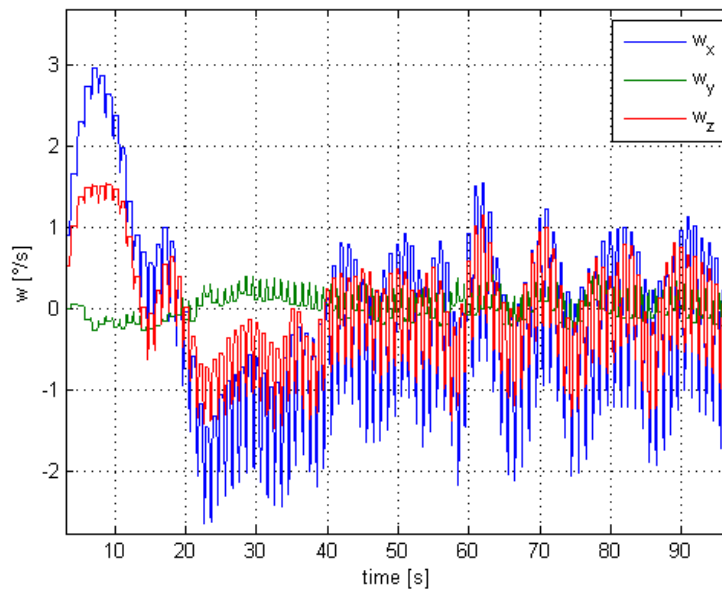
11.7 Angular rate (manoeuvre n°2)
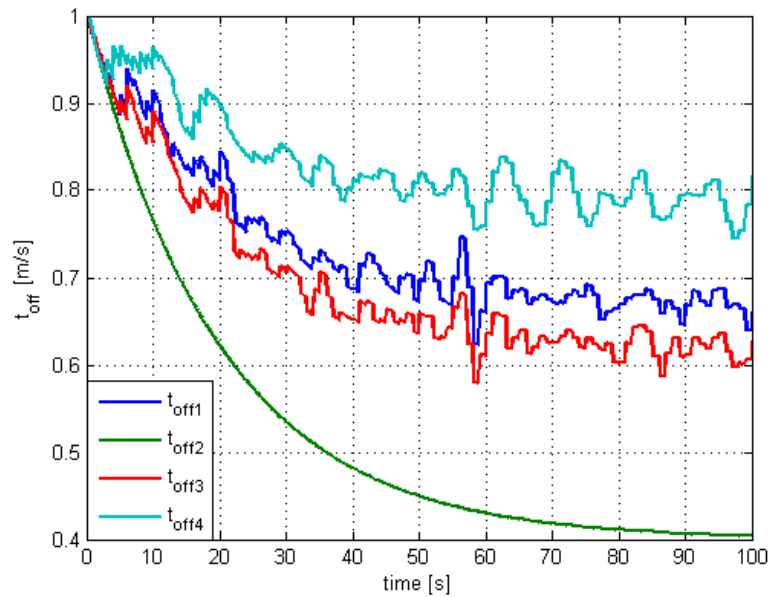
11.8 Thrusters off-time, initial transitory (manoeuvre n°2)

Manoeuvre n°3

Required $\Delta v = 142 \, m/s$

Average mass $= 145 \, Kg$

Minimum thruster off time (per sample)$= 0.6 s$

Error on the assumed moments of inertia $= -10\%$ of the actual values

Error on CoG estimation $= [4; -15.6; 23.3]\%$ of the actual values

Error on bias estimation $= -15\%$ of the actual values

Manoeuvre duration $930 \, s \, (\approx 15.5 \text{ min})$
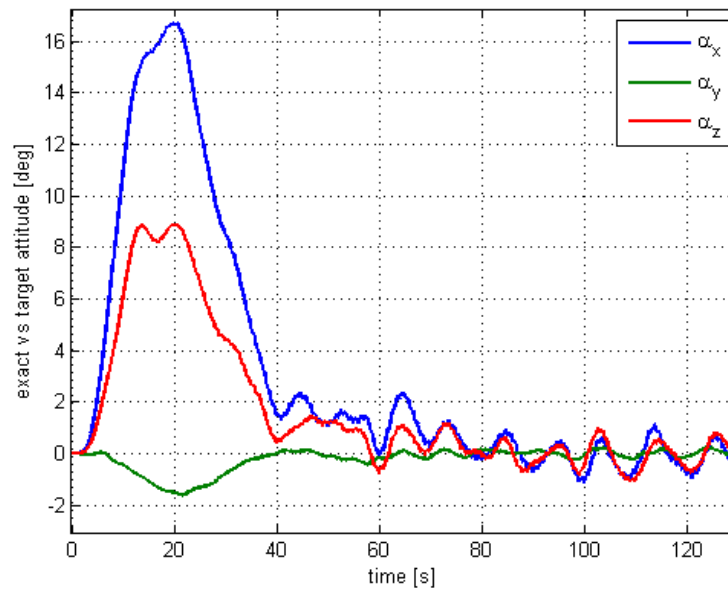
Fig 11.9 True/desired attitude error angles, initial transitory (manoeuvre n°3)

Fig 11.10 Transverse on longitudinal velocity component, percental error (manoeuvre n°3)
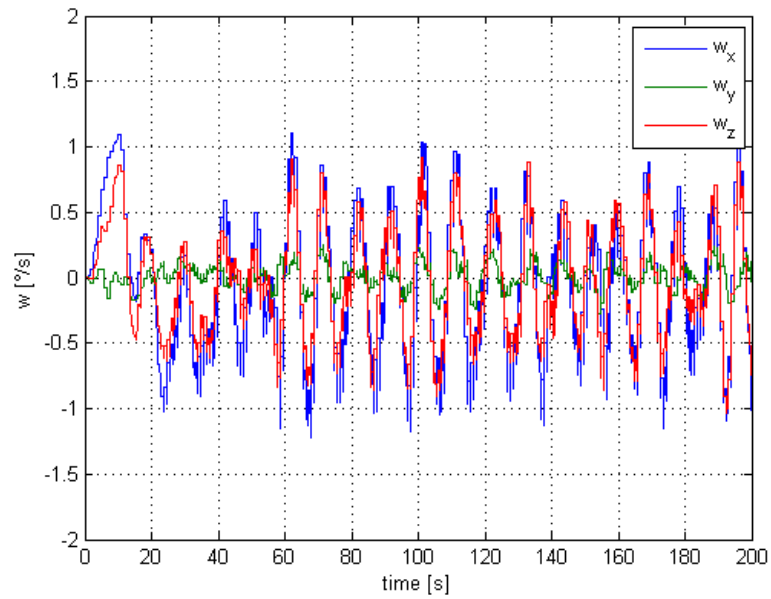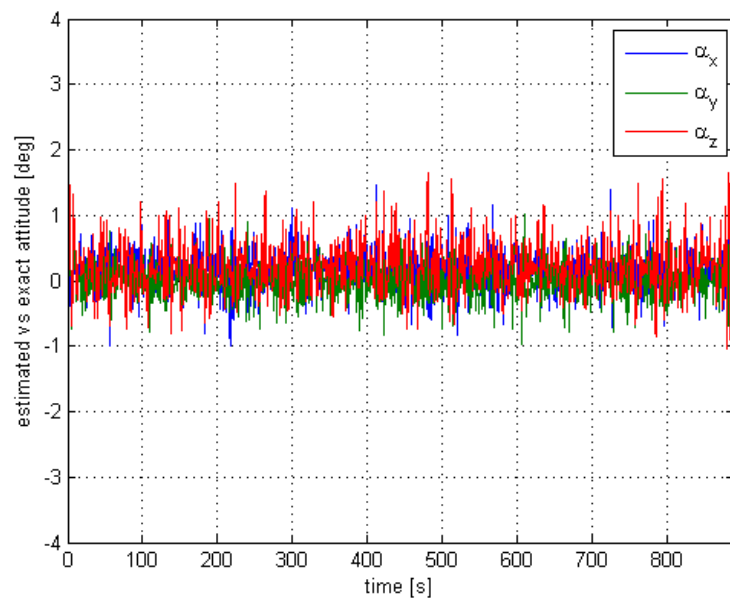
11.11 Angular rate (manoeuvre n°3)

Manoeuvre n°4

Required $\Delta v = 71 \, m/s$

Average mass $= 139 \, Kg$

Minimum thruster off time (per sample)$= 0.8 \, s$

Error on the assumed moments of inertia $= -5\%$ of the actual values

Error on CoG estimation $= \; [-15; -15; -15]\%$ of the actual values

Error on bias estimation $= -15\%$ of the actual values

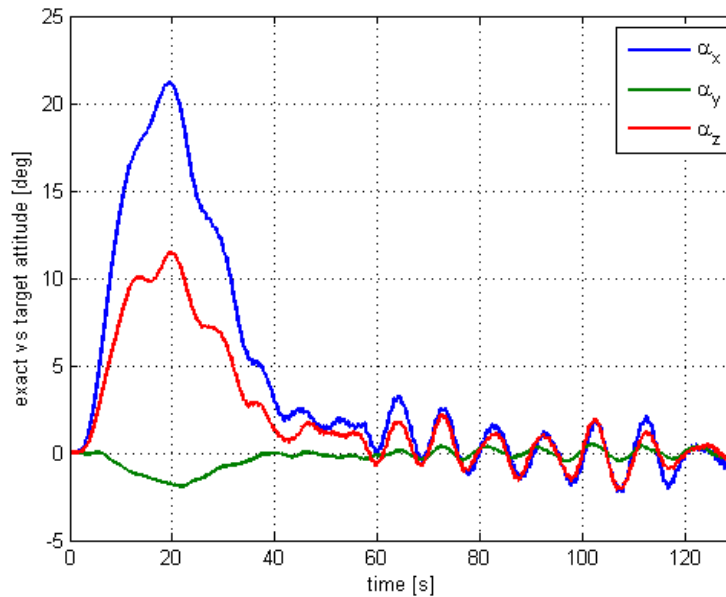Manoeuvre duration $913 \, s$ (≈ 15.2 min)

Fig 11.12 True/desired attitude error angles, initial transitory (manoeuvre n°4)
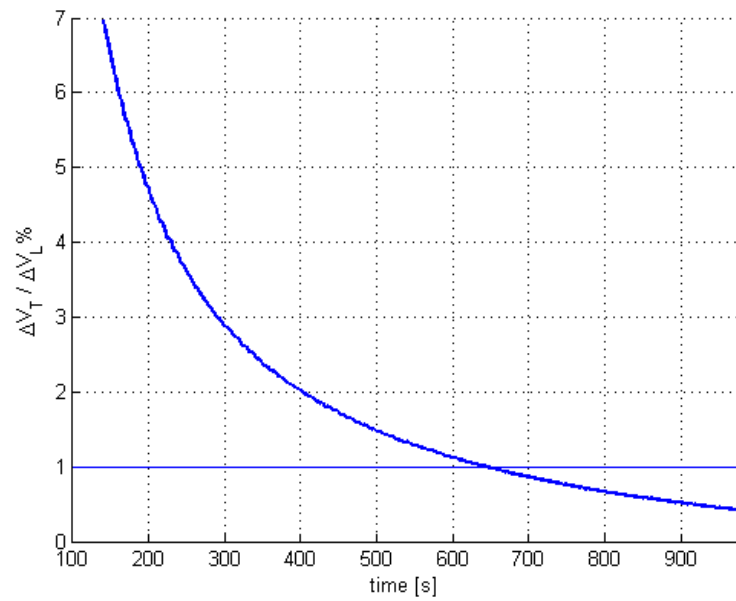

Fig 11.13 Transverse on longitudinal velocity component, percental error (manoeuvre n°4)
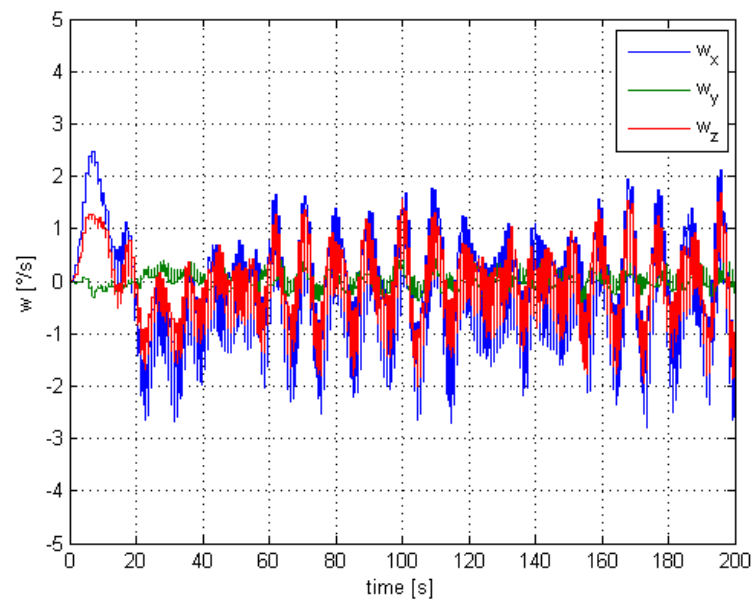
Fig 11.14 Angular rate (manoeuvre n°4)

Fig 11.15 True/estimated attitude error angles, initial transitory (manoeuvre n°4)

<u>Manoeuvre n°5</u>

Required $\Delta v = 200\ m/s$

Average mass $= 132\ Kg$

Minimum thruster off time (per sample)$= 0.5\ s$

Error on the assumed moments of inertia $= +5\%$ of the actual values

Error on CoG estimation $= [4; -15.6; 23.3]\%$ of the actual values

Error on bias estimation $= +20\%$ of the actual values

Manoeuvre duration $976\ s$ (≈ 16.2 min)

Fig 11.16 True/desired attitude error angles, initial transitory (manoeuvre n°5)

Fig 11.17 Transverse on longitudinal velocity component, percental error (manoeuvre n°5)

Fig 11.18 Angular rate (manoeuvre n°5)

Manoeuvre n°6

Required $\Delta v = 101\ m/s$

Average mass $= 124.5\ Kg$

Minimum thruster off time (per sample)$= 0.7\ s$

Error on the assumed moments of inertia $= +5\%$ of the actual values

Error on CoG estimation $= [20; 20; 20]\%$ of the actual values

Error on bias estimation $= -15\%$ of the actual values
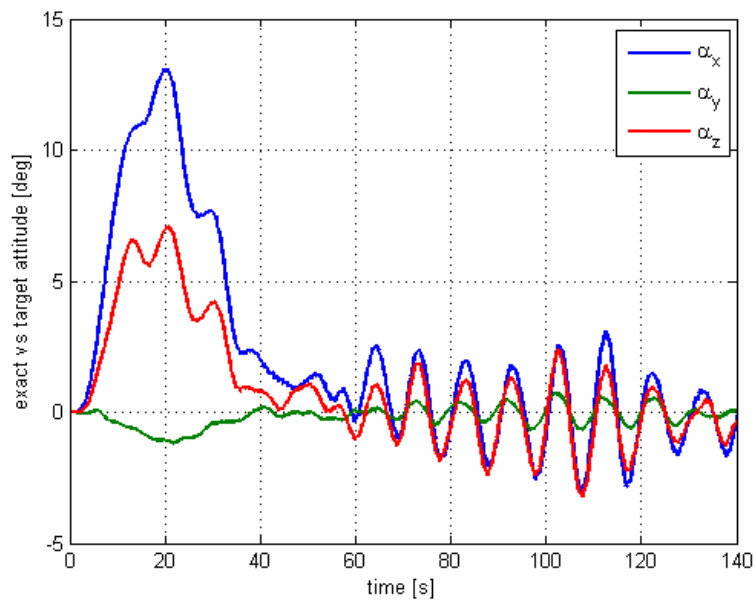
Manoeuvre duration 779 s ($\approx$ 13 min)

Fig 11.19 True/desired attitude error angles, initial transitory (manoeuvre n°6)

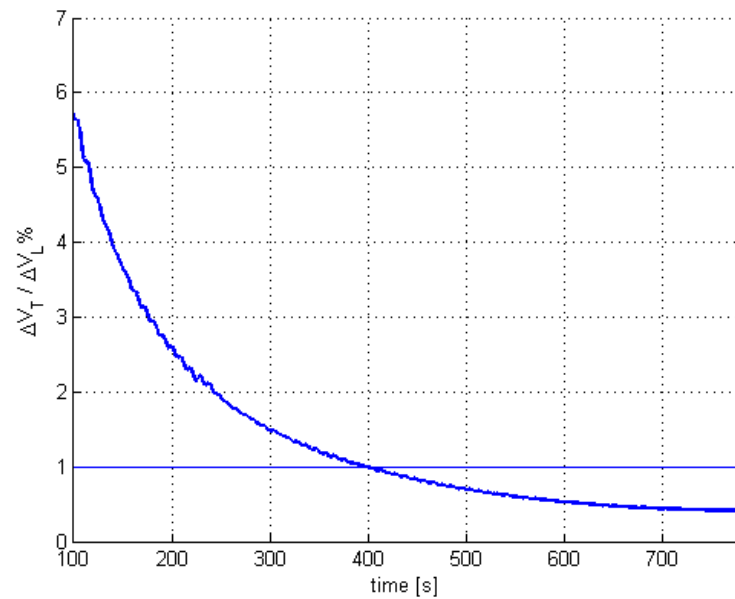The following graph shows the percental Δv error (defined in section 2.2) versus time.

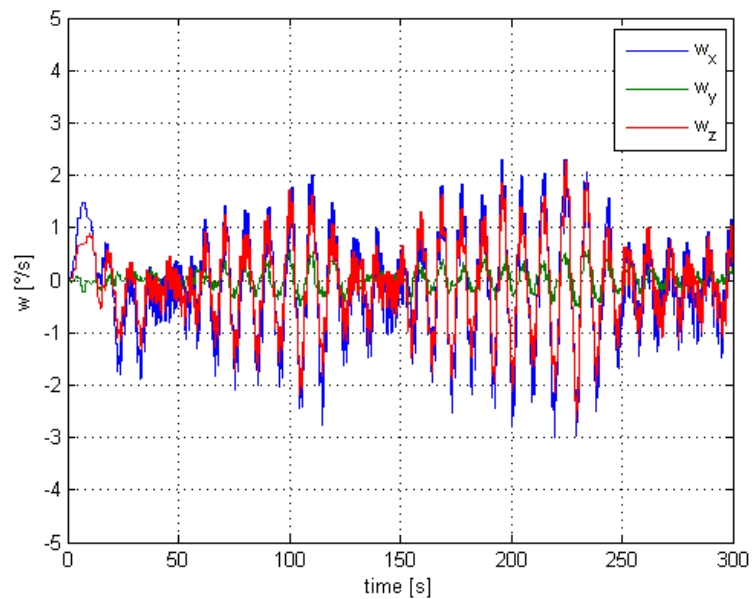Fig 11.20 Transverse on longitudinal velocity component, percental error (manoeuvre n°6)

Fig 11.21 Angular rate (manoeuvre n°6)

A 6 m/s manouvre is required by the mission analysis team. It is very difficult to perform such a small Δv with so powerful engines. The cold gas thrusters could be employed to perform it, if their strength is increased (say 2 N), even assuming

a small specific impulse (say 68s), less than 1.5 Kg of gas is required. This is just a proposal which requires to be investigated.

11.1 Parameters role

Simulations pointed out how designing the compensator with a phase margin smaller or just above 30 deg produces an oscillating response. The oscillations are moderate ($\pm 10°$) and they do not affect the system performances but they are significantly reduced ($< 1°$) by simply increasing the phase margin of a few units. It is important to distinguish this kind of *attitude oscillations* from the one generated by the angle error dead band encounter (which are normally associated with the on/off modulation scheme) and finally from the one induced by fluctuations of the estimated attitude around the actual one.

The amplitude of actual *angular rate oscillation* increases proportionally to the thrusters maximum on-time: for a strong manoeuvre (max on time = 0.9s) it ranges between $\pm 2°$/s (for t > 80s) with bigger values during the initial transitory phase (two peaks of 4.5 °/s). For a weak manoeuvre (max on time = 0.3s) it ranges between $\pm 3°$/s but the values depend also to the error on the assumed moments of inertia as showed before.
The biggest angular acceleration introduced by the MEN firing is less than $13°/s^2$, for both strong and weak manoeuvres, obviously it doesn't matter how long is the engines on time because angular acceleration depends only on thrusters induced torque and not on impulse.

In order to evaluate how uncertainties on moments of inertia affect the system response manoeuvre 6 is analyzed considering the following situations:

Error on CoG estimation = $[4; -15.6; 23.3]\%$ of the actual values

Error on bias estimation = 11.5% of the actual values

The effects of errors on system response:

System response related to errors on the assumed moments of inertia of -10, +5 and +10 per cent are showed respectively in figures 11.16, 11.17 and 11.18
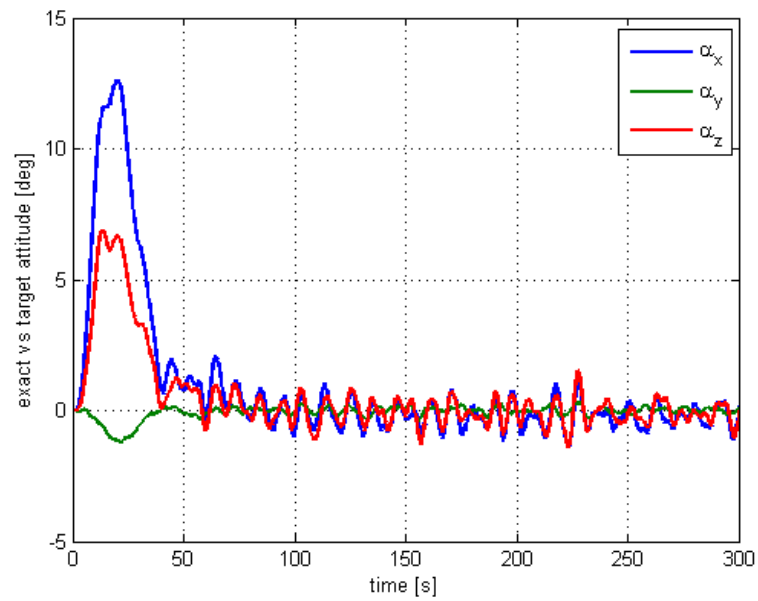
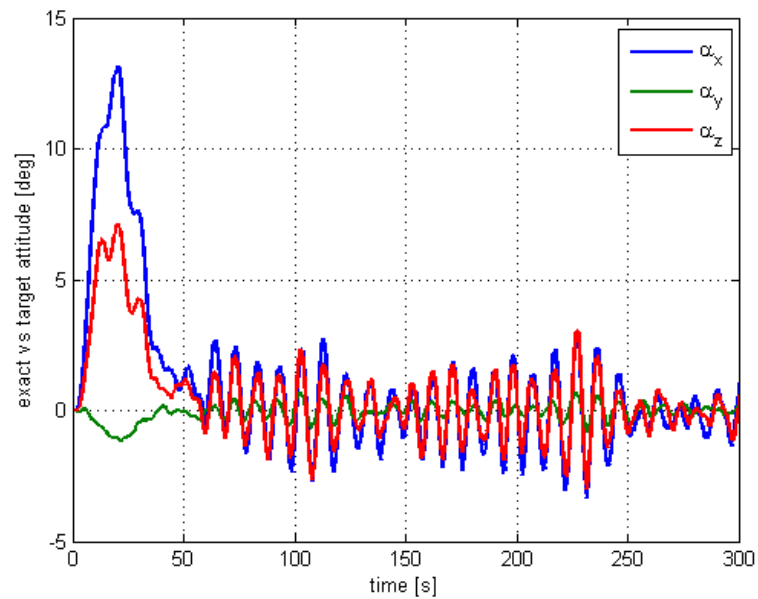Fig 11.22 True/desired attitude error angles, initial transitory (manoeuvre n°6, $I_{err} = -10\%$))

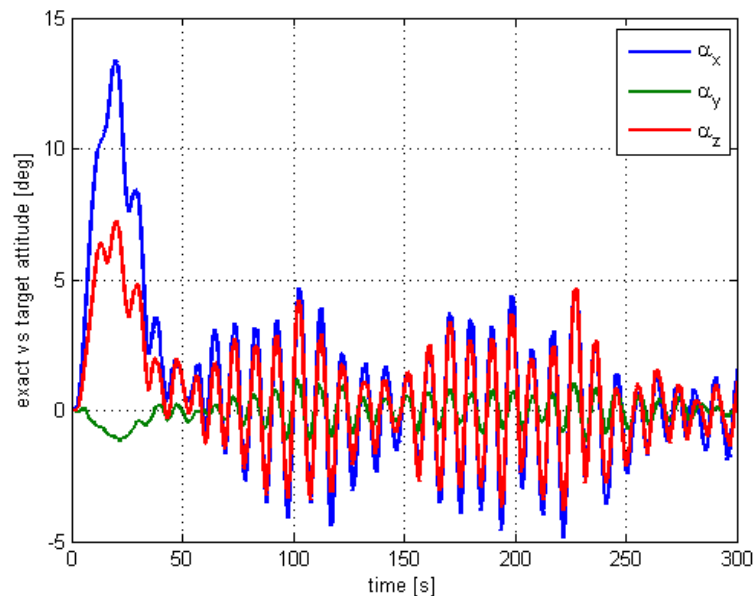Fig 11.23 True/desired attitude error angles, initial transitory (manoeuvre n°6, $I_{err} = +5\%$)

Fig 11.24 True/desired attitude error angles, initial transitory (manoeuvre n°6, $I_{err} = +10\%$)

The overestimation originates undesired oscillations because the compensator is designed to meet moments of inertia bigger than they actually are. Anyway system is stable but the manoeuvre get longer and more propellant is required. Therefore an underestimation of moments of inertia, as long as it is limited, is preferred rather than an overestimation.

Diverse uncertainties on gyros bias have been considered , under/over estimation does not change the results. An explanation to this fact can be found in gyro inability of properly catching the system angular rate oscillations. Therefore the Kalman filter semi-automatically[9] weights the sensors contributions giving less importance to gyros.

The Centre of Gravity shift is now considered. First, it is studied how errors on the assumed CoG position affect the system.
Manoeuvre 4 is simulated varying the error on the effective centre of gravity shift. The following situation is considered:

Error on bias estimation $= 11.5\%$ of the actual values

Errors on moments of inertia $=-5\%$ of the actual values

---

[9] semi-automatically is used instead of automatically because several degrees of freedom of the filter such as S_D, S_G σ_{SCS}etc.. are set by the analyst.

Errors on the assumed Centre of Gravity shift of -30,+15 and +30 per cent are considered.
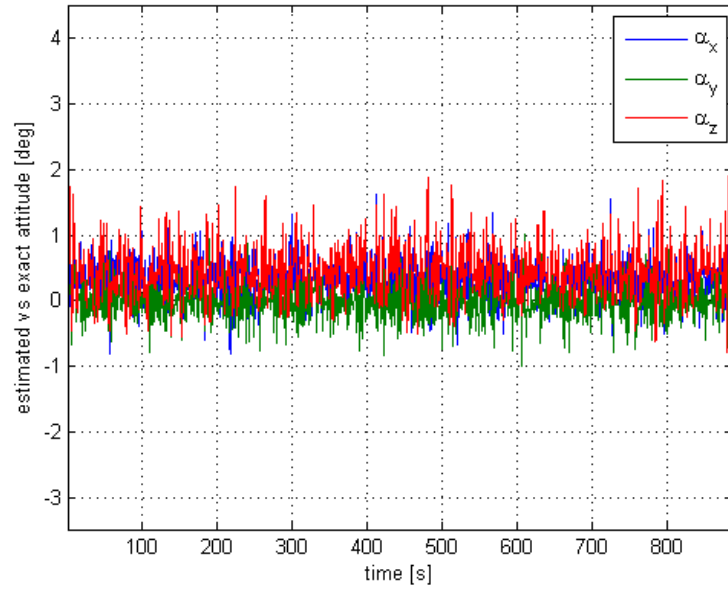

Fig 11.25 True/estimated attitude error angles with 30% underestimation of the actual CoG shift (manoeuvre n°4)
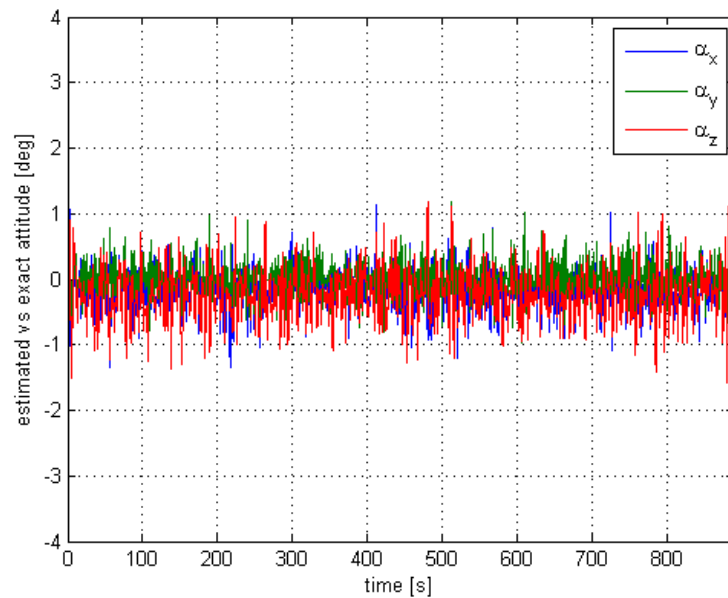

Fig 11.26 True/estimated attitude error angles with 15% overestimation of the actual CoG shift (manoeuvre n°4)
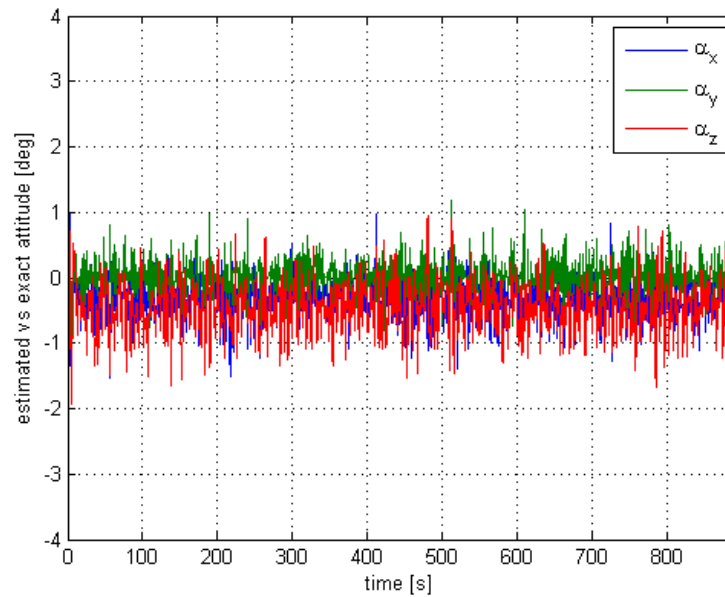
Fig 11.27 True/estimated attitude error angles with 30% overestimation of the actual CoG shift (manoeuvre n°4)

Looking carefully to the graphs a mean value for each signal can be identified. Fig. 9.8 shows that exact propagation drives to a zero mean error, while Fig. 11.25, Fig. 11.26 and Fig. 11.27 testify that errors in estimating the CoG position generate non zero mean errors on the estimated attitude.
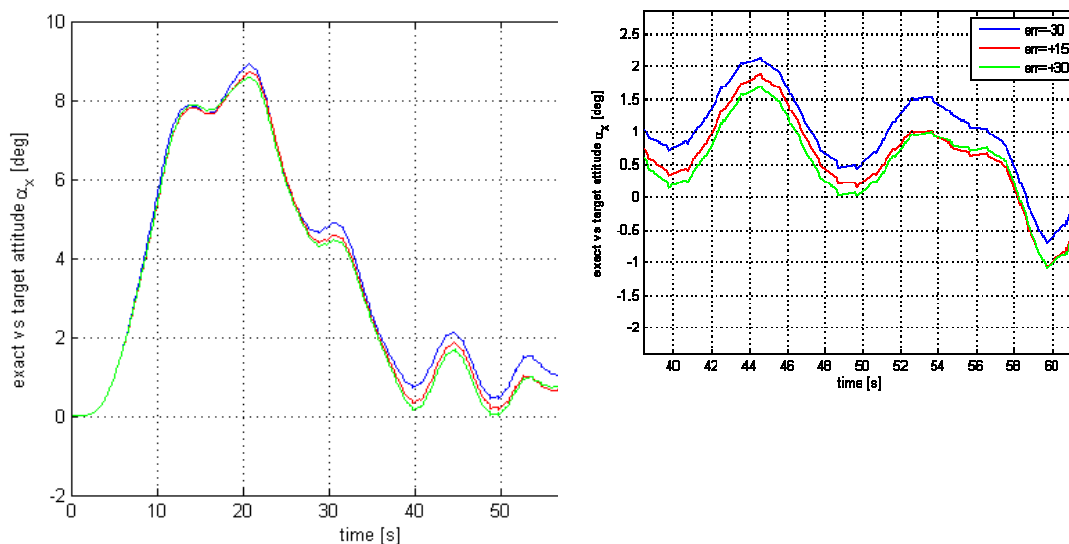

Fig 11.28 True/desired attitude first Euler angle. Effects of over/under estimating the CoG shift (manoeuvre n°4)

The important consequences of error in estimating of the CoG position regard system performances.
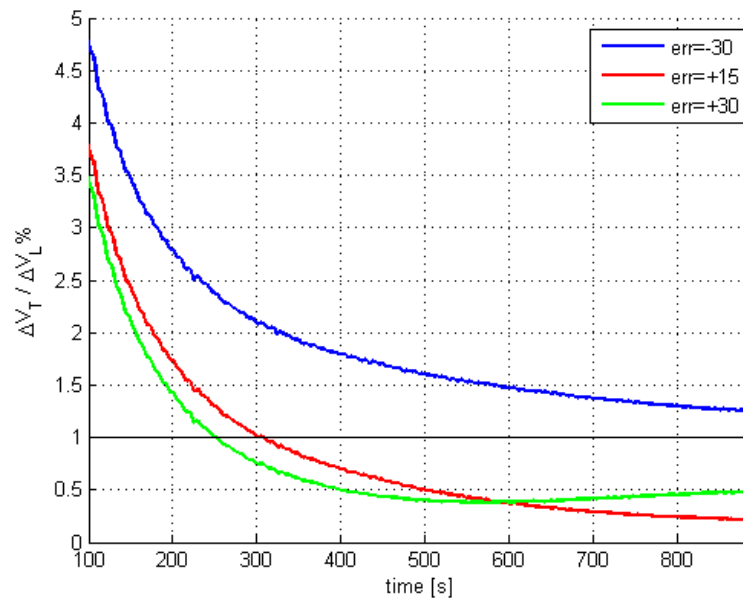

Fig 11.29 Transverse on longitudinal velocity component, percental error. Effects of over/under estimating the CoG shift (manoeuvre n°4)

the analyses results show how an overestimation of the CoG shift is preferred rather than an underestimation. This is due to the fact that the error on Cog estimation forces the error on attitude to oscillate around a constant non zero value (see Fig.11.19, 11.20 and 11.21) whose value in half of the cases is opposite to the one of the initial peak. This fact makes the compensation of the initial peak faster, or slower in case the sign is the same, than the one in absence of any error on the evaluation of the CoG position.

Now the effects of shifting the Centre of Gravity from the ideal position but within the given band are analyzed[10] considering manoeuvre 3 and the following data:

Error on moments of inertia knowledge $= -10\%$ of the actual values

Error on CoG estimation $= 0\%$ of the actual values

Error on bias estimation $= 1.5\%$ of the actual values

---

[10] It is important to distinguish between the error on the assumed centre of gravity shift and the effective centre of gravity shift, which is now considered

The following graphs compare three situations, 20, 50 and 75 % of the maximum CoG shift
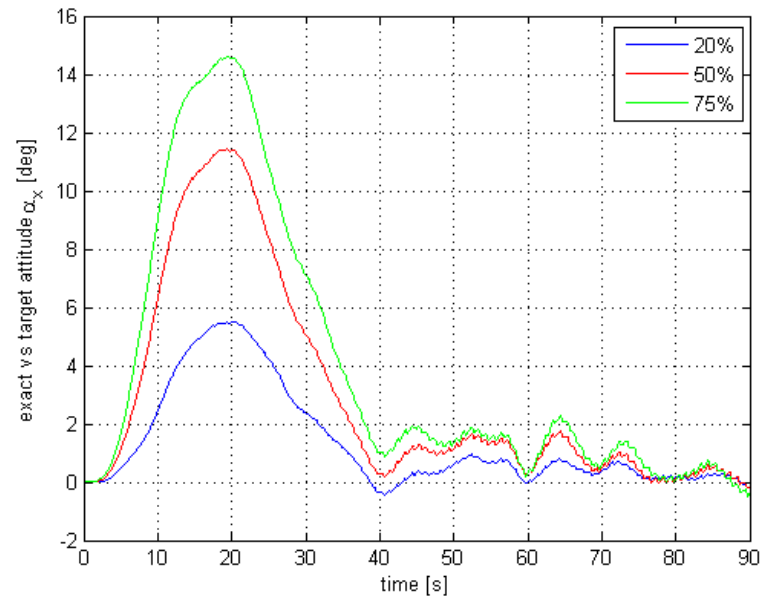

Fig 11.30 True/desired attitude first Euler angle. Effects of the CoG shift (manoeuvre n°3)
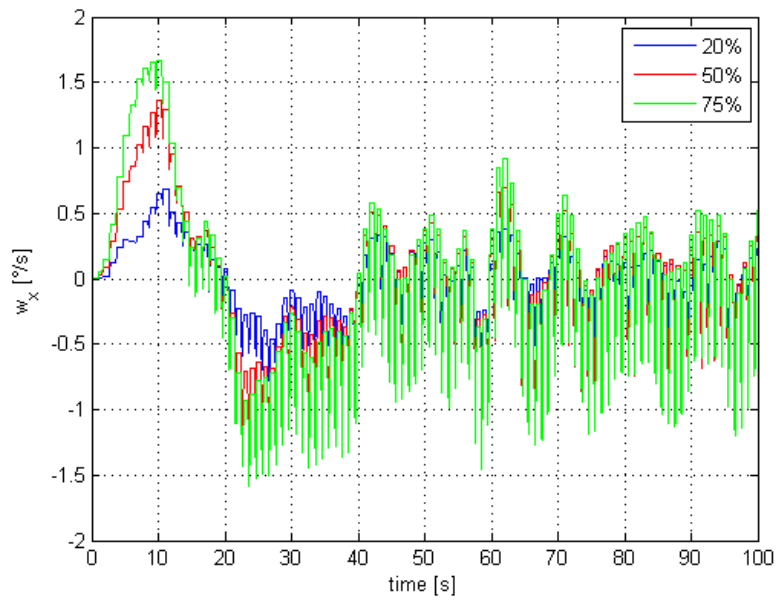

Fig 11.31 Angular rate about the x axis. Effects of the CoG shift (manoeuvre n°3)
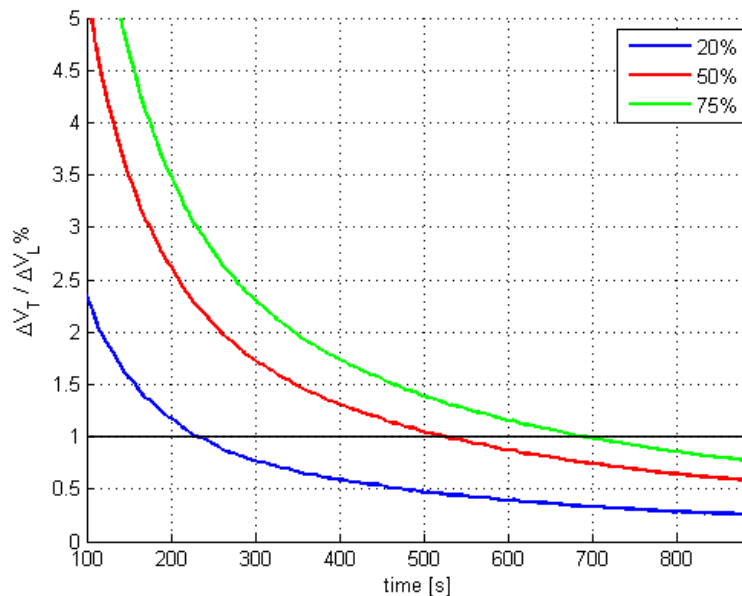
Fig 11.32 Transverse on longitudinal velocity component, percental error. Effects of the CoG shift (manoeuvre n°3)

Comparing figure 11.26 with figure 11.7 it looks that better performances are achieved in presence of errors on the estimated CoG rather than in their absence. This phenomenon has just been explained (last paragraph above).

11.2 Initial Peak

It is important to remember that the assumed initial peak is an overestimation of the effective value, therefore actual results will surely be less critical.
Several aspects produce the initial displacement:

-   The main engines are very powerful. The bigger is the minimum thruster off time the smaller is the initial peak and the longer is the manoeuvre .
-   Line delay and sample and hold force the control system design to keep low gains not to destabilize the system. The bigger is the line delay the bigger is the initial peak.

Considering manoeuvre 1, as the line delay is cut out and the compensator parameters are updated (to obtain the same gain and phase margin of the delayed case) the system response looks dumped and shows smaller displacement.

Even if the peak is smaller, the attitude error on each axis keep the same sign for all the transitory. This fact is negative looking to performances. Indeed the initial slow and wide oscillation around the desired attitude, showed by the delayed configuration, partly compensates itself and paradoxically gives a smaller final error on the applied Δv.
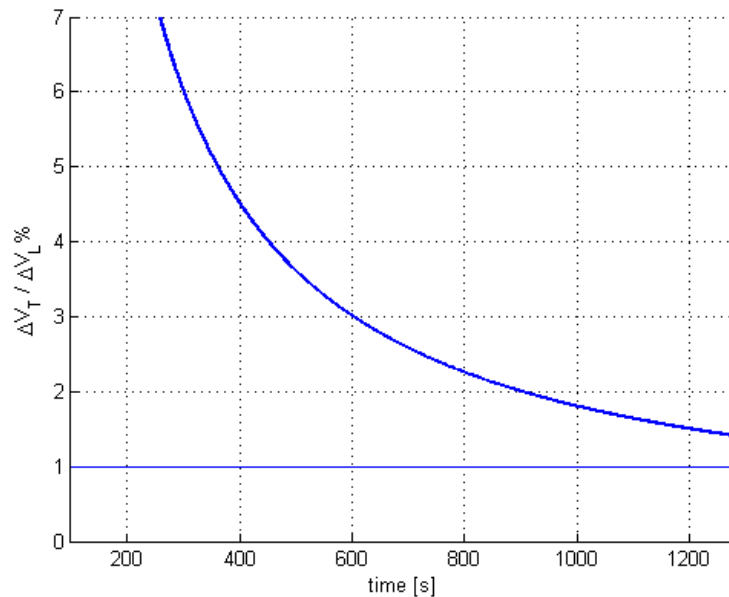
Fig 11.33 Transverse on longitudinal velocity component, percental error (manoeuvre n°1) no line delay

Several artifices have been adopted to get rid of the initial peak:

Previously to the manoeuvre the firing axis is pointed away from the desired Δv direction so that the initial kick pushes the s/c close to the desired attitude.
No improvements have been obtained and this solution has been discarded.
Considering the CoG shift it is important to distinguish between the effective CoG position and its approximation. The first one, as stated above, is directly related to the initial peak while the precision in the knowledge of the CoG position affects the attitude estimation process and especially performances. Error in attitude estimation and uncertainty on system moments of inertia do not sensibly modify the initial peak.

Effective compensation of the peak has been obtained predicting the disturbance torques related to the control action. Then the difference between desired and supplied torque is summed to the required torque.

Since the thruster off time is obtained assuming a symmetric configuration for thrusters the applied impulse is different from the required one. An approximation of that difference is calculated

$$\underline{T}_{err} = \hat{\underline{T}}_c - \underline{T}_a \qquad\qquad 11.3$$

$\underline{T}_a$ is a representative torque which is not effectively applied but multiplied by the sampling interval t_S represents the actual applied impulse

$$\underline{T}_a t_S = \underline{T}_{ON}\left(\underline{1} - \underline{t}_{OFF}\right) \qquad\qquad 11.4$$

$\underline{\underline{T}}_{ON}$ is a 3x4 matrix containing on each column an approximation of the torque introduced by each thruster firing; $\underline{1}$ is a unit vector. Therefore $\underline{\underline{T}}_{ON}\left(\underline{1} - \underline{t}_{OFF}\right)$ approximates the provided impulse on each axis during a single sample.
Therefore torque request is updated

$$\hat{\underline{T}}_c = \underline{T}_c + \underline{T}_{err} \qquad\qquad 11.5$$

This strategy has been applied to manoeuvre 1because it is characterized the biggest peak. Remembering its data

Required $\Delta v = 404 \ m/s$

Average mass $= 176 \ Kg$

Minimum thruster off time (per sample) $= 0.1 \ s$

Error on the assumed moments of inertia $= -10\%$ of the actual values

Error on bias estimation $= 11.5\%$ of the actual values

Error on CoG estimation $= [4; -15.6; 23.3]\%$ of the actual values

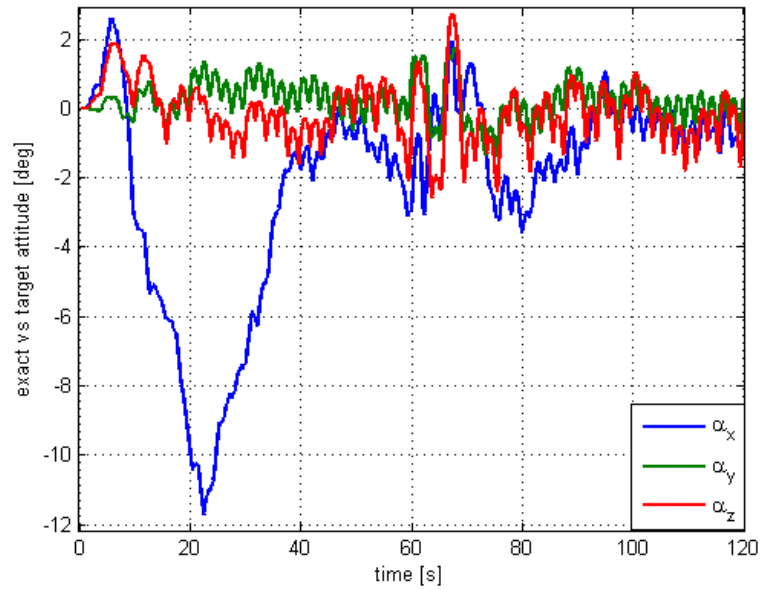In this case the manoeuvre becomes slightly longer: $1555 \ s$ (26 min)

Fig 11.34 True/desired attitude error angles, initial transitory (manoeuvre n°1, error on CoG= $[\mathbf{4}; -\mathbf{15}.\mathbf{6}; \mathbf{23}.\mathbf{3}]$%)

Comparing figure 11.29 with figure 11.1 the benefic action of pre-compensating the disturbances is highlighted.
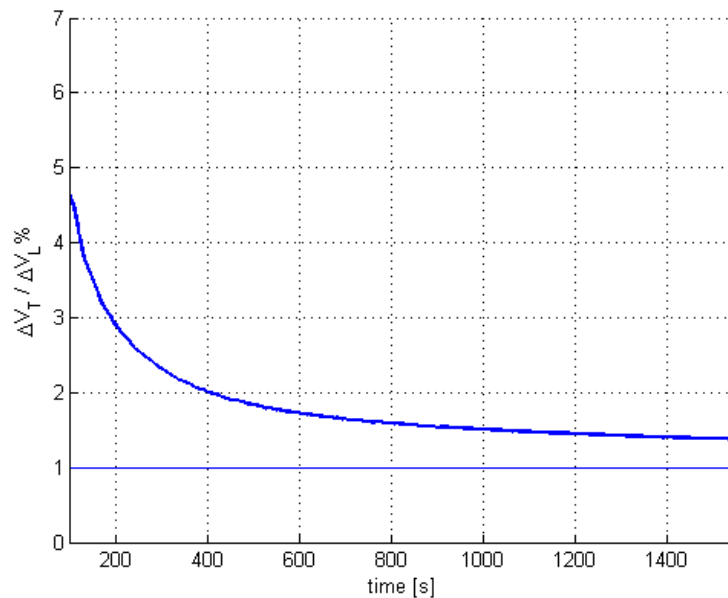

Fig 11.35 Transverse on longitudinal velocity component, percental error (manoeuvre n°1, error on CoG= [4;-15.6;23.3]%)
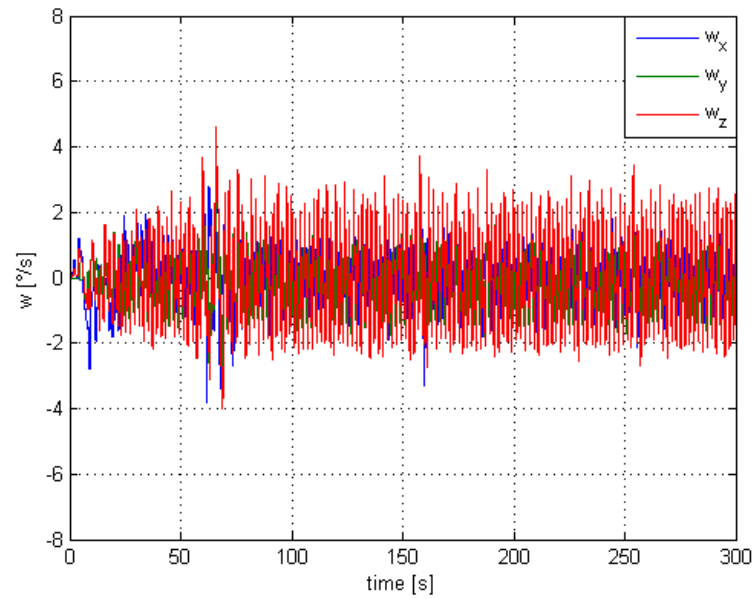
Fig 11.36 Angular rate (manoeuvre n°1, error on CoG= [4;-15.6;23.3]%)

Benefits of this strategy are very sensitive to precision in estimating the CoG position. Different values of accuracy have been considered and results are now exposed.

Error on CoG estimation = -20% of the actual value

Fig 11.37 True/desired attitude error angles, initial transitory (manoeuvre n°1, error on CoG= -20%)

Fig 11.38 Transverse on longitudinal velocity component, percental error (manoeuvre n°1, error on CoG= -20%)

Fig 11.39 Angular rate (manoeuvre n°1, error on CoG=-20%)

In this case an underestimation is preferred. Provided that the 1% constraint is raised of a few units, acceptable results are obtained even with -20% of error in estimating the CoG position.

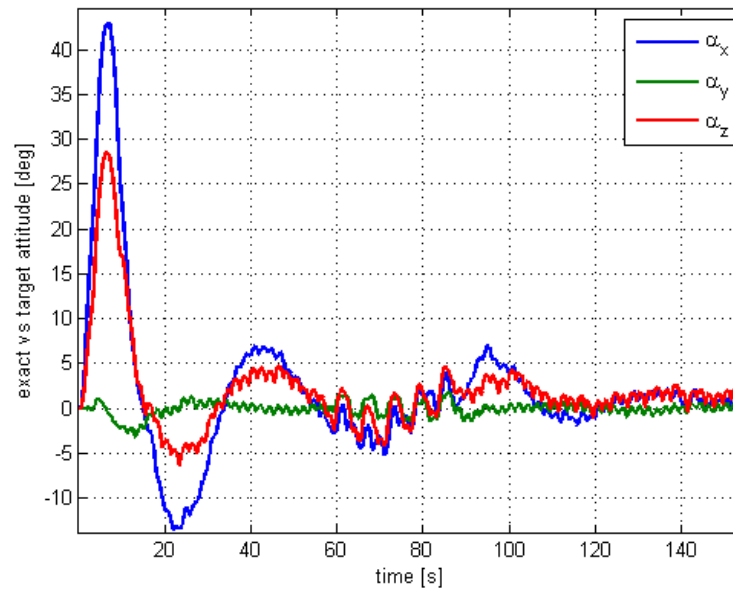Overestimation of the CoG shift is now analyzed:

Error on CoG estimation = +10% of the actual value
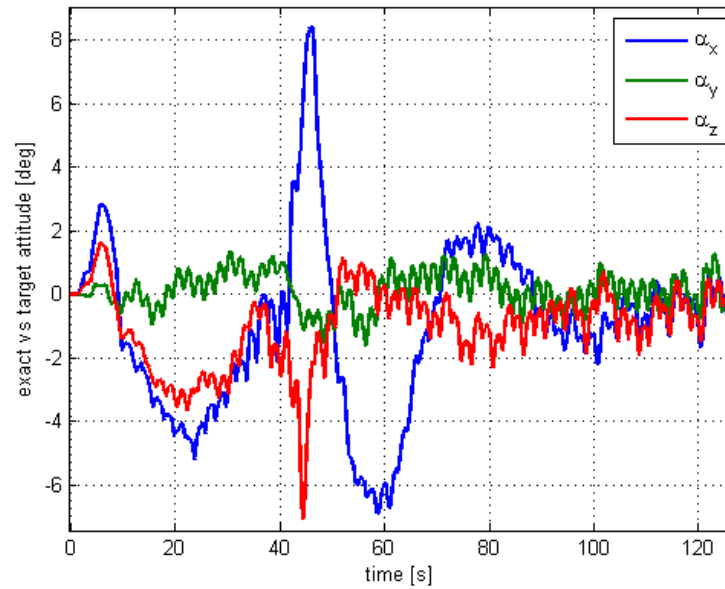
Fig 11.40 True/desired attitude error angles, initial transitory (manoeuvre n°1, error on CoG= +10%)
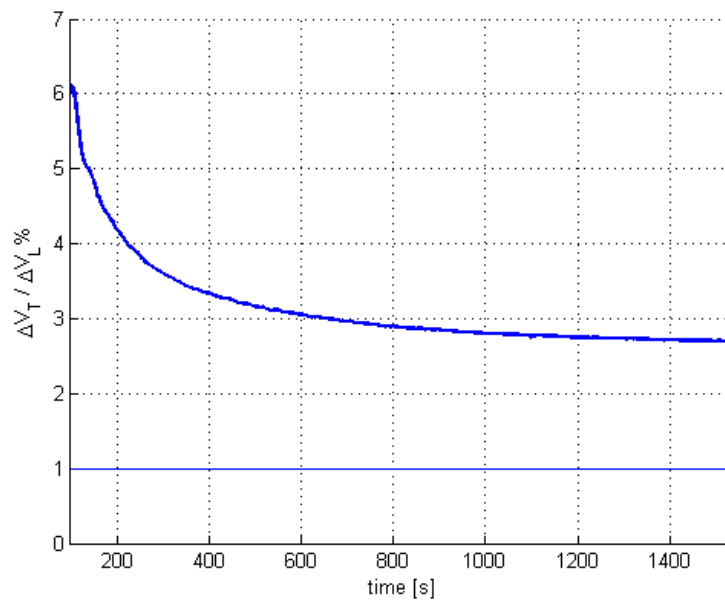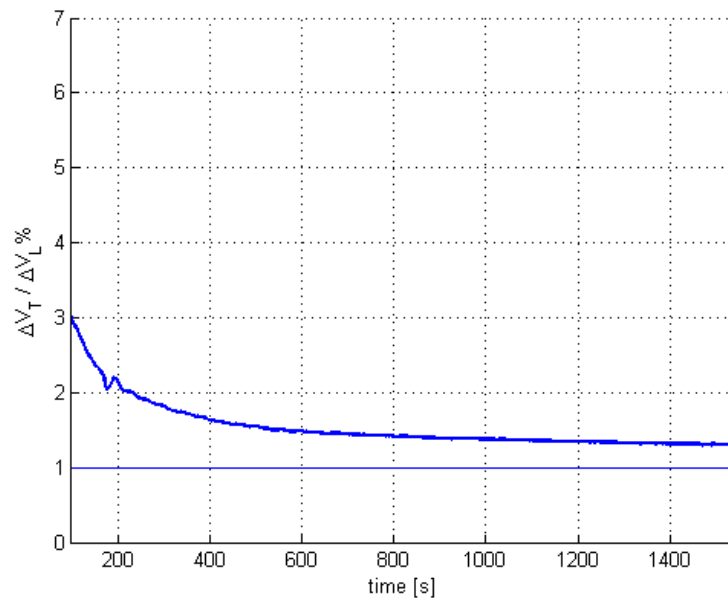

Fig 11.41 Transverse on longitudinal velocity component, percental error (manoeuvre n°1, error on CoG= +10%)
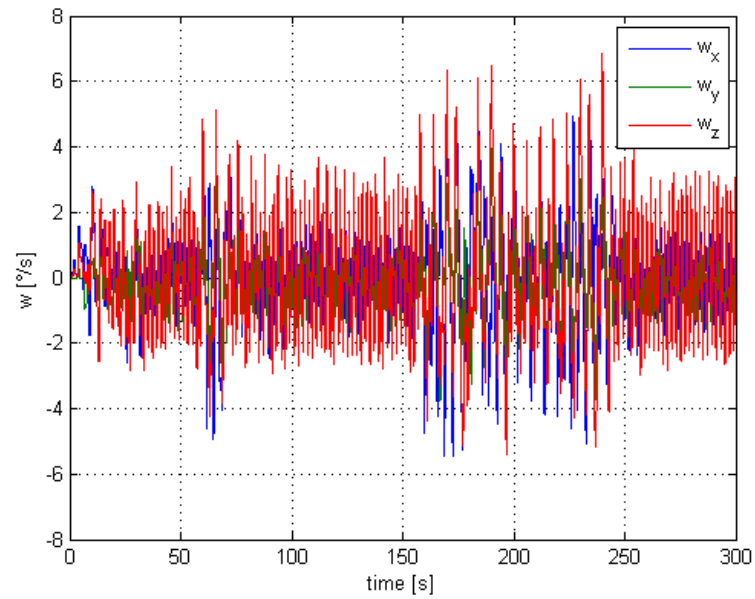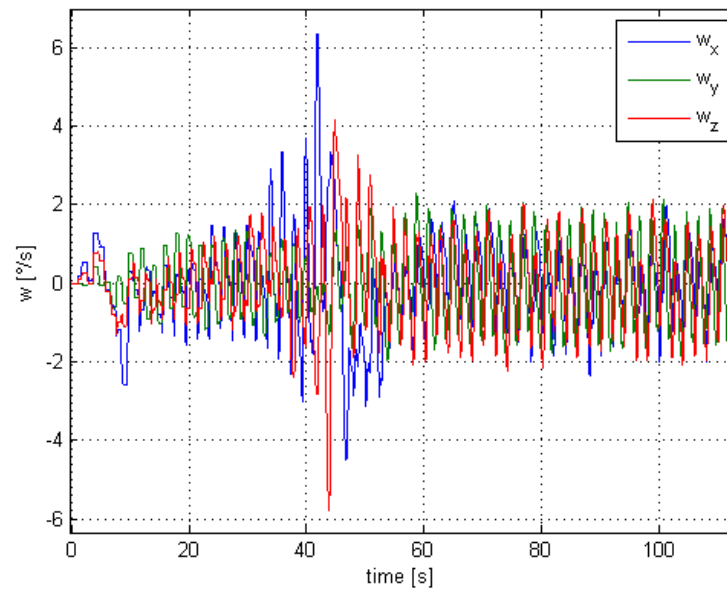
Fig 11.42 Angular rate (manoeuvre n°1, error on CoG=+10%)

The overestimation of the centre of gravity shift means accentuated compensation, which becomes undesired oscillations of attitude and angular rate.

Another way to confine the initial peak is found in passive designing e.g. limiting the effective centre of gravity shift or even moving mass to modify its position.

Chapter 12 Conclusions

A reliable configuration capable of accomplish the mission has been defined. The designed system is able to perform all the manoeuvre respecting requirements and its efficiency has been verified against parameters variation. In order to correctly estimate the attitude a second vector sensor is required being operative during the manoeuvre. Another way is to process gyro measurements at 10 Hz; in this case drift of the estimated attitude (and consequently of the actual attitude) appears but only around the sun vector. This solution is viable as the requirement on manoeuvre accuracy is stretched by the mission analysis team.
The typical initial displacement can be significantly reduced modifying the required control torque given an estimation of disturbances. The efficacy of this compensation depends strictly on the accuracy in approximating the centre of gravity shift.

12.1 Requests to other subsystems

The following requirements flowed down from the analyses of the impulsive trajectory manoeuvres:

Structure team
- A relation between CoG shift and moments of inertia is required to better estimate the CoG position.

Propulsion team
- The MEN are switched on and off during the manoeuvre. Off (on) time of 20 to 1000 ms is required.
- The MEN are canted (10° outwards).
- A time resolution of 1 ms has been assumed for thruster off times that are bigger than MOT (minimum off time = 20ms).

Mission Analysis team
- A more tolerant requirement is demanded at least for the shortest manoeuvres (3÷5%)

Mission Analysis & Configuration teams
- Sun shall be in the Sun sensor field of view during all the manoeuvre

Mission Analysis & Propulsion teams
- The s/c shall cope with reduced thrust (about 55N when the CoG is max shifted).

Mission Analysis & Software & Propulsion teams
- Applied Δv_L, therefore manoeuvres duration, is real time determined as the thrusters off-time is on board calculated.

Software team
- Transmission delay of torque commands shall not exceed 0.7 seconds.
- Processing Gyro measurements at 10 Hz a more reliable estimation of attitude is obtained.

Star Camera team
- The star camera shall be capable of performing measurements (at least one vector) during the manoeuvre.

All the subsystems
- The s/c shall cope with variable angular rate during the manoeuvre (peak values of $30°/s$) and variable angular acceleration (peak values of $16°/s^2$)
- Any components or spacecraft part shall not have natural frequencies close to 1 Hz, because that is the control system frequency.

12.2 Future work

The orbital dynamic is now considered, at some point the beginning of the manoeuvre is commanded. In all the analyses previously exposed that command was assumed being a step but the response could be relaxed imposing a smoother function. This solution is hard to be implemented because the main engines admit only on/off control and any kind of thrust modulation.
Another solution is to introduce 2 accelerometers in the prow of ESMO. Measuring the accelerations along x and z direction it is possible to anticipate

the control action in order to counterbalance disturbances more promptly than using only rate and angular sensors.

Another strategy is to plan the on time sequence previously to the manoeuvre. As soon as the centre of gravity position is estimated with the procedure exposed in chapter 10, a thrusters on sequence covering some fractions of second is guessed . Main engines are fired accordingly to that sequence and after that the spacecraft angular rate is estimated. Then another sequence is planned trying to wipe out any residual angular rate. When the best sequence is determined it is recursively commanded to the thrusters for the whole manoeuvre. As long as the definitive sequence ensures quite fine balancing of torques the cold gas thrusters are suitable to compensate errors in attitude and residual angular rate.

The easiest solution which should be discussed with Mission Analysis team is to split the manoeuvre in multiple firing and to use every break to reset gyro drift.

Appendix

Script description

The Simulink blocks used in modeling the whole system, including sensors, actuators and the external environment are presented.
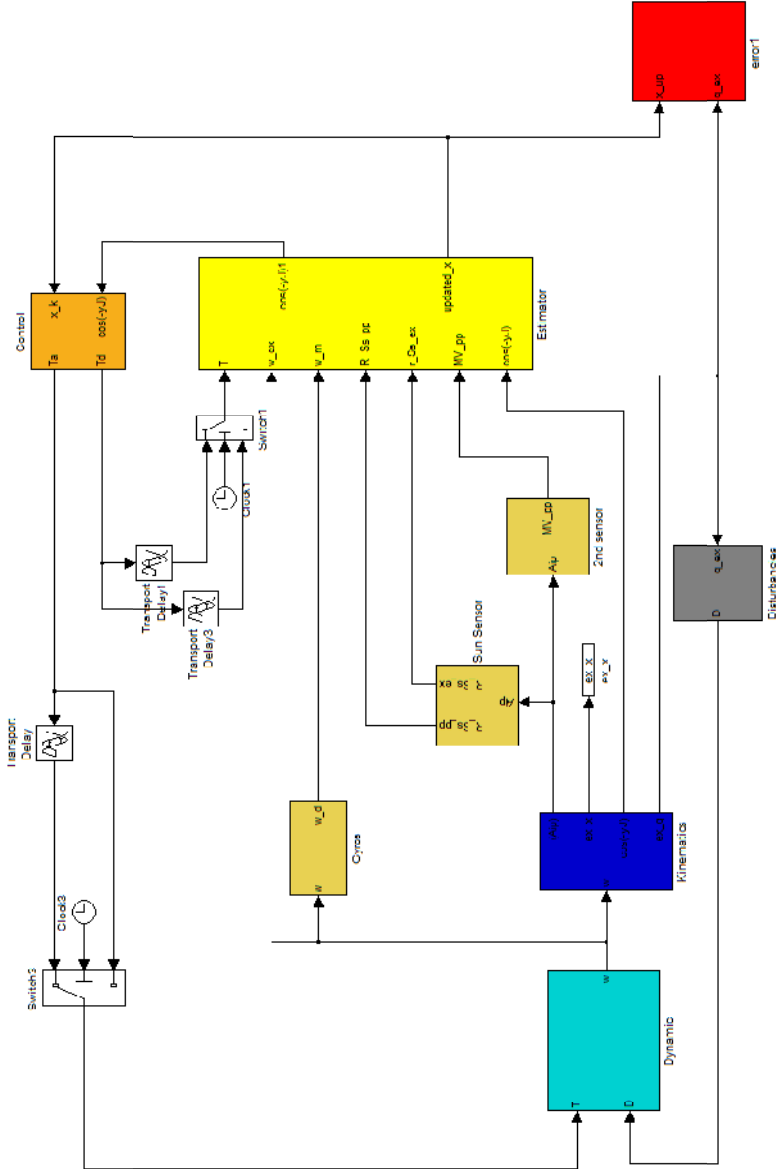
Fig A.1 Simulink Blocks modelling the whole system (level 0)

The blue and light blue blocks in Fig.A.1 contain the exact dynamic and kinematic which is corrupted in the sensors block (ocher color) to simulate the real measuring process. The estimator is implemented into the yellow box, while the actuators and compensator equations are in the orange one.

Fig A.2 Simulink Blocks modelling the estimator (level 1)

Fig.A.2 shows the content of the control block of level zero. Attitude and error covariance matrix are propagated in the light blue boxes. The updating of the propagated variables is performed into the green box using the Kalman gain which is calculated in the light green block.

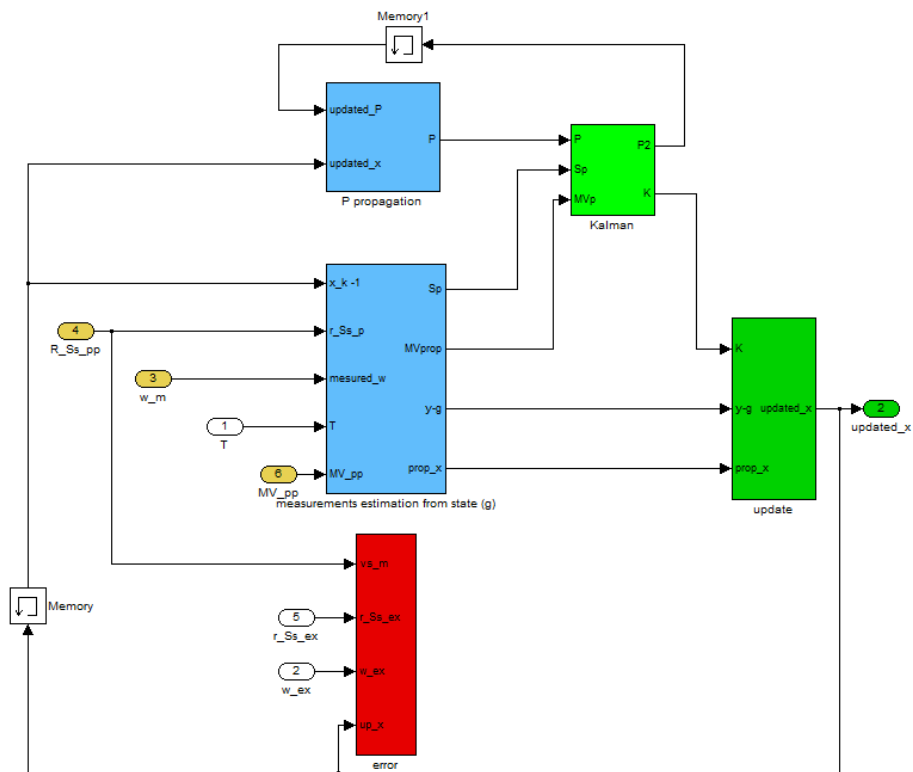Fig A.3 Simulink Blocks modelling the compensator (level 1)

Fig.A.3 shows the content of the control block of level zero. The estimated state vector is the input here while the effective applied torque is the output. Actuators are represented in the teal box while the gray one contains the compensation torque described in section 11.2. The orange block accommodates the discrete control law. Non linear terms and wheels contribution are in the olive and the brown blocks respectively. All the terms that flow into the

rectangular sum contribute in defining the desired control torque as explained at the beginning of chapter 6
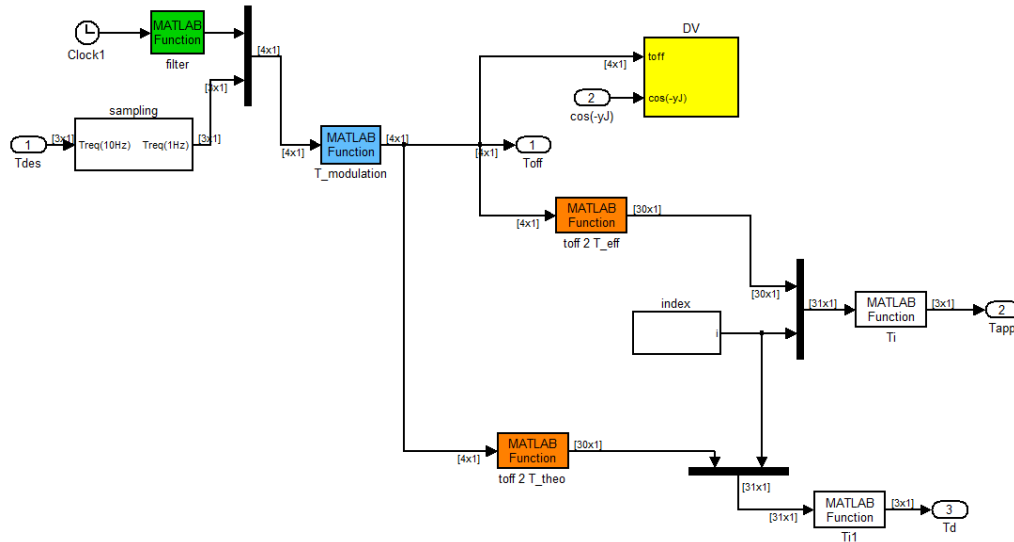

Fig A.4 Simulink Blocks modelling the actuators (level 2)

Torque request is the input, applied torque and its approximation are the output. The blue block converts torque request into thruster off time as explained in section 5.5, while the orange defines the torque time history (exact and approximated) accordingly to the desired off time. The yellow box calculates (in real time) the performed velocity increment as described in section 2.2. The green filter gives the exponential shape to the minimum off time.

Bibliography

[1] James R. Wertz, *Spacecraft Attitude Determination and Control,* Kluwer Academic Publishers, The Netherlands,1978

[2] Robert Grover Brown and Patrick Y.C. Hwang *Introduction to Random Signals and Applied Kalman Filtering, 3rd Edition*, Hardcover, John Wiley & Sons, 1992

[3] Yoshi Hashida, *ADCS for UoSat Standard Platform with Wheels*, SSTL document, October 2007

[4] Tony Holt, *AOCS Thruster Mode Limit Cycling*, SSTL document, August 2006

[5] Kalman, R.E., *A New Approach to Linear Filtering and Prediction Problems*, Transactions of the ASME, Journal of Basic Engineering, Vol. 82, March 1962

[6] Paolo Rocco, *Dispensa del corso di Automatica*, Milano, Ottobre 2001

[7] Paolo Rocco, *Dispensa del corso di Controlli Automatici*, Milano, Gennaio 2004

[8] Marcel J. Sidi, *Spacecraft Dynamics And Control - A Practical Engineering Approach*, Israel Aircraft Industries Ltd. and Tel Aviv University, Cambridge University Press, 1997

[9] Franco Bernelli Zazzera, *Appunti del corso di Dinamica e controllo d'assetto*

[10] W . Larson, J. Wertz, *Space Mission Analysis And Design 3Rd Ed* , Academic Publishers Kluwer, 1999

[11] Andrew Carrel, *N2 Attitude estimation design,* SSTL document July 25, 2008

[12] K. Dutton, S. Thompson and B. Barraclough *The art of control engineering*, Addison-Wesley, Longman, 1997

[13] Kaiser Marqardt , *Model R-6CSR 5 LBf (22 Newton) Bipropellant rocket engine performance and operating characteristic*

[14] Andrew Carrel, *Is Maths Model*, SSTL document, April 2009

[15] Quang M. Lam, Nick Stamatakos, Craig Woodruff, Sandy Ashton, *Gyro Modeling and Estimation of Its Random Noise Sources,* AIAA Guidance, Navigation, and Control Conference and Exhibit, Austin, Texas, August 2003

[16] E.J. Lefferts, EL. Markley, M .D. Shuster, *Kalman Filtering for Spacecraft Attitude Estimation,* AIAA 20th Aerospace Sciences Meeting, Florida, January 1982

[17] Renato Zanetti, Robert H. Bishop, *Quaternion Estimation and Norm Constrained Kalman Filtering,* AIAA/AAS Astrodynamics Specialist Conference and Exhibit, Keystone, Colorado, August 2006

[18] Lerner G.M., *Three-Axis Attitude Determination*, *Spacecraft Attitude Determination and Control,* edited by J.R. Wertz, D. Reidel Publishing Co., Dordrecht, The Netherlands, 1978

[19] Ilaria Roma, *ESMO System Design Summary*, March 2009

[20] R.M.O. Gemson, M.R. Ananthasayanamt, *Importance of initial state co variance matrix for the parameter estimation using an adaptive extended kalman filter*, American Institute of Aeronautics and Astronautics, 1998

[21] Sungkoo Bae, Bob E. Schutz, *Icesat_Glas Attitude Determination Using A batch Least Squares Estimator During Star Tracker Starless Periods,* AIAA/AAS Astrodynamics Specialist Conference and Exhibit, Monterey, California, August 2002

[22] Björn Wittenmark, Karl J. Åström, KarlErik Årzén, *Computer control,* Department of Automatic Control, Lund Institute of Technology, Sweden